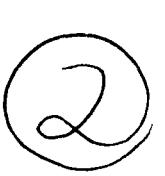

Experimental and Theoretical Investigation of RF Absorption and Reflection from Preformed Plasmas

Final Progress Report

Submitted to

Air Force Office of Scientific Research

Submitted by

Electrical Engineering Department and Institute for Plasma Research

University of Maryland, College Park, MD 20742

W. W. Destler

Principal Investigator

REPORT DOCUMENTATION PAGE

Form Approved
OMB No. 0704-0188

1. AGENCY USE ONLY (Leave blank)	2. REPORT DATE	3. REPORT TYPE AND DATES COVERED
		FinalrReport 30 Sep 89 to 30 Sep 93

4. TITLE AND SUBTITLE
Experimental and Tehoretical Investigation of RF Absorption and Reflection from Preformed Plasmas

5. FUNDING NUMBERS
AFOSR-89-0488

6. AUTHOR(S)
Professor
William Destler

7. PERFORMING ORGANIZATION NAME(S) AND ADDRESS(ES)
University of Maryland
Department and Institute for Plasma Research
College Park MD 20742

8. PERFORMING ORGANIZATION REPORT NUMBER
AFOSR-TR

9. SPONSORING / MONITORING AGENCY NAME(S) AND ADDRESS(ES)
AFOSR/NE
110 DUNCAN AVENUE STE B115
Bolling AFB DC 20332-0001

ROBERT J. BARKER

10. SPONSORING / MONITORING AGENCY REPORT NUMBER
2301/ES

11. SUPPLEMENTARY NOTES

12a. DISTRIBUTION / AVAILABILITY STATEMENT
UNLIMITED

12b. DISTRIBUTION CODE

13. ABSTRACT (Maximum 200 words)

SEE PAGE #3 FOR ABSTRACT

14. SUBJECT TERMS

15. NUMBER OF PAGES

16. PRICE CODE

17. SECURITY CLASSIFICATION OF REPORT	18. SECURITY CLASSIFICATION OF THIS PAGE	19. SECURITY CLASSIFICATION OF ABSTRACT	20. LIMITATION OF ABSTRACT
UNCLASS	UNCLASS	UNCLASS	UL

Research Progress Report

Title: Experimental and Theoretical Investigation of RF Absorption and Reflection from Preformed Plasmas

Submitted to: Air Force Office of Scientific Research

Submitted by: Electrical Engineering Department and Institute for Plasma Research

University of Maryland, College Park, MD 20742

Principal Investigator: William W. Destler, Professor and Chairman of Electrical Engineering, University of Maryland

Period of Research: October 1, 1992 to September 30, 1993

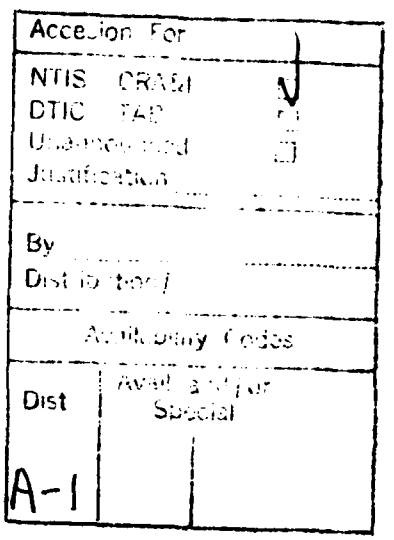

I. Introduction

This report constitutes the final progress report for a program of experimental and theoretical research on the reflection, absorption, and scattering of VHF and microwave radiation from plasma-covered conductors. A principal goal of this research is to determine to what extent plasmas can be used to reduce the radar cross-section of highly rf-reflective objects. This work was first funded by AFOSR starting October 1989. The major goals of this program have been:

1) To study rf absorption and reflection from a plasma-covered plane conductor to determine under what conditions the presence of the plasma can result in a significant reduction in the backscattered rf.

2) To conduct such studies under a wide range of plasma (overdense and underdense) and rf (frequency, power density, and pulse duration) conditions.

3) To establish a solid theoretical foundation for the understanding of experimental observations.

To date, these studies have been largely completed and the results have proven both encouraging and surprising. Experimental studies of rf reflection and absorption from plasma-covered plane conductors indicate that the presence of the plasma can significantly reduce the backscattered rf (by as much as 40 dB) even when the plasma is essentially collisionless. Since collision-free plasmas are inherently easier to create and maintain than are collision-dominated plasmas, this result may allow a very significant reduction in the costs of using ionized gases as microwave absorbers in real systems. In addition, this reduction in the backscattered rf occurs

over a very wide range of rf power densities and is therefore probably not a strongly nonlinear phenomena.

It is clear that a collisionless mechanism that significantly reduces backscattered rf from a reflecting surface without envoking cyclotron resonance absorption would have real advantages over other concepts being explored for this purpose. Such a configuration inherently requires not applied magnetic field and therefore might have additional cost advantages over other schemes.

In this report a summary of research progress made during the course of this program is presented in the next section. Copies of research papers prepared under this program are enclosed in the Appendix.

II. Summary of Research Progress

During the past grant period considerable progress has been made in our experimental and theoretical studies of rf absorption and reflection from a plasma-covered plane conductor. This work is summarized briefly below, and detailed in papers enclosed in the Appendix.

Experimental Research - First year experiments in this program were concentrated on studies of the reflection, absorption, and transmission of high power microwave radiation from a plasma-covered plane conductor. This work is detailed in a paper "Experimental Studies of High Power Microwave Reflection, Transmission, and Absorption from a Plasma-Covered Plane Conducting Boundary", published in the May 1991 issue of the Journal of Applied Physics, and enclosed in the Appendix. For these experiments, microwaves from a high power Large Orbit Gyrotron (10GHz, 30 ns, 10-200 kw/cm^2) were beamed at a 30 cm diameter plane conducting plate in hard vacuum (10^{-5} Torr). In this work, the presence of an optimally configured collisionless plasma on the surface of the plane conductor resulted in a reduction in the backscattered rf by 20-33 dB. Experiments were also conducted to determine if the high microwave power employed in these studies could result in nonlinear effects that might account for the strong rf absorption, with negative results.

In a further effort to study this phenomena over a wider range of experimental conditions and to investigate possible nonlinear effects, experiments have been conducted using low power microwave sources at similar frequencies. The basic experimental configuration was essentially the same as that used for the high power experiments, but the microwave power densities (0.01-

10 mW/cm^2) and pulse durations (10 microseconds - cw) were considerably different. Experiments were conducted at both 9 GHz and 13 GHz to explore frequency dependencies.

Results of these experiments are reported in the paper "Experimental Study of the Interaction of Microwaves with a Non-Magnetized Pulsed Plasma Column", published in the September 1992 issue of the Journal of Applied Physics and enclosed in the Appendix. The most important results of this study can be summarized as follows:

1) Backscattered rf can be reduced by the plasma by 30-40 dB below that observed in the absence of the plasma.

2) The mechanism accounting for the reduction in the backscattered radiation was thought to be a combination of efficient side-scattering of radiation at the critical density layer (accounting for no more than 20% of the incident radiation) and resonant absorption at the critical density layer.

3) The phenomena resulting in the reduced backscatter appears to be linear over a very wide range of incident microwave power densities.

4) Remarkably, backscattered radiation appears to increase as the pressure of the ambient background gas in the chamber is increased to make the plasma more collisional. This may actually be a result of the increased difficulty in creating and maintaining the plasma under collisional conditions.

Experimental Research over the last year has been focused primarily on obtaining a better understanding of the plasma conditions that have resulted in the observed reduction in the backscattered rf. Extensive studies of the spatial and temporal profiles of the pulsed plasma used in the microwave reflection experiments have been conducted and are summarized in the draft

paper "Spatial and Time Profiles of a Pulsed Plasma Column, and Their Correlation with Backscatter of Microwaves from the Plasma", to be submitted to the Journal of Applied Physics and enclosed in the Appendix. In addition to detailed information on the plasma density as a function of position and time, electron temperatures have been measured and radial variations in plasma density have been observed. This more detailed picture of the plasma covering the plane conductor should provide a much firmer basis for theoretical and numerical modeling of these systems.

Theoretical Research - Efforts to formulate possible mechanisms to account for the observed reduction in the backscattered rf have included studies of collisional absorption closely following those of Vidmar[1] (see Singh, et al, in the Appendix) and investigations of nonlinear instabilities as well (see Destler, et al, in the Appendix). Results of these studies indicate that collisional absorption alone cannot explain the observed reduction in the backscattered rf in either the high power or low power experiments, and experiments have confirmed that the process is not a result of nonlinear phenomena. As a result, it is presently believed that the mechanism accounting for the reduction in the backscattered radiation a combination of efficient side-scattering of radiation at the critical density layer (accounting for no more than 20% of the incident radiation) and resonant absorption at the critical density layer enhanced by radial spatial variations in the plasma density[2].

1. R. J. Vidmar, IEEE Trans. Plasma Sci. **18**, 733, 1990.

2. H. L. Rowland, "Anomalous Absorption of Electromagnetic Radiation", submitted to Phys. of Fluids, 1992.

Appendix

Experimental studies of high-power microwave reflection, transmission, and absorption from a plasma-covered plane conducting boundary

W. W. Destler, J. E. DeGrange, H. H. Fleischmann,[a] J. Rodgers, and Z. Segalov
Electrical Engineering Department and Laboratory for Plasma Research, University of Maryland, College Park, Maryland 20742

(Received 3 December 1990; accepted for publication 25 January 1991)

Experimental studies of the reflection, transmission, and absorption of high-power microwave pulses from a plasma-covered plane conducting boundary are presented. Under optimum conditions, backscattered rf power is attenuated by more than 30 dB over values measured in the absence of the plasma. Measurements of the radial and axial plasma density profiles and the neutral gas pressure near the plane conductor indicate that collisional absorption processes are not the primary source of the observed attenuation in the backscattered microwave signal, and that the plasma density exceeds the critical density over much of the volume nearest the conductor. The effects of a tenfold reduction in the microwave power density on the reflection and absorption characteristics of the system are also reported.

I. INTRODUCTION

Interest in the propagation of coherent electromagnetic radiation in plasmas has been sustained for many years as a result of applications of such studies in such diverse areas as the rf heating of fusion plasmas, plasma-filled microwave tubes and devices, and atmospheric and ionospheric propagation. In recent years, however, the possibility of using artificially produced plasmas in the atmosphere to reflect electromagnetic radiation and allow over-the-horizon radar and communication systems at microwave frequencies has been proposed.[1] In addition, studies have been initiated at several laboratories on the extent to which plasmas can be used in place of more conventional microwave absorbers in certain applications.[2-8] In particular, plasmas may be capable of absorbing microwave radiation over a wider frequency range than can conventional absorbers, and are in principle more controllable.

In the studies reported in this paper, high-power microwave radiation was beamed at a plane conducting surface, and reflected and transmitted rf was carefully measured to provide a baseline against which plasma-induced effects could be compared. A hydrogen plasma was created on the surface of the conducting plate by a number of coaxial plasma guns embedded in the plate, and microwave reflection and transmission was then measured over a wide range of plasma conditions. Side-scattered radiation was also measured in some experiments to determine if the incident radiation was absorbed or scattered by the plasma. Finally, the microwave power density was decreased by an order of magnitude to determine if nonlinear effects could be responsible for the observed attenuation in the reflected microwave signal.

In this paper, the experimental measurements are detailed in Sec. II, and a discussion of possible theoretical causes for the observed absorption is presented in Sec. III. Conclusions are drawn in Sec. IV.

II. EXPERIMENTS

The general experimental configuration used for studies of microwave reflection, transmission, and absorption from plasma-covered plane conductors is shown in Fig. 1. High-power microwave radiation from a large orbit gyrotron (10 GHz, 100 MW, 30 ns FWHM) is beamed at a 30-cm-diam brass plate inserted as the endstop in a 150-cm-long acrylic vacuum chamber. The vacuum chamber is directly connected to the Gyrotron vacuum system and a vacuum of less than 10^{-4} Torr is maintained throughout the entire experimental system. The phase stability of the large orbit gyrotron (which is driven by a 2-MeV, 2-kA, 30-ns pulse line accelerator) is relatively poor, thus ensuring that any observed reductions in reflected microwave signals are almost certainly not due to standing wave effects. A plasma is created on the surface of the plate by 19 embedded coxial plasma guns discharged using a laser flashlamp pulser. The discharge end of each coaxial plasma gun was coated with a titanium-hydride mixture to ensure a hydrogen-rich plasma. Because the plasma is essentially stationary on the time scale of the microwave pulse, some control over the axial and radial plasma density profile can be achieved by varying the firing delay between the plasma guns and the microwave source and/or the charging voltage on the laser flashlamp pulser.

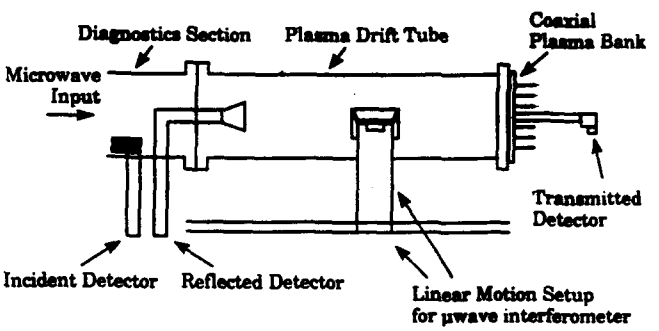

FIG. 1. General experimental configuration.

[a] Permanent address: Department of Applied Physics, Cornell University, Ithaca, NY 14853.

 0021-8979/91/096313-06$03.00

Measurements of the radial and axial plasma density profiles in the region upstream of the brass plate have been obtained using Langmuir probe measurements and 10 GHz microwave interferometry. Representative Langmuir probe signals 60 cm upstream of the brass plate on-axis are shown in Fig. 2 for 2- and 5-kV flashlamp pulser charging voltages. These results indicate that both the duration and the magnitude of the plasma density waveform at this point can be readily varied by simply controlling the amount of energy supplied to the coaxial plasma guns. Results of detailed studies of the axial plasma density profile (all data taken on axis) as a function of time are shown in Figs. 3 and 4 for 2- and 5-kV flashlamp pulser charging voltages. Plasma density measurements above the critical density for the 10-GHz interferometer (1.2×10^{12} cm $^{-3}$) were inferred by using both the interferometer data and the Langmuir probe waveforms.

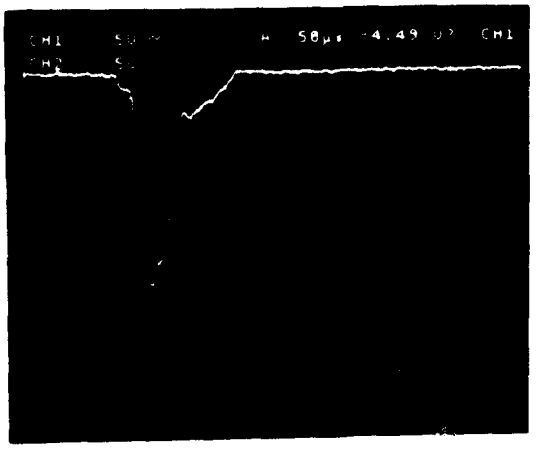

(a)

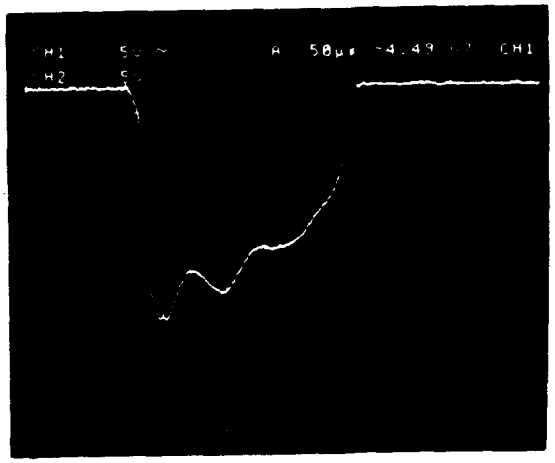

50 µsec

(b)

FIG. 2. Typical Langmuir probe waveforms: (a) 2-kV charge on laser flashlamp pulser. (b) 5-kV charge.

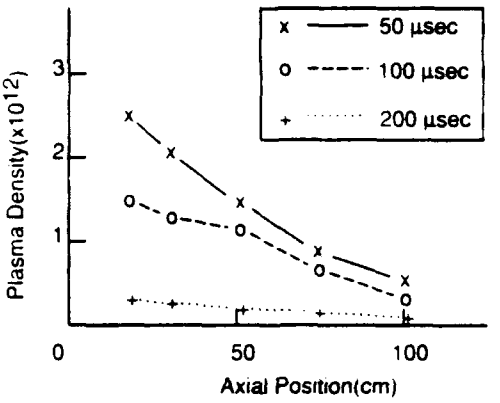

FIG. 3. Axial plasma density distributions at various delay times after plasma gun firing, 2-kV charge on laser flashlamp pulser.

Langmuir probe measurements of the radial plasma density profile 60 cm upstream of the brass plate are shown in Figs. 5 and 6 for 2- and 5-kV flashlamp pulser charges, respectively. To determine shot-to-shot variability in the measurements, two measurements were made for each radial position. The nonreproducibility of the data is attributed to the fact that not all of the coaxial plasma guns were observed to fire on every shot, resulting in some shot-to-shot inconsistency in the plasma density profile even well upstream of the brass plate.

The microwave diagnostic setup used in the experiments is shown schematically in Fig. 1. Additional details on the incident and reflected rf monitors are provided in Fig. 7. Not shown in the figure is a standard gain horn employed in the reflected microwave monitor to ensure sufficient directionality. As shown in Fig. 1, a third microwave monitor was inserted right in the brass plate to provide information on the microwave power that was able to propagate through the plasma. A number of tests of the diagnostic system were conducted in advance of the plasma absorption tests, including a test in which the brass endplate was covered with conventional microwave absorber of known attenuation at 10

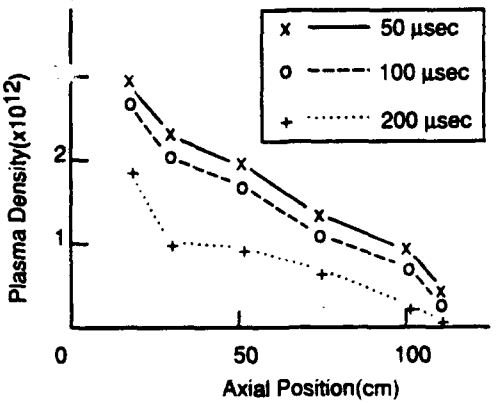

FIG. 4. Axial plasma density distributions at various delay times after plasma gun firing, 5-kV charge on laser flashlamp pulser.

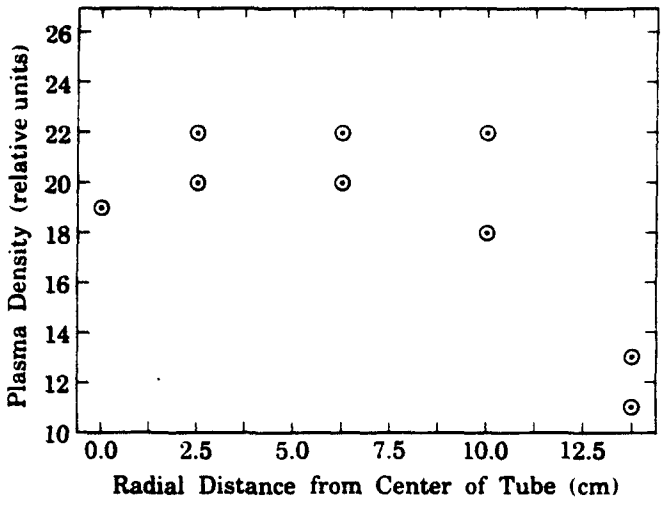

FIG. 5. Radial plasma density distribution 60 cm upstream of plane conductor 70 μs after plasma gun firing, 2-kV charge on laser flashlamp pulser.

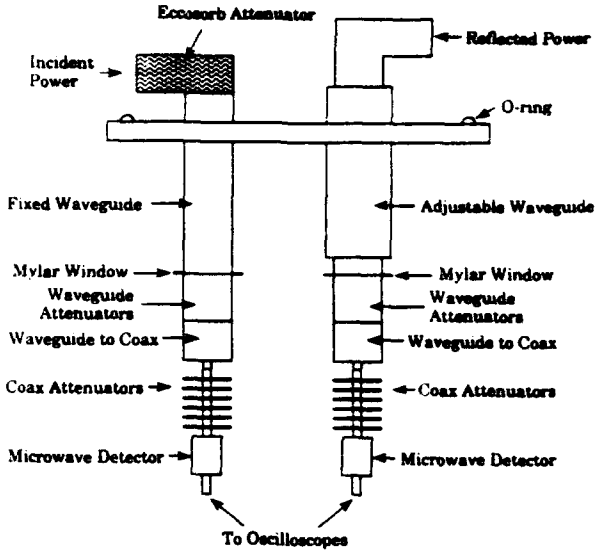

FIG. 7. Incident and reflected microwave detector configurations.

GHz. The attenuation of the reflected microwave signal observed in these experiments compared to that received with no absorber in place was in good agreement with the manufacturer's specifications for the absorber. In a second test, the incident and reflected microwave receiving antennae were each covered with copper foil in turn, and observed microwave signals dropped to levels below ambient noise levels. This test was conducted to ensure that rf leakage around waveguide flanges or coax connections would not corrupt microwave measurements. Finally, the radial profile of the microwave radiation produced by the large orbit gyrotron was measured by rotating the reflected rf antenna so that it received the incident microwaves. This antenna was then moved radially and the microwave power received was normalized to that received by the incident rf monitor, as shown in Fig. 8. Several measurements were obtained for each radial position. As can be seen, the incident microwave radiation is fairly uniform over the cross section of the 30-cm-diam vacuum chamber, with the approximately 6 dB increase in the incident microwaves measured by the "reflected" rf monitor attributable to the 6-dB standard gain horn used on that detection system. Shot-to-shot variations, however, are relatively large.

Typical reflected microwave signals with and without plasma are shown in Fig. 9. It is readily seen that under optimum conditions the presence of the plasma results in a significant reduction in the reflected microwave signal. Figures 10 and 11 present results of extensive measurements of the reflected rf signal (normalized to the incident rf on each shot) as a function of the firing delay between the coaxial plasma guns and the microwave pulse. The system reflection baseline limits represent the range of results obtained with

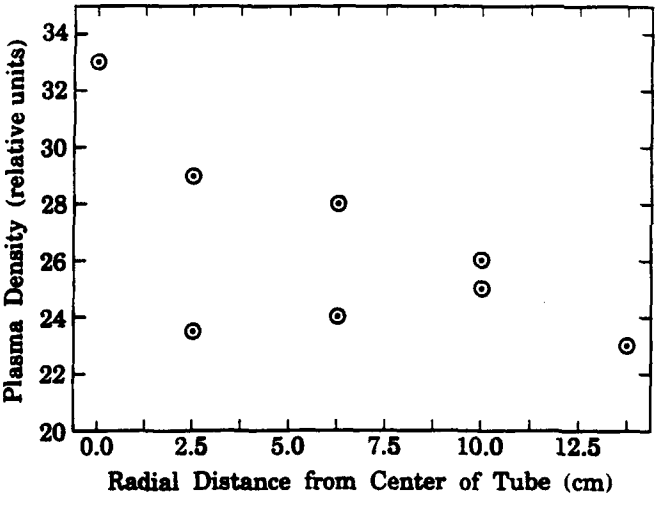

FIG. 6. Radial plasma density distribution 60 cm upstream of plane conductor 70 μs after plasma gun firing, 5-kV charge on laser flashlamp pulser.

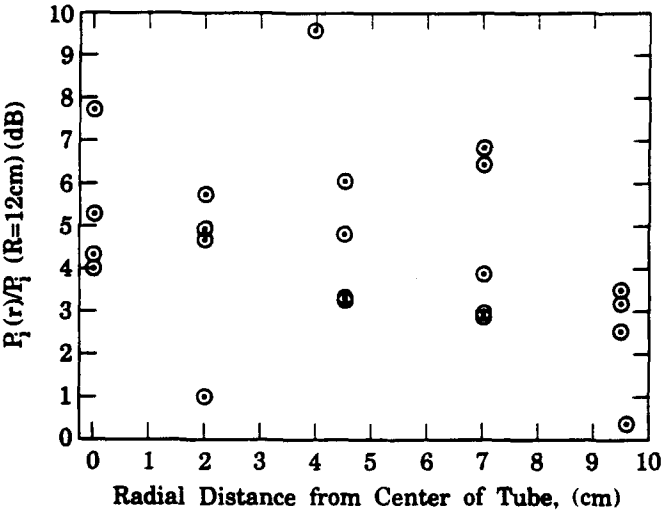

FIG. 8. Normalized incident microwave power density vs radius 150 cm upstream of plane conductor.

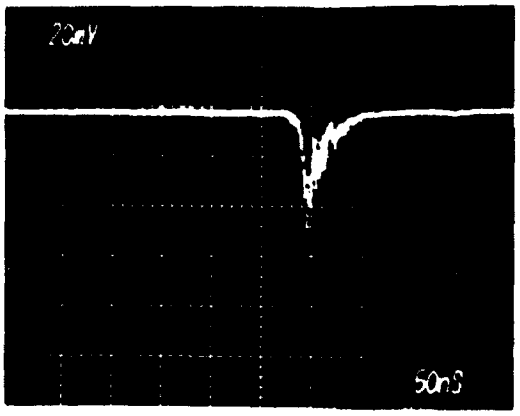

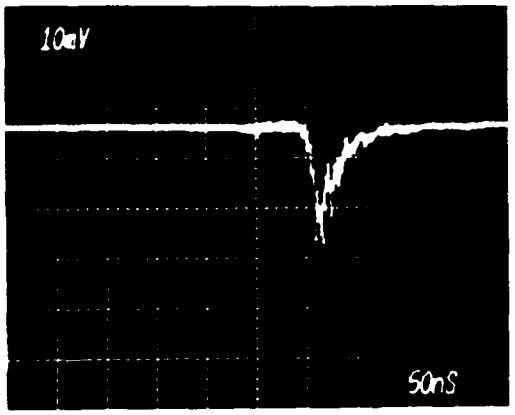

(b)

FIG. 9. Typical rectified reflected microwave waveforms: (a) no plasma, 56-dB fixed attenuation, (b) with plasma (5-kV charge, 50 μm delay), 36-dB fixed attenuation.

no plasma over many shots. Data are once again shown for 2- and 5-kV charging voltages on the laser flashlamp pulser. It is evident that the maximum attenuation of the reflected signal due to the presence of the plasma is in the range 20–33 dB under optimum conditions in both cases. The range of firing delays over which significant attenuation is observed is much more narrow for the 2-kV charging voltage, however, consistent with the much shorter plasma lifetime associated with this condition. It is interesting to note that some attenuation is observed for firing delays as large as 200 μs, even though the Langmuir probe measurements indicate that the plasma pulse duration is no more than about 100 μs, 60 cm upstream of the plane conductor. Reflected rf was also found to be fairly uniform over the cross section of the 30-cm vacuum chamber, at least at the axial position of the reflected microwave monitor.

Results of measurements obtained from the transmitted rf monitor located on the brass plate are shown in Fig. 12. The magnitude of the normalized baseline measured without plasma is related to the coupling of rf to the receiving waveguide and should not be used as an indication of the absolute microwave power density reaching the plate. Nevertheless, it is clear from the figure that this signal is strongly attenuated over the same range of firing delays that resulted in significant attenuation of the reflected rf signal, although not at as high a rate as simple evanescent decay of the wave in the overdense region near the plate would imply.

In order to ensure that the plasma was not simply scat-

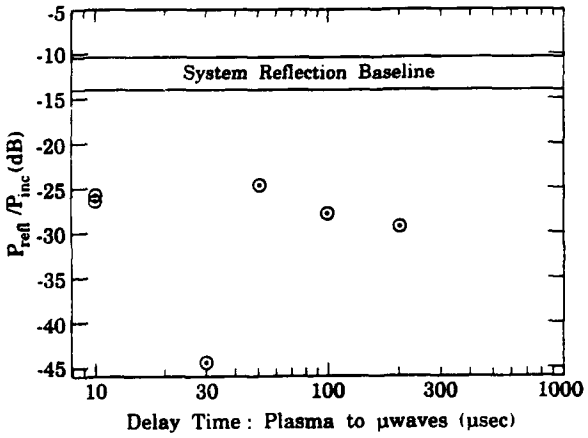

FIG. 10. Normalized reflected microwave power as a function of delay time between firing of plasma guns and the microwave pulse, 2-kV charge.

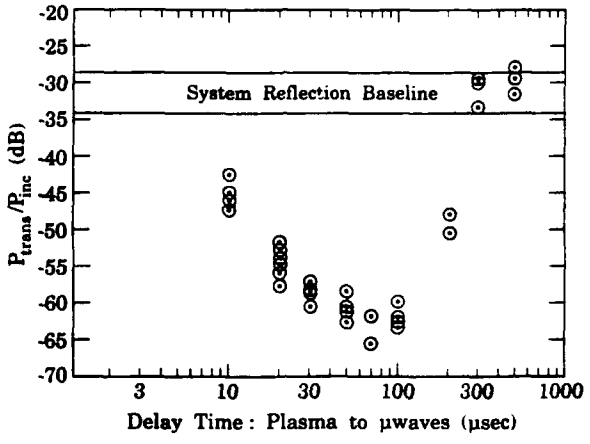

FIG. 12. Normalized transmitted microwave power as a function of delay time between firing of plasma guns and the microwave pulse, 5-kV charge.

tering the rf out the sides of the acrylic vacuum chamber, a third microwave detector was mounted on the side of the vacuum chamber at an axial distance of 75 cm from the brass plate. This detector measured rf exiting radially out of the vacuum chamber and the standard gain horn employed had an acceptance angle of about 30°. Results of these measurements, shown in Fig. 13, indicate that there is not a significant increase in side-scattered rf at firing delays corresponding to significant reductions in the reflected rf signal. In fact, side-scattered rf appears also to be reduced by the presence of the plasma, especially at a firing delay of 50 μs. In this figure, the zero delay time data corresponds to not firing the plasma guns, and therefore approximates the normalized baseline for these measurements.

In a final experiment, the total microwave power from the large orbit gyrotron was reduced by an order of magnitude to about 10 MW to determine if nonlinear effects were an important cause of the observed rf absorption. As shown in Fig. 14, the maximum attenuation of the reflected signal under optimum plasma conditions in this case was about 20–25 dB below the normalized baseline, compared to about 30 dB for the higher power experiments. Thus it is possible that nonlinear effects may play a role in explaining the observed effects.

III. THEORETICAL DISCUSSION

Many mechanisms can produce electromagnetic wave energy absorption in plasmas, including electron-ion and electron-neutral collisional absorption, cyclotron resonance absorption, instabilities, and other nonlinear effects. In this section we will briefly address each of these possibilities with the exception of cyclotron resonance absorption. We are omitting this possibility because there is no applied magnetic field in the wave-plasma interaction region.

The damping constant for an electromagnetic wave propagating in a homogeneous plasma in which the electron-ion collision rate ν_{ei} is given by

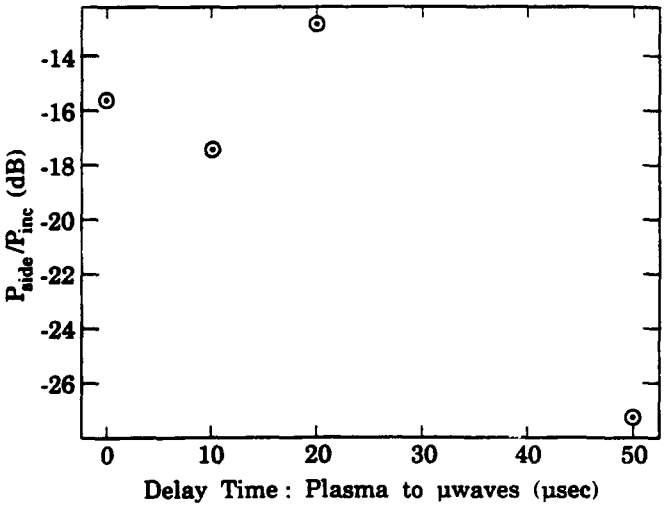

FIG. 13. Normalized side-scattered microwave power as a function of delay time between firing of plasma guns and the microwave pulse, 5-kV charge.

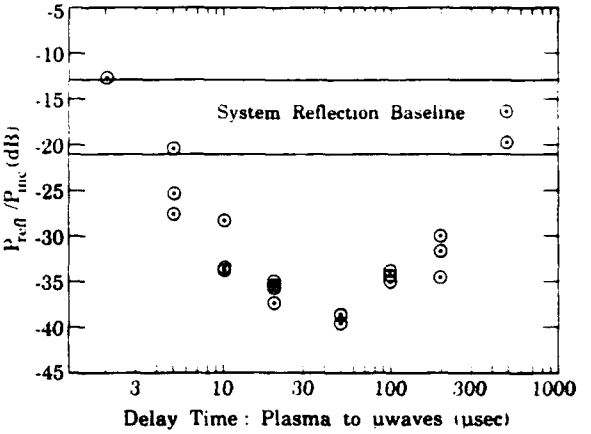

FIG. 14. Normalized reflected microwave power as a function of delay time between firing of plasma guns and the microwave pulse, 5-kV charge, reduced microwave power density.

$$k = \frac{\omega_{pe}^2}{\omega_0^2}\left(\frac{1}{1-\omega_{pe}^2/\omega_0^2}\right)\frac{\nu_{ei}}{c}, \tag{1}$$

where ω_0 is the wave frequency, $\omega_{pe} = (ne^2/\epsilon m)^{1/2}$ is the electron plasma frequency, ϵ is the permittivity of free space, and c is the velocity of light in vacuum.[9] Here m is the electron rest mass, e is the electronic charge, and n is the electron density. For inhomogeneous plasmas the damping factor is somewhat different, although not so different as to change the overall picture. Clearly wave damping will be strongest near $\omega_0 = \omega_{pe}$. To see effective wave damping from electron-ion collisions, therefore, $(\nu_{ei}/c)\,L \gtrsim 0.5$ near $\omega_0 = \omega_{pe}$ where L is a characteristic scale length for the plasma. If $L = 10$ cm, the electron-ion collision frequency must therefore be at least $10^9\ s^{-1}$. At the critical density of $n = 1.2\times10^{12}\ cm^{-3}$, and taking $T_e = 2$ eV (a value approximately equal to the electron oscillation energy in the wave electric field), the electron-ion collision frequency is estimated to be $2.5\times10^7\ s^{-1}$. Thus for these experiments the electron-ion collision frequency is simply too small to account for significant wave damping.

A second possible collisional absorption process is wave energy loss to electron-neutral collisions, in which it is assumed that the plasma is immersed in a dense neutral background. Electron-neutral collisional absorption has been observed in high-power microwave propagation experiments[10] in which a high-power microwave pulse is used to break down the atmosphere and subsequent wave energy is coupled to the neutral background by the plasma electrons. For electron-neutral collisions to be a significant source of wave energy damping, however, the ambient neutral gas pressure must be at least 1 Torr assuming $n = n_{crit}$ and $T_e = 2$ eV as discussed previously. Since the actual ambient pressure in the vacuum chamber is initially about 1 mTorr and is not observed to rise significantly when the plasma guns are fired, electron-neutral collisions are also not a likely source of the observed wave attenuation.

A number of instabilities are also candidates for wave energy loss, including the oscillating two-stream instability,[11] the ion acoustic decay instability,[12] the two-plasma

decay instability[13] and instabilities driven by stimulated Raman scattering[14] and stimulated Brillouin[15] scattering. Of these, even at the high microwave intensity associated with the experiments, the oscillating two-stream instability appears to be the only one with sufficiently high growth rates to significantly affect the wave amplitude on the 30 ns time scale of the experimental microwave pulse. This instability occurs near $\omega_0 = \omega_{pe}$, and for a homogeneous plasma has a threshold for instability given by

$$\left(\frac{v_{osc}}{v_e}\right)^2 > 4\frac{\nu_{ei}}{\omega_0}, \tag{2}$$

where v_{osc} is the electron oscillation velocity in the wave field, and v_e is the electron drift velocity. The oscillating two-stream instability is characterized by a very high growth rate with e-folding times estimated to be subnanosecond for the experimental parameters reported here.

Another possible mechanism has been investigated by Rowland,[16] who has studied numerically anomalous absorption processes in collisionless plasmas. In this work, the presence of transverse structure in a plasma at the critical density layer is reported to increase the coupling between the electromagnetic wave and electrostatic plasma waves and lead to enhanced absorption of the radiation. Simulations show 90% absorption of the incident wave energy and a reduction in the backscattered rf by 20 dB.

IV. CONCLUSIONS

A significant (20–33 dB) reduction in the backscattered microwave signal from a plane conductor has been observed when a plasma is created on the surface of the conductor under optimum conditions. Measurements of the plasma and ambient neutral densities indicate that the primary absorption mechanism is not collisional in nature. Although it is possible that either the oscillating two-stream instability or the coupling of electromagnetic wave energy to electrostatic waves resulting from a transverse density structure at the critical density layer may account for the observed attenuation in the backscattered rf, further experimental and theoretical work will be required to definitively determine the loss mechanism. For example, predetermined transverse structures can probably be created by creating plasma at only a few of the 19 coaxial plasma guns located on the brass plate. Future studies will concentrate on a careful determination of the loss mechanism and on its possible enhancement.

ACKNOWLEDGMENTS

It is a pleasure to acknowledge useful discussions with Professor C. D. Striffler. This work was supported by the Air Force Office of Scientific Research.

[1] R. J. Vidmar, IEEE Trans. Plasma Sci. **18**, 733 (1990).
[2] R. J. Barker, 1990 IEEE International Conference on Plasma Science (Oakland, CA, May 21–23, 1990), Conf. Record, p. 169.
[3] J. E. Brandenburg, W. M. Bollen, R. Seely, and D. Felinczak, 1990 IEEE International Conference on Plasma Science (Oakland, CA, May 21–23, 1990), Conf. Record, p. 170.
[4] D. G. Gregoire, J. Santoru, and R. W. Schumacher, 1990 IEEE International Conference on Plasma Science (Oakland, CA, May 21–23, 1990), Conf. Record, p. 170.
[5] M. Rader, F. Dyer, A. Matas, and I. Alexeff, 1990 IEEE International Conference on Plasma Science (Oakland, CA, May 21–23, 1990), Conf. Record, p. 171.
[6] S. P Kuo and A. Y. Ho, 1990 IEEE International Conference on Plasma Science (Oakland, CA, May 21–23, 1990), Conf. Record, p. 171.
[7] L. H. Combs, C. Liu, and J. R. Roth, 1990 IEEE International Conference on Plasma Science (Oakland, CA, May 21–23, 1990), Conf. Record, p. 151.
[8] J. E. Scharer, O. C. Eldridge, M. H. Bettenhausen, N. T. Lam, and S. W. Lam, 1990 IEEE International Conference on Plasma Science (Oakland, CA, May 21–23, 1990), Conf. Record, p. 151.
[9] W. L. Kruer, *The Physics of Laser Plasma Interactions* (Addison-Wesley, New York, 1988), pp. 46–48.
[10] C. A. Sullivan, W. W. Destler, J. Rodgers, and Z. Segalov, J. Appl. Phys. **63**, 5228 (1988).
[11] W. L. Kruer, *The Physics of Laser Plasma Interactions* (Addison-Wesley, New York, 1988), pp. 61–69.
[12] W. L. Kruer, *The Physics of Plasma Interactions* (Addison-Wesley, New York, 1988), pp. 66–68.
[13] W. L. Kruer, *The Physics of Plasma Interactions* (Addison-Wesley, New York, 1988), pp. 81–83.
[14] W. L. Kruer, *The Physics of Plasma Interaction* (Addison-Wesley, New York, 1988), p. 73.
[15] W. L. Kruer, *The Physics of Plasma Interactions* (Addison-Wesley, New York, 1988).
[16] H. L. Rowland, Phys. Fluids (submitted). [See also 1990 IEEE International Conference Plasma on Science (Oakland, CA, May 21–23, 1990), Conf. Record, p. 150.]

Experimental study of interaction of microwaves with a nonmagnetized pulsed-plasma column

A. Singh, W. W. Destler, P. Catravas,[a] and J. Rodgers
Laboratory for Plasma Research, University of Maryland, College Park, Maryland 20742

(Received 19 December 1991; accepted for publication 8 May 1992)

The time evolution of backscattered and sidescattered microwaves from a plane conductor covered by a pulsed-plasma column has been studied; transmitted signals along the axial and transverse directions of the column have also been studied. The incident microwaves are at a cw power level varying from a few milliwatts to a few watts. The cw nature of the signal makes it possible to observe the fine structure in the time evolution of the interactions. The plasma is generated by an array of plasma guns embedded in the conducting plate. The plasma density has a gradient in the axial direction and contains regions of subcritical and supercritical plasma density. Reductions in the backscattered radiation down to the lowest measurable levels with available equipment are observed for durations that are an order of magnitude longer than the duration of the current pulse that generated the plasma. Variations caused by changes in the charging potential on the plasma gun capacitor bank, the pressure of the background gas, and the frequency and power level of the incident microwaves are reported. The attenuation in the backscattered radiation decreases with increasing pressure, especially at lower charging potentials. There is a close correlation between the timing and location of sidescattered signals and the transition of the critical density layer across the axial position of the detectors for the scattered signal. The amplitude of the scattered signal was also measured. Estimates have been made for the percentage of incident power accounted for by scattering. Models are discussed for absorption of microwaves in the plasma.

I. INTRODUCTION

Compared to conventional absorbers of microwaves, plasmas offer the possibility of a wider frequency coverage, switchability, and tunability. The reduction in microwave backscatter and effective absorption of microwaves by plasmas have thus been the subject of investigation at a number of laboratories.[1-8] The nature of the plasmas studied has included isotropic and magnetized plasmas, those generated by photoionization or by arc discharge, those that are collisional or collisionless, and those that are confined in waveguides, cones, or enclosures. We have reported previous studies at this laboratory dealing with experiments using pulsed microwaves of 30 ns duration at megawatt power levels.[9] Attenuation of the order of 30 dB in the backscattered microwave signal from a conducting plate was achieved by generating a pulsed plasma in front of the plate using plasma guns embedded in the plate. Various phases of the time evolution of the interaction process were studied by varying the time lag between the triggering of the plasma and the firing of the source of microwaves (a large-orbit gyrotron). The background pressure was of the order of 0.1 mTorr. At such a pressure electron-neutral collisions were not considered to be a major cause of the observed attenuation. Different parametric instabilities were considered as possible causes, and threshold values were estimated. Consequently, in spite of the high microwave power level, only the oscillating two stream instability appeared to have a sufficiently high growth rate to significantly affect the wave amplitude. The possibility of enhanced absorption due to a transverse structure at the critical density layer was also noted.

The present study was motivated by a desire to understand more clearly the nature of the underlying phenomenon, and thus to be able to optimize its application. To this end, the experiment was modified so as to use continuous-wave microwaves in the power range of a few milliwatts to a few watts. Consequently, the fine structure in the sequence of development of the microwave-plasma interaction can be studied systematically. The resultant digitally stored data can be analyzed to give a time resolution down to nanosecond range. In addition, the lower-power microwave sources allow a much larger number of experiments in a given span of time and thereby permit a much more complete exploration of the parameter space. Finally, the low-power experiments allow for an investigation of the rf-plasma interactions at power densities seven orders of magnitude lower than the previous studies, thereby shedding additional light on the presence of any nonlinear effects. The operating parameters that were varied included the charging potential on the capacitor bank that fed the plasma guns, the pressure of the background gas, and the frequency and power level of the incident microwaves.

In Sec. II of this paper the experimental setup and techniques used are described. The dependence of backscattered and axially transmitted microwave signals on operating parameters is presented in Secs. III and IV, respectively. Results on the time evolution of both sidescattered and transverse transmission signals are given in Secs. V and VI, respectively, and their correlation is presented in Sec. VII. Observations on the amplitude of the sidescat-

[a]Present address: Department of Electrical Engineering, Massachusetts Institute of Technology, Cambridge, MA.

 0021-8979/92/171707-13$04.00

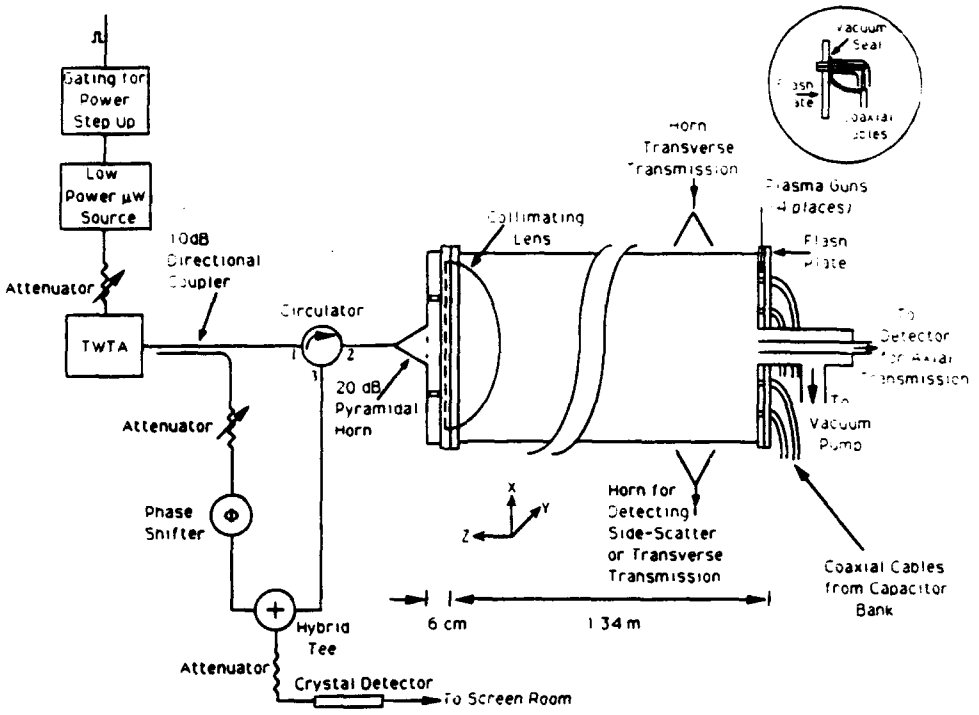

FIG. 1. Schematic diagram of the experimental setup.

tered signal and estimation of its power as a percentage of the incident signal are given in Secs. VIII and IX, respectively. Results of simulations of reduction in backscattered signal in a transversely homogeneous plasma are presented in Sec. X, the effects of the process of generation of the plasma on its lack of homogeneity are discussed in Sec. XI, and a model based on resonance absorption in a transversely inhomogeneous plasma is outlined in Sec. XII. Conclusions are summarized in Sec. XIII.

II. THE EXPERIMENTAL SETUP AND TECHNIQUES USED

A schematic diagram of the setup is shown in Fig. 1. The microwave-plasma interaction occurred in an acrylic tube 1.35 m long with a diameter of 30 cm. The plasma was generated by an array of four plasma guns embedded in a stainless-steel plate attached to one end of the tube. Each gun consisted of a spark plug with the space between inner and outer conductors filled with an epoxy containing titanium hydride. These guns produced what was essentially a hydrogen plasma when an arc discharge current was passed through them.

The other side of the tube was closed by a plexiglas plate, or a microwave lens for measurements at 10 GHz. The incident microwaves were launched by a standard-gain horn having a gain of 20 dB. Its distance from the lens was adjusted to minimize changes in the backscattered signal when a shorting plate was moved axially back and forth on the other end of the acrylic tube. A minimum of 1.5:1 in the ratio of highest to lowest values of backscattered signals was obtained for a frequency of 10 GHz when the distance between the mouth of the horn and the front (flat) face of the lens was 6 cm. This procedure was adopted so as to obtain as good an approximation as possible of a plane-wave front emerging from the curved rear surface of the lens.

The incident microwaves were generated by two low-power (0–100 mW) sources at 10 and 13.77 GHz. Where higher power was required, a travelling-wave tube amplifier was added. Power to the 20 dB horn was fed via a circulator having a nominal directivity of 30 dB. This separated the outgoing signal from the reflected signal. The latter was detected and fed by coaxial cable to a digital oscilloscope. Using this kind of transmit-receive arrangement employing a single horn, measurements of the attenuation in the backscattered signal could be made with a dynamic range of up to about 30 dB (a figure limited by the directivity of the directional coupler).

To study the extent of delay between initiation of discharge current and the reduction in backscattered signal, the two were probed simultaneously as shown in Fig. 2. It

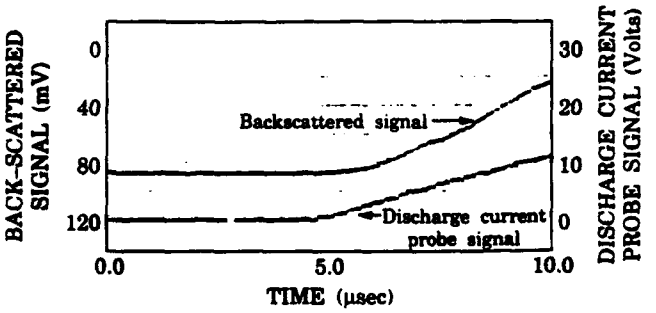

FIG. 2. Time relationship between start of plasma discharge current and the start of reduction in backscattered signal (the latter increases downward in the graph). Delay is of the order of 1 μs.

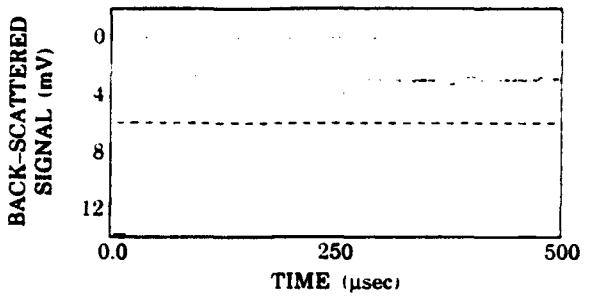

FIG. 3. Early phase of backscattered signal (without balancing out of parasitic reflection); frequency is 10 Ghz, charging potential is 8.5 kV, and pressure $\simeq$ 100 mTorr.

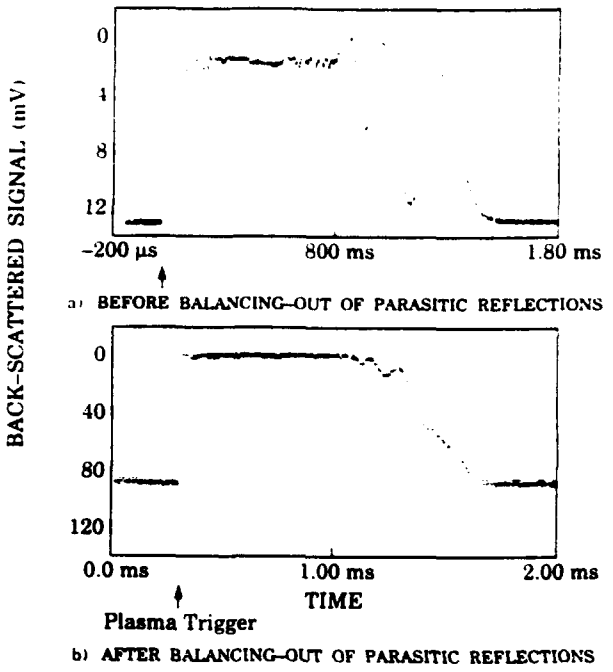

FIG. 4. Backscattered microwave signals (a) before and (b) after balancing out parasitic reflections from the lens and other surfaces. Frequency is 10 GHz, charging potential is 8.5 kV, and pressure is 100 mTorr.

is seen that the delay is of the order of 1 μs. Furthermore, in this initial phase the two traces do not indicate a highly nonlinear relationship between the backscattered signal and the discharge current (notice that in the graph, the backscattered signal increases downwards).

The reflected signal has three main components: (a) the signal propagating through the plasma to the flash plate and back; (b) the signal reflected from the front surface of the plastic plate or the lens; and (c) the signal reflected from the plasma gradient itself. These three components together produce the detected signal, which has a cyclically varying nature and which contains information on the amplitudes as well as the relative phases of both the rf signals. In the first 200 μs or so, the fluctuations in the detected signal often showed segments of different periodicity, with a phase reversal in between. An example of such a trace is shown in Fig. 3. A possible explanation is that the backscattered signal is slightly shifted in frequency. This can be attributed to a Doppler shift by reflection from a layer whose location travels across the tube due to changes in the density profile.

Shifts in frequency can also result from rises and falls in density of the plasma with time.[10] The relatively slow fluctuations in the backscattered signal toward the end of the interaction period can be attributed to the effect of plasma density slowly decaying below critical value. This changes the effective dielectric constant of the plasma and produces a phase shift between reflections from the front and the rear ends of the tube.

The fluctuations in the detected backscattered rf signal are indicative of interference fringes resulting from its beating with parasitic reflections. While observations of interference fringes do provide useful information, they can also prevent accurate measurements of the amplitude of the backscattered signal. With this in view, a bridge circuit using a hybrid tee was included in the detector system as shown in Fig. 1. A signal tapped from the incident wave was used to cancel parasitic reflections such as from the surface of the lens. The amplitude and phase of the cancelling signal were adjusted to minimize the composite detected signal when the metal end plate was substituted temporarily by an anechoic box. Figure 4 shows the backscattered signal (a) without and (b) with the balancing out of parasitic reflections, in a typical case. It is seen that the fringes are considerably reduced, though not completely eliminated.

In the case shown in Fig. 4(b), and other similar cases where the attenuation in backscattered signal is the highest, the trace becomes almost indistinguishable from the zero line. In order to increase the dynamic range of the measurement, a gating circuit was added to the amplitude modulation facility provided in the low-power oscillator. The timing of the gate was set in such a way that the power would be stepped up by a known factor in a time period when the attenuation due to the plasma was high. Thus, the detector could measure both the large backscattered signal without the plasma but with low incident power and also the attenuated backscattered signal at a higher incident power level without saturating the detector. Figures 5(a) and 5(b) show the detected traces without and with the gated upshift in power level of incident microwaves. In this way attenuation of the order of 30 dB could be measured. In our configuration where the same horn acts as the sending and the receiving horn, the accuracy was restricted by the limitation in directivity of the circulator employed as well as the microfluctuations in the plasma itself. These fluctuations also show up in the enhanced level of backscattered signal when the power is stepped up during the selected time gate, as seen in Fig. 5(b).

Observations on the axial transmission through the plasma column were also conducted. In this case an open-ended waveguide was used to sample the received signal at the surface of the flash plate.

For observations on sidescattered and transversely

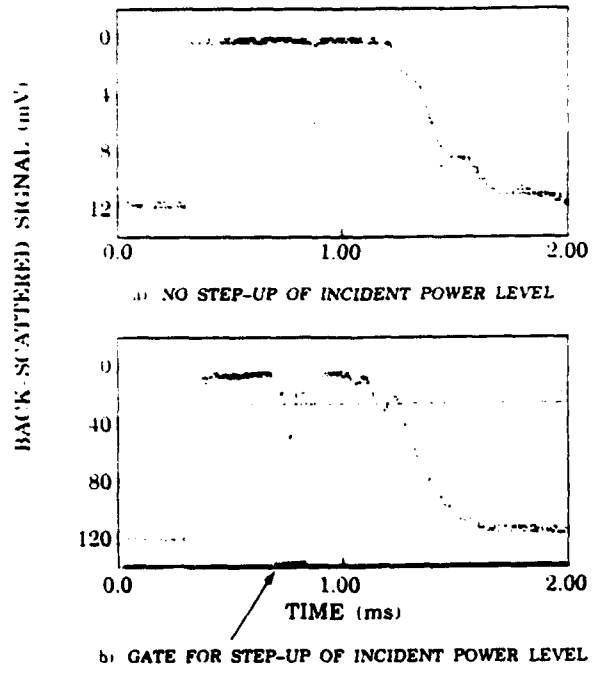

FIG. 5. Increase in dynamic range of measurement of attenuation by gated stepup of incident power level; frequency is 10 GHz, charging potential is 8.5 kV, and pressure is 100 mTorr.

transmitted radiation, auxiliary horns were used that were oriented radially, as shown in Fig. 1. Their locations and orientation are discussed in greater detail in Sec. V.

III. DEPENDENCE OF BACKSCATTERED SIGNAL ON OPERATING PARAMETERS

Using the setup described in the previous section, a series of experiments was conducted on the time evolution of the backscattered microwave signal as a function of various parameters. Typical results are summarized below.

Figure 6 shows the time evolution of the backscattered signal for different values of background pressure ranging from 15 mTorr to 10 Torr, when the charging potential was 8.5 kV. It is noticed that the duration of maximum attenuation is of the order of 600–800 μm. (The duration of the discharge current that generates the plasma is approximately 40 μm.) In general the duration is an order of magnitude higher than the duration observed in our high microwave power experiment.[9] In the present experiments there is a lens or a partition at the end of the tube opposite to the flash plate. This and the pressure of background gas are possible parameters helping to retain higher plasma densities for a longer time than in the previous studies where there was a direct connection to a large-orbit gyrotron at low background pressure with no interface in between.

Figure 7 shows the time evolution of the backscattered signal for plasma gun capacitor bank charging potentials of 8.5, 6.0, and 3.5 kV. The duration of the maximum attenuation decreases with reductions in the charging potential. It is seen that for 3.5 kV charging potential, the trace shows a decrease in attenuation followed by another in-

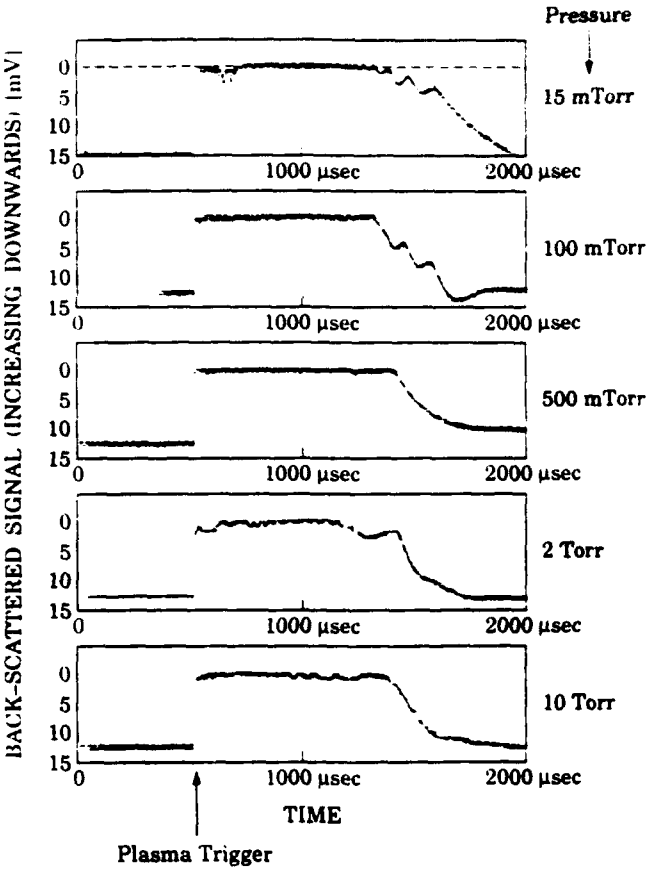

FIG. 6. Time evolution of backscattered signal at different values of background pressure; frequency is 10 GHz, and charging potential is 8.5 kV.

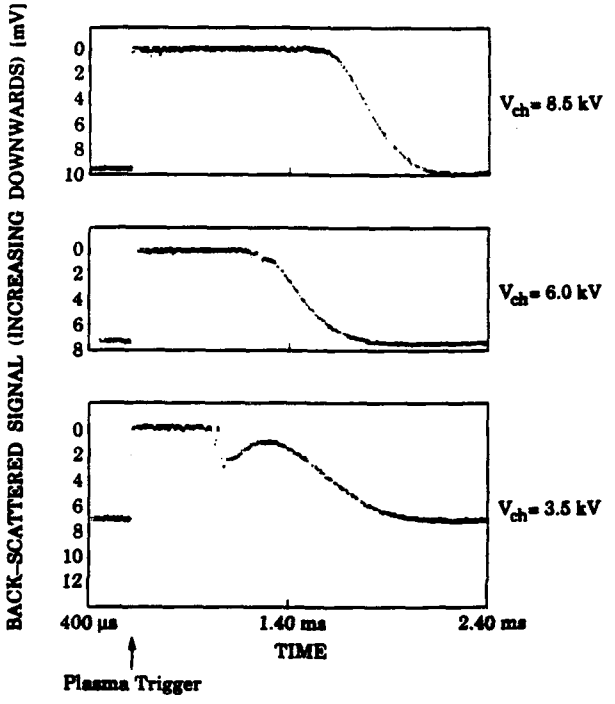

FIG. 7. Backscattered signal level as a function of time, at different values of charging potential V_{ch}; frequency is 10 GHz, pressure is 12 mTorr.

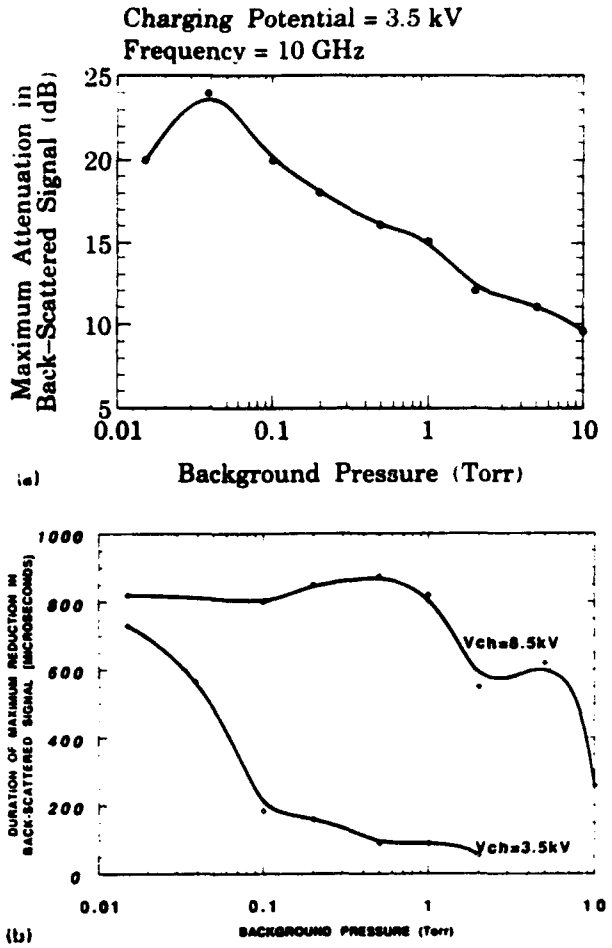

FIG. 8. (a) Variation of maximum attenuation in backscattered signal as a function of background pressure for a low value of charging potential (viz. 3.5 kV); frequency is 10 GHz. (b) Duration of maximum reduction in backscattered signal as a function of background pressure for charging potentials of 3.5 and 8.5 kV; frequency is 10 GHz.

crease. At higher charging potentials these two regimes appear to merge. It has also been observed that, when the charging potential is low, the maximum attenuation in each shot decreases with increase in pressure, as seen in Fig. 8(a) for the case of 3.5 kV. However, for 8.5 kV the variation of maximum attenuation with pressure could not be determined, because the detection system accuracy was limited in attenuation measurements to 30 dB or less. Figure 8(b) shows the duration of the maximum reduction in backscattered signal as a function of background pressure. It is seen that it falls noticeably for pressure above 0.1 Torr, for the case of 3.5 kV charging potential. However, for 8.5 kV charging potential it remains nearly constant up to 1 Torr and falls rapidly above 5 Torr.

The time evolution of the backscattered signal as a function of the incident microwave power level is shown in Fig. 9. The three traces represent a variation of 7:1 in the level of microwave power backscattered from the flash plate in the absence of the plasma. The sensitivity of the scale was adjusted to accommodate the received signal level. The bridge circuit was not fully balanced in this case, so that the traces do show the various phases of evolution of the plasma. The traces are not identical. However, over

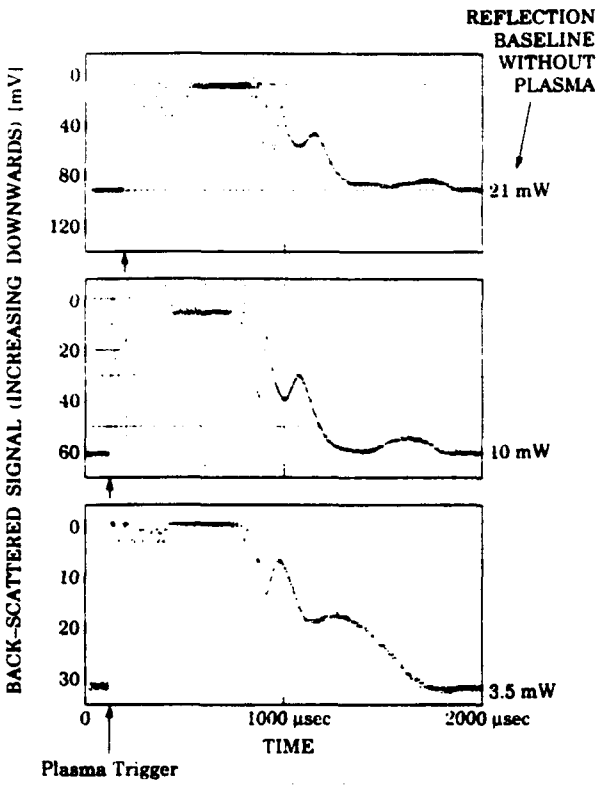

FIG. 9. Effect of variation of incident power level on time evolution of backscattered signal; frequency is 10 GHz, pressure is 24 mTorr.

this power range the general nature of the behavior does not change significantly.

IV. DEPENDENCE OF AXIAL TRANSMISSION ON CHARGING POTENTIAL

In this set of experiments the microwave power level reaching the flash plate was sampled by an open-ended waveguide inserted into the flash plate on axis (as shown in Fig. 1). The time evolution of the received signal at charging potentials of 8.5, 6.0, and 3.5 kV is shown in Fig. 10. The period of high attenuation is followed by an increase in the signal, which in turn is followed by another period of increased attenuation. This effect is more prominent at the lowest charging potential of 3.5 kV. It is also reminiscent of a similar effect in the case of backscattered signal. The duration of the first period of high attenuation as a function of the charging potential is shown in Fig. 11. The variation is seen to be an almost linearly increasing function of charging potential. This can be attributed to the higher plasma density achieved with the larger charging potential, which then takes a longer time to deplete below the critical value at every location.

V. TIME EVOLUTION OF THE SIDESCATTERED SIGNAL

In studying the physical phenomena responsible for the reduction in the backscattered signal, it is also of importance to observe the nature of the sidescattered signal. This was done by detecting the signal picked up by a horn

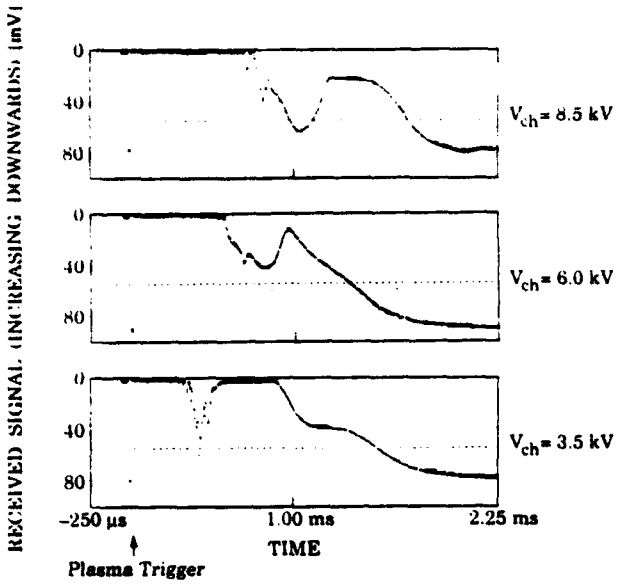

FIG. 10. Time evolution of axial transmission at different values of charging potential V_{ch}; frequency is 10 GHz, pressure is 15 mTorr. Microwaves turned on only briefly before plasma trigger.

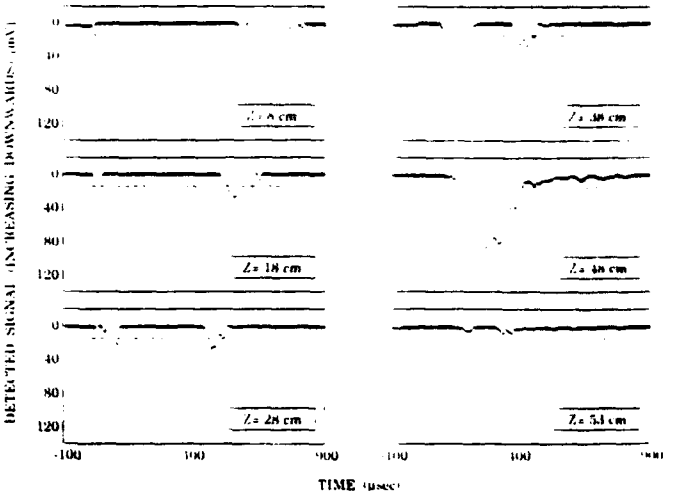

FIG. 12. Time evolution of sidescattered signal at various distances z from flash plate. Both sending and receiving horns have polarization of E field in the x direction (i.e., vertical). Frequency is 10 GHz, pressure is 15 mTorr, charging potential is 8.5 kV, and incident signal amplified by traveling-wave tube amplifier.

which pointed in the radial direction and which could be set at various distances from the flash plate in the axial direction (Fig. 1). Several orientations of the launching and receiving horns were studied. The orientation studied most extensively was one in which the E vectors of the two horns were aligned parallel to each other, which was referred to as the x direction. In another combination, the E vector of the receiving horn was oriented in the z direction. Finally, the launching horn was turned by 90° (its E vector now being in the y direction), which had the same effect as if the receiving horn and its supporting structure had been turned around in azimuth by 90°.

The sidescattered signal at various distances z from the flash plate is shown in Fig. 12 for the orientation of x and x for the horns. It is observed that the scattered signal consists of two groups of pulses. These are well separated in time at small values of z and tend to coalesce at larger values; they merge near $z=48$ cm. Beyond this distance the amplitude drops dramatically. As discussed in more detail later, the broad nature of this phenomenon is attributed to the fact that the sidescattering takes place mainly during those time periods when a layer of critical density transits across the given axial location of the receiving horn.

In a further study of possible nonlinear effects, the sidescattered power for the above orientations of horns was observed at a frequency of 13.774 GHz, while varying the incident power level over a range of 30 dB. Figure 13 shows the relationship of the two on a log-log scale. It is seen that the curve is nearly a straight line, with a slope of 1.046. These observations point to the fact that the incident and scattered power levels are linearly related over a 1000:1 power range.

Figures 14 and 15 show the sidescattered signal with its E vector in the z direction, for the cases where the sending horn had its E vector in the x and y directions, respectively. The feature of the two groups of pulses that

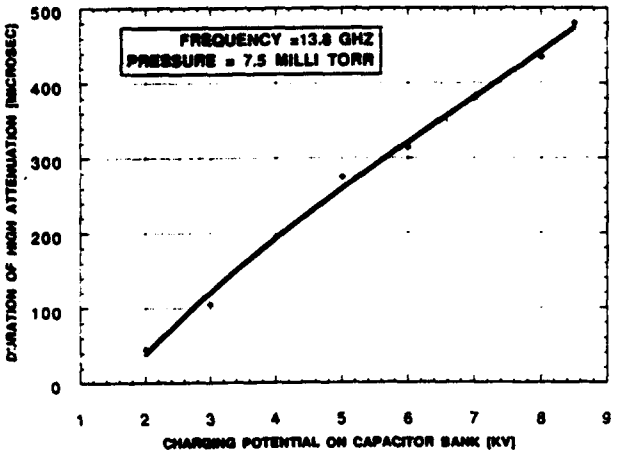

FIG. 11. Duration of period of high attenuation in axial transmission at different values of charging potential V_{ch}.

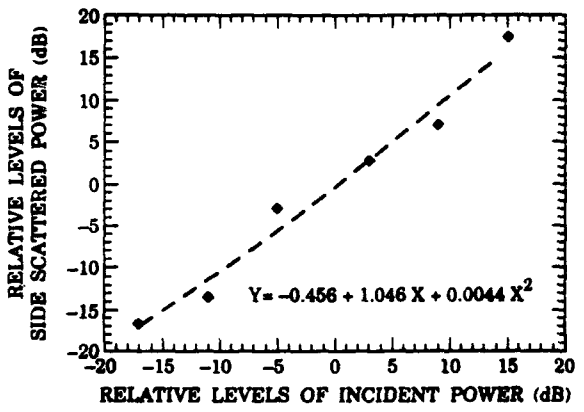

FIG. 13. Sidescattered power Y as a function of incident power level X.

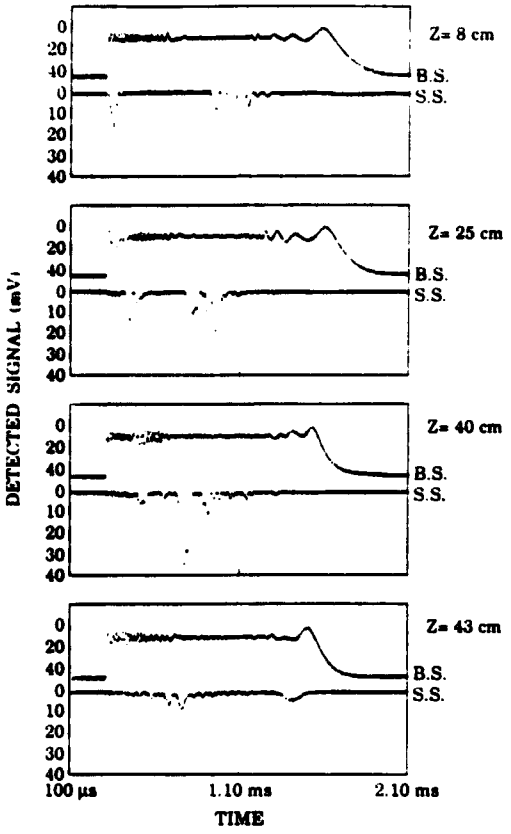

FIG. 14. Time evolution of backscattered signals (upper traces) and sidescattered signals (lower traces), at different distances z from flash plate; polarization of incident signal in x direction and that of scattered signal in z direction. Frequency is 10 GHz, charging potential is 8.5 kV, and pressure is 72 mTorr.

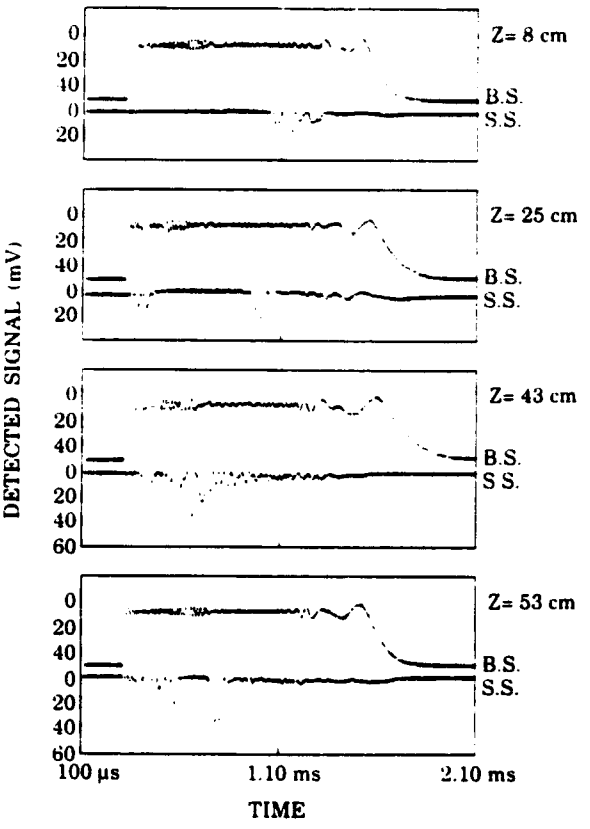

FIG. 15. Time evolution of backscattered signals (upper traces) and sidescattered signals (lower traces) at different locations z; polarization of incident signal in y direction and of scattered signal in z direction. Frequency is 10 GHz, charging potential is 8.5 kV, pressure is 72 mTorr, and reflection baseline (flash plate without plasma) is 7.5 W.

their separation diminishes with z is common among these figures and Fig. 12. The power levels, however, are significantly lower, when the setting of attenuators is taken into account. In a comparison of the peak power levels made at 13.77 GHz for scattering in the x-x orientation versus the x-z orientation, the former was higher by a factor of ≈ 10 dB in the general vicinity of the flash plate. The ratio decreased at greater distance from the flash plate.

Also included in Figs. 12, 14, and 15 are simultaneous traces of the backscattered signal, (denoted by B.S. in the margin of the graphs, while the sidescattered signal is denoted by S.S.). Here the bridge was not fully balanced, so that the backscattered signal also includes phase-shift information.

VI. TIME EVOLUTION OF TRANSVERSE TRANSMISSION

Measurement of the transverse transmission of microwaves across the plasma at various locations and time periods provides a means of studying the time history of the regions of supercritical density in the plasma. These observations were taken by using a radially located horn as the sending horn with another one located opposite to it for receiving the signal (see Fig. 1). The axial location of the two horns could be varied. When the transmission is almost completely cut off, a region of supercritical density can be assumed between the horns.

Figure 16 shows the time evolution of transverse transmission at various locations for a charging potential of 3.5 kV, background pressure of 13 mTorr, and frequency of 10 GHz. At each location three observations of successive plasma shots were superimposed, so as to give an indication of shot-to-shot variations. The diagram also shows the wave form of a current pulse sent through the plasma guns, for comparison of duration. The general nature of the traces shows that near the flash plate the transverse transmission is cut off almost in synchronism with the rise of the discharge current. Transmission is blocked for nearly 300 μs which is nearly an order of magnitude longer than the full width at half-maximum (FWHM) duration of the current discharge (even for this relatively low value of charging potential). At greater distances from the flash plate the duration of the cutoff in the transverse transmission is reduced. Furthermore, there is an intermediate period of reduced transmission whose duration increases with distance z. After the period of complete transmission cutoff, the transmission slowly increases.

Figures 17(a) and 17(b) show the time evolution of transverse transmission for three different charging potentials for a background pressure of 13 and 45 mTorr, respectively. The duration of complete transmission cutoff

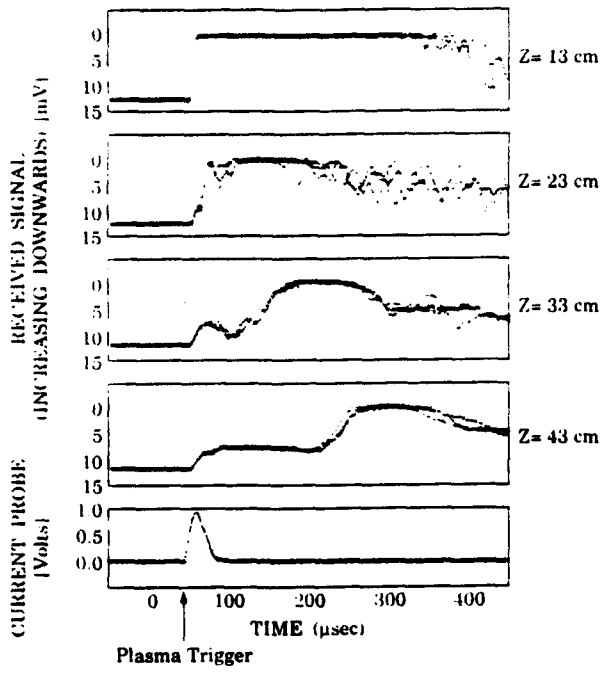

FIG. 16. Time evolution of transverse transmission at various distances z from the flash plate; frequency is 10 GHz, pressure is 13 mTorr, and charging potential is 3.5 kV. Three shots superimposed for each value of z.

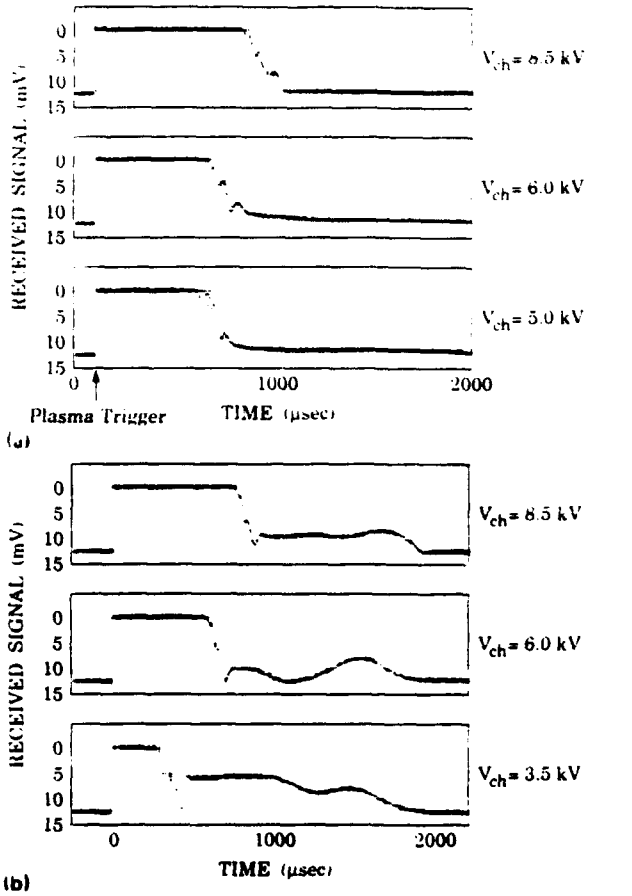

FIG. 17. (a) Time evolution of transverse transmission near flash plate (z=8 cm), for different charging potentials V_{ch}; frequency is 10 GHz, pressure is 13 mTorr. (b) Time evolution of transverse transmission near flash plate (z=8 cm), for different charging potentials V_{ch}; frequency is 10 GHz, pressure is 45 mTorr.

diminishes as the charging potential is reduced. This cutoff period is followed by a period of rapid fluctuations. The received signal rises to almost the full value that existed prior to firing the plasma guns for the case of 13 mTorr pressure. However, for 45 mTorr pressure the signal falls again and reaches a plateau followed by some further undulations, until the original level is restored.

VII. THE CRITICAL DENSITY BOUNDARY AND ITS CORRELATION WITH SIDESCATTERED SIGNALS

Based on the observations made of transverse transmission, plots have been made of the position of the critical density plasma layer as a function of time. Two such curves for the case of charging potentials 8.5 and 3.5 kV are shown in Fig. 18. As may be expected, the boundary for the latter lies inside the former, the duration of the supercritical boundary being shorter in the latter case. Another noteworthy feature is the plumelike shape appearing at large values of z.

Measurements of the position of the peak sidescattered signal (horns in the orientations x and x) as a function of time have also been made, and are shown along with the critical density boundary in Figs. 19(a) and 19(b) for the cases of charging potential 8.5 and 6 kV, respectively. As can be readily seen, the sidescattered signal appears to originate at or near the critical density layer.

An experiment to test the correlation of the sidescattered microwaves with the position of the critical density layer was also conducted at 13.77 GHz. Results are plotted in Fig. 20. For these measurements the charging potential was 8.5 kV, and the orientation of the horns corresponded to x-x polarization. It is seen that the duration of supercritical plasma density is less than for the 10 GHz studies. This is as expected since the critical plasma density is

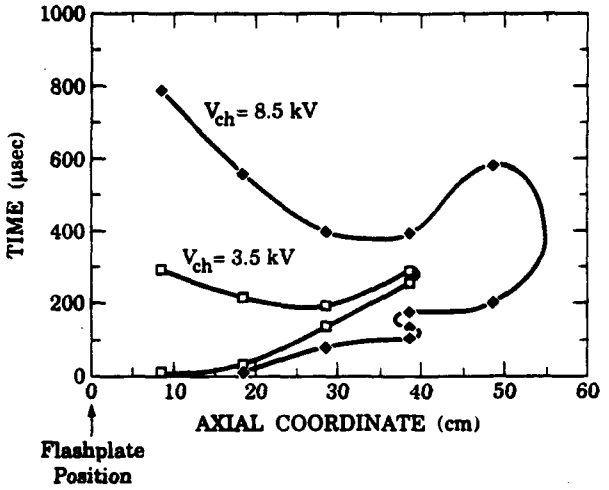

FIG. 18. Time evolution of critical density boundary as a function of location for charging potentials of 8.5 and 3.5 kV; frequency is 10 GHz, background pressure is 45 mTorr, and microwave power ≈30 mW.

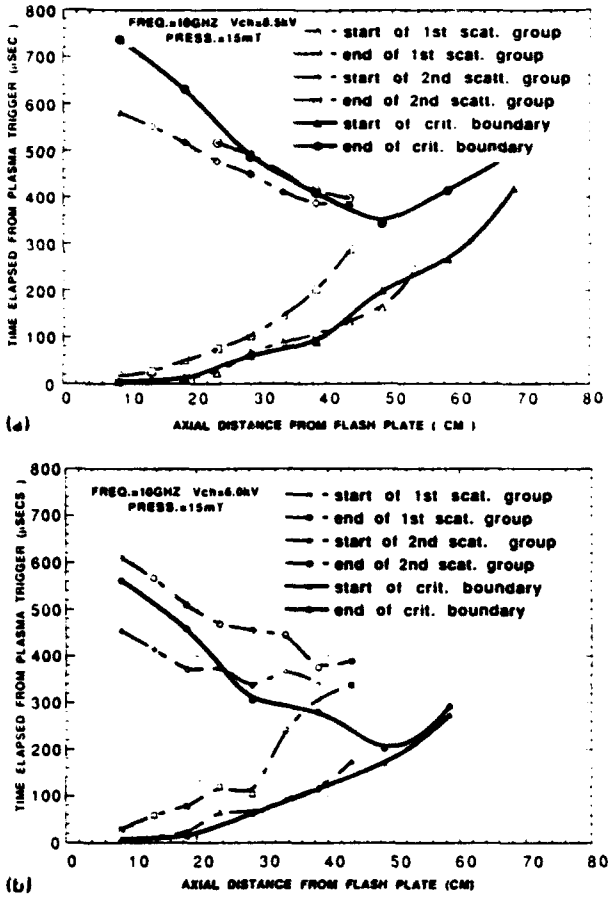

FIG. 19. (a) Correlation of sidescattered signal with critical density boundary; frequency is 10 GHz, pressure is 15 mTorr, incident microwave power level is 19 W, and charging potential is 8.5 kV. (b) Correlation of sidescattered signal with critical density boundary; frequency is 10 GHz, pressure is 15 mTorr, incident microwave power level is 19 W, and charging potential is 6 kV.

higher in this case. Once again, the sidescattered radiation appears to originate at or near the critical density layer.

VIII. AMPLITUDE OF THE SIDESCATTERED SIGNAL AND ITS 3D PLOT

Apart from correlations of the timing and location of the sidescattered radiation with those of the critical density layer, we have studied the amplitude of the scattered radiation. Figure 21 gives the variation of the peak of sidescattered signal with axial distance from the flash plate. The curves in the graph show the peak values averaged over eight shots for the two groups of sidescattered pulses when the plasma density is rising and falling, respectively. An interesting feature is the dip in the vicinity of 30 cm axial distance. It is attributable to attenuation of incident microwaves caused by a short-lived plume of a low-density plasma that proceeds ahead of the main body of the plasma as it propagates away from the flash plate. An indication of shot-to-shot variations can be had from the data points included in the diagram for single shots instead of the averaged eight shots.

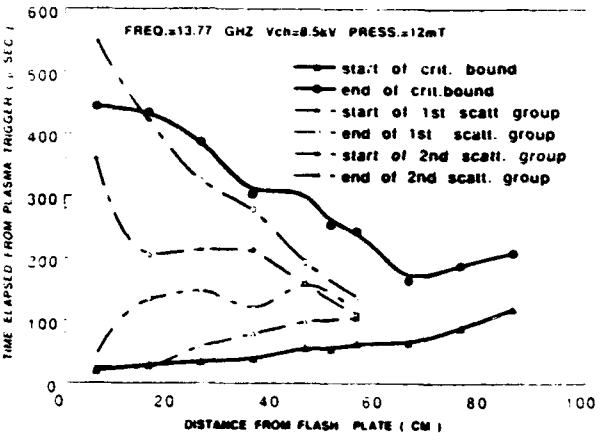

FIG. 20. Correlation of sidescattered signal with critical density boundary; frequency is 13.774 GHz, charging potential is 8.5 kV, and pressure is 12 mTorr.

In order to get an overview of the trends of amplitude variation, we approximated the envelope of each of the two sidescattered signal groups with the least-squares fit of a Gaussian curve. The coordinates interpolated from the Gaussian curves provide arrays of data for the two groups. These were then used to produce three-dimensional plots which give the shape of the envelopes as a function of time and axial distance. In this process the details regarding individual pulses or fluctuations that ride on the envelope are smoothed out. Hence the 3D plot represents general trends and not the fine structure. The 3D plot shows the peaks at 11 discrete values of axial coordinate, which makes them stand out in an isolated fashion. A dotted line has been added to the plot to indicate a continuous ridge, as a closer approximation. Figure 22 shows such a plot. The two ridges are far apart near the flash plate and tend to merge into one ridge farther away. They are reminiscent of the two-dimensional graphs in Figs. 19(a) and 19(b) even though the precise layout in time and axial coordinate is somewhat different.

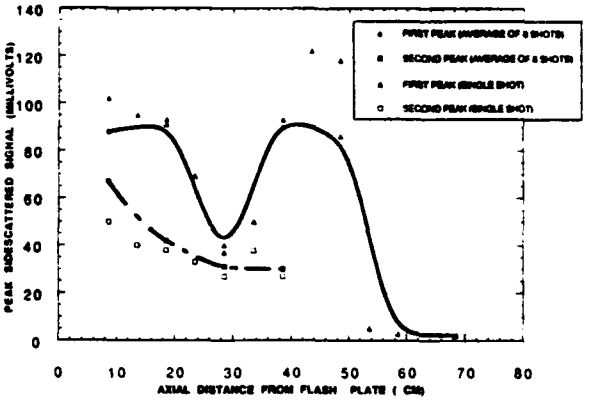

FIG. 21. Time evolution of peak sidescattered signal averaged over eight shots, at various axial distances from flash plate. Some data points from single shots are also shown for comparison.

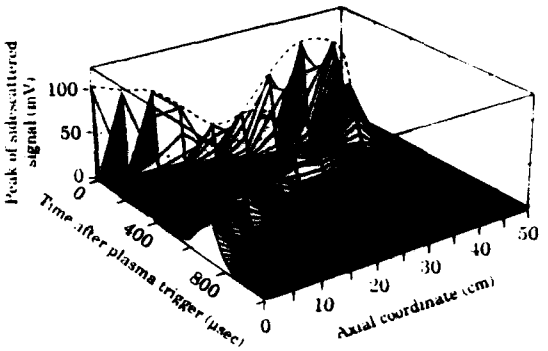

FIG. 22. Three-dimensional plot of the envelope of sidescattered radiation with respect to time and axial distance coordinates. The pulses and fluctuations in the scattered signal are smoothed by a Gaussian approximation of the envelope of the sidescatter signal.

IX. ESTIMATION OF PERCENTAGE OF SIDESCATTERED SIGNAL

In order to estimate the fraction of the incident power that is sidescattered, it is necessary to integrate the measured power density over the entire circumference of the plasma tube as well as over an axial length greater than that of a horn at a single position. In addition, contributions can also come from different polarizations. The orientations of the transmitting horn and the horn that receives the sidescattered signal can be adjusted in four different combinations. They represent the two orientations of the incident E field, namely along x and y axes in combination with the orientations of the received E field, namely along x and z axes, according to the direction of the three axes shown in Fig. 1. Rotation of the receiving horn provides data on the two possible planes of polarization of the scattered signals. Rotation of the plane of polarization of the incident microwaves provides information on the variation of the scattered radiation with polar angle. This last variation provides two values for the scattered signal equivalent to putting the receiving horn at azimuthal angles, $\phi=0°$ and $\phi=90°$. Furthermore, it is necessary to estimate the values obtained for other azimuthal positions. Making use of system symmetries and because diffusion and recombination in plasma can be considered as smoothly varying processes, we assume that the variation of scattered power with ϕ goes as

$$p(\phi)=c_1+c_2\sin^2\phi,$$

where $c_1=P_{\min}$, $c_2=(P_{\max}-P_{\min})$, and $P_{\max}$ and $P_{\min}$ are the measured scattered power for the two azimuthal positions. It was observed that $P_{\min}$ was $\approx 0.65P_{\max}$ near the flash plate, while the ratio of $P_{\min}$ to $P_{\max}$ became nearer to unity near the opposite end of the tube. This could be attributed to the homogenizing effect of stray reflections within the tube.

The following simplifying assumptions were made regarding the receiving horn: (a) the power density of radiation is uniform across the aperture of the horn; (b) the effective area of the horn for purposes of determination of directivity is $(8/\pi^2)AB$, where A is the length and B the width of the mouth of the horn[11]; (c) most of the power enters within the main lobe of the radiation pattern of the horn.

The power received over a strip around the plasma tube whose length is the same as the dimension of the horn that is parallel to the axis is obtained by integrating $p(\phi)$ over the azimuthal range. In the case where the horn is oriented to receive E_x,

$$p_{\text{strip}}=(2\pi r/B)(c_1+0.5c_2),$$

where r is the radius at which the receiving horn is located. The denominator is replaced by A when the receiving horn is oriented to receive E_z. A summation of p_{strip} for strips down the length of the tube provides an estimate of the total scattered power flux at a given instant of time. The process can be repeated at numerous other instants of time and the scattered energy over a given interval of time can thus be evaluated. This result was compared initially with the energy reflected when no plasma was present.

A time interval of 80 μs was chosen for the integration of the sidescattered power producing the energy estimate. In this period practically all the scattered energy is in the vicinity of the flash plate. For the case where E_z is the received polarization, this time interval is covered by three axial positions of the receiving horn at 4.5, 12.5, and 21.0 cm from the flash plate. At each position eight shots of the pulsed plasma were used to determine an average so as to minimize the effects of shot-to-shot jitter. The E field of the incident signal was in the y direction. The ratio of the measured scattered energy to the energy reflected without the presence of plasma was evaluated as described earlier, and is calculated to be 5%.

In the case of E_x polarization for the scattered signal, the receiving horn has its large dimension A in the axial direction. Thus nearly the same axial length is covered in two positions of the horn. Fewer shots were taken in this case. The contribution of scattering is of the same order. This indicates that the ratio of the scattered energy to the reflected energy without plasma is about 10% including both polarizations, E_z and E_x, of the scattered signal. It is estimated that with no plasma the reflected energy received at the transmitting horn is about 10% lower than energy incident on the flash plate. The ratio of scattered energy to the energy incident on the flash plate is correspondingly reduced to an estimated value of 9% from the above measurements.

Using the same basic techniques without integration with respect to time, we evaluated the ratio of the peak value of instantaneous scattered power to that of reflected power without plasma. These peak ratios are shown in Table I, for various parameters regarding charging potential, polarization of incident and scattered waves, and background pressure. A trend that is noticeable is that the ratio of peak scattered power to incident power increases as the pressure of the background gas is increased. The instantaneous peak power levels for different parameters and polarizations cannot be added directly as the exact timing of the peaks may not be the same. These figures are presented here so as to provide an estimate of percentages

TABLE I. Ratio of peak scattered power to incident microwave power, for different values of charging potential, polarization, and pressure of background gas.

V_{charge} (kV)	Polarization		Pressure of background gas (mTorr)	Ratio of peak scattered power/ incident power
	Incident	Scattered		
8.5	E_ν	E_z	75	17%
8.5	E_τ	E_z	75	15%
8.5	E_τ	E_τ	52	13%
6.0	E_ν	E_z	72	22%
6.0	E_τ	E_τ	56	13%
6.0	E_τ	E_τ	15	10%
3.5	E_τ	E_τ	56	10%
3.5	E_τ	E_τ	15	5%

even at the peak levels of scattered signal. Since this scattered signal accounts at best for no more than about one-fourth of the incident signal, it is clear that other mechanisms are responsible for the bulk of the reduction in the backscattered signal.

X. ESTIMATION OF REDUCTION IN BACKSCATTER FROM COLLISIONAL EFFECTS IN A TRANSVERSELY HOMOGENEOUS PLASMA

Collisional effects would play a minimal role when the background pressure is low, as in our high-power experiments,[9] where it was 0.1 mTorr. However, the same cannot be said for higher pressures, as was the case in the present experiments. A study of the reduction in backscatter due to collisional effects was made for the parameter range of interest here. The approached used is that employed by Vidmar in Ref. 1, and briefly outlined here. The plasma density is assumed to be homogeneous in the transverse direction and to have an Epstein profile in the axial direction, given by the relation

$$n = n_0/[1+\exp(-z/\sigma)],$$

where σ represents the rate of variation of plasma density n, which goes from 0 to n_0 as z goes from $-\infty$ to ∞. Microwaves propagating up the density gradient get partially reflected. The component that is partially transmitted proceeds toward the conducting plate and gets reflected. The absorption is evaluated by integrating the imaginary part of the propagation constant in the collisional plasma over the forward as well as backward path. This returning signal is added to that reflected from the plasma profile. Subject to the approximations made in modeling the plasma, the approach gives the estimated total reduction in backscatter caused by the presence of this plasma. The values are a function of the gradient scale factor of the density profile, the momentum-transfer collision frequency, the angle of incidence, and the relative values of the frequency of incident microwaves and the maximum plasma frequency. Using the above approach and assuming a gradient scale factor of 10 cm, a maximum plasma frequency of 10 GHz, and normal incidence of microwaves of 10 GHz frequency, the peak reduction in backscatter varies from 2 to 25 dB as the momentum-transfer collision frequency varies from 2×10^7 to 2×10^8 s^{-1}. An increase in the angle of incidence makes for a reduction in the peak attenuation occurring at resonance between the two frequencies.

The momentum-transfer collision frequency is a function of the gas composition, the pressure, and the electron temperature. This last had been earlier estimated[9] to be ≈ 2 eV, based on Langmuir probe measurements. Taking the case of dry air and a typical pressure of 15 and 75 mTorr in the low-power experiments, and using curves in Fig. 7 of Ref. 12, the momentum-transfer collision frequency is estimated as 5×10^6 and 2.5×10^7 s^{-1}, respectively. This indicates that based on this model the contributions to reduction in backscatter due to collisional effects would be rather small for parameters relevant to these experiments.

In fact, in the experiments an increase of the background pressure produced a decrease in the maximum attenuation in the case of 3.5 kV as charging potential (Fig. 8), but did not alter it significantly from the maximum observable attenuation for the case of 8.5 kV charging potential. The greater sensitivity of the observation in the former case gives a clue as to the nature of the underlying physical phenomena. With increases in background pressure the collision frequency between the electrons and neutrals would tend to increase. As discussed above, an increase of the collision frequency would by itself tend to increase the maximum attenuation. Consequently, it is clear that additional mechanisms must be responsible for the attenuation besides collisions between electrons and neutrals.

XI. SOME FEATURES OF THE PHYSICAL PHENOMENA UNDERLYING THE GENERATION OF THE PLASMA

The four plasma guns are discrete sources of plasma generation whose lateral dimensions are small ($\approx$0.5 cm) compared with the tube diameter ($\approx$30 cm). The flow of discharge current through the inner conductor generates a magnetic field that surrounds the conductor. Thus the charged particles in the arc would have axial Lorentz forces exerted on them by the magnetic field.[13] These are seen to be directed away from the opening in the coaxial conductors that generate the arc. Because of their lighter mass, the electrons would achieve higher velocities than ions. They would thus streak out of the ports of the plasma guns, causing ionization by collision with molecules of the residual gas in their path. The plasma so generated is likely to be inhomogeneous in the transverse direction. This means that the layer of critical density would not be a plane surface. The curvature and ripples in it would cause the local incident angle to be nonzero, even when the overall geometry of the experiment implies normal incidence. This in turn influences absorption as well as sidescatter.

The observations on the time and location of the critical density layer (determined from transverse transmission data) (Figs. 18–20) indicate that a plume of the plasma proceeds rapidly away from the flash plate and

begins to decay. It is followed by another component of the plasma which moves and decays more slowly than the plume. The charged particles causing the plume could thus be the above-mentioned streams of fast electrons shot out from the plasma guns by Lorentz forces acting on the discharge current. In its path the plume would generate ionization by collision, and create less-energetic electrons and ions which constitute the more slowly moving and slowly decaying component of the plasma.

The data on transverse transmission taken at a low value of charging potential (3.5 kV) lend further support to the above viewpoint. It is seen from the trace for $z=43$ cm in Fig. 16, that there is a plateau in the reduction of received signal starting just after the end of the discharge current and lasting for about 100 μm. In this period the transmission is not fully blocked, but is attenuated. It is followed by a period in which the attenuation rises to near total blockage. In other words, at somewhat distant points from the flash plates there exists a precursor to the main body of the plasma. It blocks the transverse transmission only partially presumably because of subcritical density, or incomplete filling of the plasma tube in the radial direction at that distance.

The timing of the observed sidescattered microwave signals correlates closely with the transitions of the critical density layer past the receiving horns (Figs. 19 and 20). This shows that the sidescattered signal originates at or near the layer of critical density.

XII. RESONANCE ABSORPTION IN A TRANSVERSELY INHOMOGENEOUS PLASMA

Considering that the plasma is generated by four plasma guns, it is likely that the layer of critical density will have ripples and turbulence as discussed above. Recombination of plasma at the walls would also tend to give radial variations of plasma density, resulting in a curved geometry for the layer of critical density. Accordingly, the angle of incidence of microwaves on the layer of critical density would be nonzero at most places, unlike what could be anticipated from a simple model of the experiment. An additional source of instability in the plasma resulting in transverse inhomogeneity can arise from a non-Maxwellian distribution of energy of electrons. The resulting "free energy" can be transferred to fluctuating fields.[14]

It is relevant to examine the phenomenon of "resonance absorption" occurring when electromagnetic radiation propagates up the density gradient in a plasma at a finite incident angle with respect to a layer of critical density. When θ is nonzero, an electromagnetic wave, which has its electric vector lying in the plane of incidence (p polarization), has a finite component of E field parallel to the density gradient. This results in electron oscillations which build up resonantly near the critical density, and cause a density fluctuation. This appears as electron plasma waves which contribute to enhanced scattering[15] as well as resonance absorption.[16,17] It may also be noted that this effect has a broad maximum at a value of θ lying between 0° and 90°. It is small near $\theta=0$ as the E-field component parallel to the gradient tends to vanish. It is also small at values of θ approaching 90° as the electromagnetic wave gets reflected at a layer well ahead of the critical density; so that the evanescent E field reaching the resonance layer is very small. The peak resonance absorption is of the order of 0.5,[18] for the optimum incident angle for a laterally homogeneous layer of critical density.

The effect of ripples on the layer of critical density has been studied by Rowland using numerical as well as analytical techniques.[19] The ripples enhance the absorption. A parameter $k_f L/k_t a$ has been defined in which L is the density gradient scale factor, k_t is the propagation factor for the ripples on the layer of critical density, and a is the amplitude of the same. In a simplified model the absorption scales as $\exp(-k_f L/k_t a)$. Simulations show cases of up to 90% absorption of incident energy.

As a consequence of the preceding analyses, it is believed that a major part in the reduction of backscatter is caused by the lateral inhomogeneity in the plasma and by the process of resonance absorption. Sidescatter and collisional absorption play lesser roles. The relative values would be dependent on the array of input parameters. The absorption can thus be explained without invoking nonlinearities caused by the power level of incident microwaves. This agrees with experimental observations.

XIII. CONCLUSIONS

Backscatter, sidescatter, transverse transmission, and axial transmission of low-power microwaves interacting with a pulsed plasma have been studied experimentally over a range of parameters. Measurements of the time evolution of the position of the critical density layer indicate that a plume propagates rapidly away from the flash plate and is followed by a more slowly moving plasma front of higher density. This plume decays more rapidly than the main body of the plasma. A possible cause of the observed phenomena is the presence of more than one plasma species emanating from the plasma guns.

A reduction in backscatter was obtainable down to the limits of our observational accuracy ($\approx$30 dB attenuation). The timing of the observed sidescattered microwave signals correlates closely with the transitions of the critical density layer past the receiving horns. It is therefore evident that the sidescattered signal originates at or near the critical density layer. The sidescattered signal is linearly dependent upon the incident power over three orders of magnitude.

The processes of resonance absorption and sidescatter at the layer of critical density can account for a large part of the observed reduction in backscattered signal. Attenuation due to collisional effects between electrons and neutrals is not significant at pressures below 10 mTorr, but can play a role at higher pressures.

ACKNOWLEDGMENTS

Discussions with Professor H. Fleischmann, Dr. R. J. Vidmar, Dr. H. L. Rowland, and Dr. W. Main were very

useful. Valuable help was rendered by Jay Pyle in the setting-up phase of the experiment. The work is supported by AFOSR.

[1] R. J. Vidmar, IEEE Trans. Plasma Sci. **PS-18**, 733 (1990).
[2] R. J. Vidmar, in International Conference on Plasma Science, Williamsburg, VA, June 3–5, 1991, p. 86.
[3] D. T. Moriarty, K. D. Vilece, M. Onozuka, R. F. Duraski, C. Yoo, and M. C. Lee, in International Conference on Plasma Science, Williamsburg, VA, June 3–5, 1991, p. 146.
[4] M. Laroussi and J. R. Roth, in International Conference on Plasma Science, Williamsburg, VA, June 3–5, 1991, p. 146.
[5] D. Gregoire and J. Santoru, in International Conference on Plasma Science, Williamsburg, VA, June 3–5, 1991, p. 86.
[6] J. E. Sharer, O. C. Eldridge, S. F. Chang, M. H. Bettenhaussen, and N. T. Lam, in International Conference on Plasma Science, Williamsburg, VA, June 3–5, 1991, p. 87.
[7] A. Y. Ho and S. P. Kuo, in International Conference on Plasma Science, Williamsburg, VA, June 3–5, 1991, p. 89.
[8] W. W. Destler, P. Catravas, J. Rodgers, A. Singh, C. D. Striffler, P. E. Latham, and H. L. Rappaport, in International Conference on Plasma Science, Williamsburg, VA, June 3–5, 1991, p. 147.
[9] W. W. Destler, J. E. Degrange, H. H. Fleischmann, J. Rodgers, and Z. Segalov, J. Appl. Phys. **69**, 6313 (1991).
[10] I. Alexeff, F. Dyer, and M. Rader, in International Conference on Plasma Science, Williamsburg, VA, June 3–5, 1991, p. 86.
[11] S. Ramo, J. R. Whinnery, and T. van Duzer, *Fields and Waves in Communication Electronics* (Wiley, New York, 1984), p. 618.
[12] R. D. Hake, Jr. and A. V. Phelps, Phys. Rev. **158**, 70 (1967).
[13] R. A. Gross and B. Miller, *Methods of Experimental Physics* (Academic, New York, 1970), Vol. 9, Part A, Sec. 5.13.
[14] W. A. Perkins, *Methods of Experimental Physics* (Academic, New York, 1970) Vol. 9, Part A, Sec. 7.3
[15] J. Sheffield, *Plasma Scattering of Electromagnetic Radiation* (Academic, New York, 1975), Chap. 10.
[16] A. V. Gurevich, *Nonlinear Phenomena in the Ionosphere*, translated by J. G. Adashko (Springer, Berlin, 1978), Sec. 6.2.
[17] Z. Sedlacek and B. Roberts, J. Plasma Phys. **41**, 97 (1989).
[18] W. L. Kruer, *The Physics of Laser Plasma Interactions* (Addison-Wesley, Reading, MA, 1988), Sec. 4.2.
[19] H. L. Rowland (unpublished).

Draft Nov. 1, 1993

Spatial and time profiles of a pulsed plasma column, and their correlation with backscatter of microwaves from the plasma

(Authors)
Institute for Plasma Research
University of Maryland, College Park, MD 20742

ABSTRACT

An unmagnetized plasma column is generated by an array of plasma guns at one end of a tube. Its spatial and time profiles have been studied using floating as well as biased Langmuir probes. The data indicate the present of two components in the plasma, one moving and decaying faster than the other. The faster one also has a higher initial electron temperature. The slower one represents the main body of the plasma. The observations have been taken with an axial as well as a radial orientation of the plasma guns. In the latter case the axial drift velocity is slower than in the former case. The effect of varying the presence of background gas in the range 1 mTorr to 200 mTorr has also been studied. It reduces the drift velocities as well as amplitude of the pick up signal. Furthermore in the pressure range above 5 mTorr plasma fluctuations are generated as evidenced by the probe pick-up signal as well as fluctuations in the backscattered signal. The spatial profile inferred from the data indicate a nonuniformity along the radial direction. The profiles along the axial direction are more complex than the Epstein profiles considered earlier. Both of these factors would provide useful inputs into more accurate modeling of the plasma and its effect on backscatter of microwaves.

1 Introduction

Backscatter and absorption of microwaves by a plasma has been the subject of study at the University of Maryland and a number of other laboratories [1-5]. Among it's chief attractions are tunability and wider bandwidth than that obtainable from conventional materials.

At the University of Maryland we have studied the phenomenon using plasma guns embedded in a conducting plate as a source of an unmagnetized pulsed plasma generated inside an acrylic tube at megawatt as well as milliwatt power levels. In both cases reduction in backscatter of the order of 30 dB was observed, the figure in some cases being limited by the accuracy of the measurement technique. This level of reduction in backscatter could not be explained on the basis of simulation in terms of a cold collisional plasma model as described in Ref. 3. Measurements on the power carried away by sidescatter of microwaves could also not account for more than 5% to 20% of the incident power level.

The objective of the present phase of our study was to gain a better understanding of the time-dependent parameters of the plasma, including the spatial profile of plasma density and electron temperature. Furthermore, the influence of the presence of background gas was evaluated. Evidence was sought for the presence of lateral non-uniformities in the plasma, as this can also have a significant effect on the level of backscatter.

The Langmuir probe technique is one that can provide insights into a number of plasma parameters [6]. Its relative simplicity lends itself to extensive exploration of parameter space relating to the experiment, and was used accordingly. A floating probe arrangement was used initially to provide an indication of the general nature of the profiles of plasma density as a function of time and axial locations. Later the Langmuir characteristic was synthesized by varying the bias potential from shot to shot. It was possible to measure the electron temperature and plasma density for a few parameters, by adjusting the experimental conditions for optimum reproducibility from shot to shot.

In order to eliminate the possible effect of ultraviolet radiation originating from the plasma guns and causing photoemission from the probe, a modified configuration of guns was also tried out. In this the guns were mounted radially instead of axially, and their tips

were not in a line of sight with the probe locations.

These data provide used inputs for modelling the plasma and its effect on the incident microwaves. In particular, the axial profiles are seen to be more complex than the Epstein profiles assumed in the earlier simulations. Furthermore, the manner in which they varied with time was different in the two cases of axially or radially mounted plasma guns. There had been an inference from studies of tranverse transmission of microwaves through the plasma columns that the plasma has a component that moves fast and also decays quickly, followed by a slower moving and longer lasting main body of plasma. This conclusion was further supported by the present studies using Langmuir probes.

The experimental set up is described in section 2. The trends in observed data are summarized for the floating probe case in section 3 and for biased probe in section 4. Correlation observed in the time variations of backscatter of microwaves vis-viz. the data from Langmuir probes is discussed in section 5. Conclusions are summarized in section 6.

2 The Experimental Set-up

A schematic diagram of the experimental set up used for measurement of backscatter of microwaves is shown in Fig. 1. The plasma was located in an acrylic tube 1.35 m long and having a diameter of 30 cm. The plasma guns consisted of spark plugs in which the space between the inner and outer conductors was filled with an epoxy containing titanium hydride. There were four of these located symmetrically around the axis. The set up has been described in detail in Ref. 2.

The set up for Langmuir probe measurements for the case of axially mounted plasma guns is shown in the schematic diagram of Fig. 2. The microwave horn and lens located earlier at one end of the tube were replaced by a support for the Langmuir probe located along the axis of the plasma tube. The probe leads were surrounded by a conducting tube that acted as a shield. It could be moved axially through a vacuum seal so as to alter the location of the probe vis-a-viz. the flash plate. The signal was fed to an oscilloscope. The

detection circuit is shown in Fig. 3. The traces on its CRT were photographed for further analysis. In some of the experiments a digital oscilloscope was employed and the traces obtained as hard copy directly.

The traces showed the floating potential of the probe as a function of delay time after the plasma trigger, for the case where the load resistance R_L in Fig. 3 is high, i.e. of the order of 1 MΩ. When the load resistance is low, the value of the 'floating' potential is given by the intersection point between the characteristic curve and the load line. In our case the load was kept generally at 50Ω so as to avoid reflections due to mismatch with the characteristic impedance of the coaxial line.

The measurement of electron current, or of the floating probe potential is also subject to errors due to emission of secondary electrons or photo-electrons. Among other things, it is important to have a clean surface of the probe. In our experiments the probe was cleaned first mechanically and then chemically. This was followed in most cases by a cleaning via ion bombardment for a few minutes before the beginning of each run, consisting of a range of input parameters.

For the case of biased probe measurement, the biasing and detection circuits are shown in Fig. 4. A series of shots were taken at different values of bias on the probe,. The value of pick-up signal for specific time delays was read on the successive traces obtained. This array of data was converted into graphs of $\ell n(I_s - I_p)$ versus V_B, where I_s is the current picked up by the probe at different values of the probe bias, V_b, and I_p is the ion saturation current obtained when V_b has a sufficiently large negative value. In the most general case, the variation of electron current I_e versus bias voltage V_B is as shown in Fig. 5 [6]. At $V_B = V_p$, the plasma potential, the probe picks up the saturation current I_e^* deposited by bulk electrons in the plasma. There is an exponential section of the characteristic curve for a range of V_B immediately below V_p. If an electron beam or an ion beam exists, it shows up as I_b or I_i, respectively. The ion saturation current I_p is shown somewhat exaggerated and has to be subtracted from the current I_s that is picked up so as to get the true electron current.

For non-drifting Maxwellian electrons, the probe current $I_e(V_B)$ is given by the relationship [6]:

$$I_e(V_B) = I_e^* \exp\left[\frac{-e(V_p - V_B)}{T_e}\right] \quad \text{for } V_B \leq V_p, \tag{1a}$$

$$I_e = I_e^* \quad \text{for } V_B > V_p, \tag{1b}$$

$$\text{where} \quad I_e^* = Sn_e e\sqrt{T_e/2\pi me}, \tag{1c}$$

where n_e is the plasma electron density and S is the collecting area of the probe. Thus the electron temperature T_e is given by the slope of the line showing $\ell n(I_S - I_p)$ vs. V_B. Furthermore the electron density can be derived from I_e^* after substituting the area of the probe and the electron temperature in equation (1c).

The Langmuir probe characteristics synthesized from multiple shots are prone to error from shot-to-shot variations. An attempt was made to minimize the effect of such variations by taking multiple shots at the same bias value. In these experiments the characteristic is not a simple one as attributable to a Maxwellian non-drifting electron velocity. As shown in Fig. 5, there are more than one "knee" in the curve. As such it is necessary to identify the correct nomenclature for each segment of the curve. In this it is helpful to compare the different characteristics in a set, so as to see the consistency of nomenclature allocation among themselves.

3 Trends in data observed with floating probes

A trace of pick up signal versus time, for axial location $z = 30$ cm from flash plate, and background pressure of air of the order of 1 mTorr is shown in Fig. 6a. The plasma was generated by a charge of 8 kV on the capacitor in the pulser. The magnitude of the pick-up signal increases downward in the figure.

3.1 Two components of the plasma

It is seen that there is a very rapid increases in the signal right after the plasma trigger. The signal then rises more slowly to a peak and then falls gradually. This entire trace extended

to approximately 850 μs. The quick rise is in consonance with the observations that the reduction in microwave backscatter also starts with very little delay (of the order of one microsecond in Ref. 2). Furthermore, the observation on transverses transmission reported in the same reference pointed towards more than one component in the plasma. One of these proceeds very rapidly away from the flash plate in the axial direction and also dies off relatively quickly. The second one constitutes the main body of the plasma, which moves and decays more slowly. This also is in conformity with the observed delay in reaching the peak, followed by a slow decrease.

3.2 Average velocity of the two components

The arrival of the two components of the plasma becomes better differentiated at larger distances from the flash plate, provided that one of the components has not become too small with the increased distance. An example of such a trace is shown in Fig. 6b, which is for $z = 115$ cm, other conditions being the same as for Fig. 6a. Figure 6c shows the trace for $z = 30$ cm for the case of radial orientation of plasma guns. Here we do not observe a rapid rise immediately after the trigger presumably because the initial transients near the flash plate, and the ultraviolet radiation are shielded from the probe. However, two peaks indicating two components of plasma are evident here also. We can call them the fast and the slow component, respectively.

From such traces it is possible to derive the average velocity of propagation of a peak from the flash plate up to a given distance. One can evaluate this average velocity over a range of distances. The average velocity for the two kinds of peak is shown in Fig. 7 for the axially as well as radially oriented plasma guns. The slow components are seen to be of the same order for short distances near the flash plates, after which they diverge to a ratio of nearly 4:1 in favor of the axial orientation. The fast components for the axial orientation is another nearly 3:1 faster than the slower component.

3.3 Inference of lateral inhomogeneity

These observations can be explained by recalling that axially oriented plasma guns can send the initial plume of a plasma directly into the tube, whereas that is not the case for the radially oriented guns. It is interesting to consider the reason for higher average velocity for larger axial distances, which is counter-intuitive. This is attributable to the fact that the probe is located at the axis while the plasma guns are arranged with their centers at radius 8 cm. Consequently, a cone of directed plasma which moves at a relatively high velocity will raise the plasma density to peak levels more quickly at farther distances than would be the case for the slower lateral diffusion of the plasma plumes towards the axis.

From this it can also be inferred that the plasma density is not a constant across the cross section of the tube. Apart from reduction near the walls due to recombination, there is also a reduction near the axis due to off axis location of the plasma guns.

The average velocity over the distance of $z = 0$ to 45 cm was evaluated for the two components of plasma as a function of the background pressure of air, for the case of axially oriented plasma guns, as shown in Fig. 8. It is noted that the velocities of both the components are diminished in comparable ratios as the pressure is increased. This is understandable because the mean free path of collisions goes down as the background pressure rises.

3.4 Spatial profiles

From a sequence of traces obtained at different distances z from the flash plate, it is possible to synthesize a spatial profile of the pick up signal at specific delay times after the trigger. Such profiles provide useful insights into the physical phenomena, as microwave interaction depends upon the plasma density profile and its gradient at different locations.

A set of profiles for axial plasma guns, at delay times varying from 50 microsecond to 400 microseconds is shown in Fig. 9a. It is seen that up to 300 microseconds, there is increase of signal with increase in z. This is in conformity with the discussion regarding the velocities of a fast and slow component of the plasma. Furthermore, it is noticed that in the initial

phase there is a rise in the signal as the plasma front arrives, followed by a gradual decay as time progresses. This latter phenomenon is further seen in Fig. 9b, which shows the profiles in the time period from 400 μs to 800 μs.

The corresponding profiles for the case of radial plasma guns are shown in Fig. 10 a,b. Here the signal falls in the vicinity of the flash plate also as time progresses into the declining phase of the plasma. With the plasma guns tucked away to one side the flash plate acts more like a sink for the plasma in the late phases, providing a surface for recombination of ions and electrons.

3.5 Amplitude of pick-up signal

The slower component that is the main body of the plasma, provides a major contribution to the pick up signal. The faster component, that is the plume, contributes a signal that rides on the slower counterpart, and is distinguishable as a separate entity only in limited parameter range of axial distance and time.

Figure 11 shows the variation of the maximum of the envelope for the signal from only the slower component, referred to as B-type, as a function of the axial distance z with the background pressure as a parameter. As may be expected, the signal level falls with increasing z. It also goes down with the increase of background pressure of gas. In other words, the plasma guns generate the plasma at the flash plate, and as it proceeds away from it, the plasma density gets diminished, more so when there are neutral gas molecules present. This implies that there is no significant multiplication of ionization and that energies of the primary electrons are likely to be less than the ionization potential of the gas.

Contours of constant value of the pick up signal value with axial distance and time delay as coordinates are shown in Fig. 12a for the case where plasma of background gas was less than 1 mTorr and Fig. 12b for background pressure of 20 mTorr. The presence of a 'plume' is noticeable for short delays and at larger axial distance. The general nature of the contours agrees with those obtained for the boundary of the layer of critical density drawn against the same coordinates for a background pressure of 15 mTorr as shown in Fig. 13 from Ref. 2.

4 Trends observed with biased probe

Biased probe measurements were undertaken so as to provide estimates of the electron temperature, the plasma density and their variations with the time delay and axial location. As discussed in section 2, the characteristics of the Langmuir probe were synthesized from multiple shots which had different bias voltages on the probe. It is to be recalled also that the accuracy of measurement depends critically on shot-to-shot reproducibility of the characteristic. The present observations can lead to general conclusions about the trends.

Figure 14 shows a synthesized characteristic for the case of an axial location of 75 cm from the flash plate and a time delay of 200 μs for a charging potential of 8 kV. The curve shows more than one relatively flat and sloping regions, respectively. This feature has been encountered in numerous other synthesized characteristics. It is indicative of a multi-component plasma with different temperatures and densities. In most cases, two components can be identified.

Shot-to-shot variation can arise from amplitude jitter as well as time jitter. As such, characteristics were synthesized also by tracking the individual peaks of the fast and slow components of the plasma as they arrived at specific locations. Figures 15a and 15b show such characteristics for $z = 50$ cm for the fast and slow components of plasma, respectively. The electron temperature and plasma density for these cases are shown in Table 1. It is seen that the fast moving component of plasma has a higher temperature than the slow moving component. Furthermore, Fig. 15b indicates a two component plasma. They are represented by number shapes in the characteristic, one in the bias range from 5 to 20 V and the other one in the range -10 to 5 V. The lower density componeth appears to be the residue of the initial fast component after a delay of 300 μsecs.

Figure 16 shows the time evolution of the plasma density at $z = 75$ cm, for radially oriented plasma guns with probes charged to 8 kV. For plasma density the general trend is a rise with time followed by a comparatively slower decline. This is consistent with observations using floating drives.

Figure 17 is a trace of pick-up signal versus time obtained for $z = 75$ cm, with an applied

Table 1:

Axial Distance from Flash Plate (cm)	Fast Moving Component of Plasma		Slow Moving Component of Plasma	
	Electron Temperature (eV)	Plasma Density (cm^{-3})	Electron Temperature (eV)	Plasma Density (cm^{-3})
50	6.08	6.04×10^{10}	2.32	1.117×10^{10}
75	4.57	3.11×10^{10}	2.23	7.42×10^{10}

bias of -10 V on the probe. It shows a narrow peak followed by a broader one with a gap in between. This is further confirmation of the phenomenon of an initial fast component of the plasma followed by a slower one. The former has more energetic electrons. The gap between the two humps in the trace is caused by the fact that after the faster component decays, there is a time gap before electrons with sufficient energy to overcome the probe bias arrive in the main body of the plasma.

5 Backscatter of microwaves

A schematic diagram of the set-up for measurement of backscatter of microwaves by the plasma is shown in Fig. 18. Microwave signal was generated at 13.77 GHz and amplified by a travelling wave tube (TWT) amplifier. Initially the flash plate was replaced by a microwave absorber, viz. ecosorb. The E-H tuner was adjusted to give minimum reflection as measured by a network analyzer. The flash plate was then put back on again.

The backscattered signal for axially oriented plasma guns had been studied extensively and reported in Ref. 2. The experiments reported here refer to radially oriented plasma guns. Figure 19 shows two traces obtained with different setting of sensitivity, namely 1

and 5 mV/division, for the case of background pressure = 2mTorr. The traces have gone below the zero line, presumably because the stored charged in the diode does not follow large and rapid changes in the microwave signal amplitude. In any case this implies that the actual value of the attenuation was more than what can be measured by the set-up. For more accurate evaluation, it would be necessary to add a power step up arrangement for a limited time in the duration of the probe as had been done earlier in the case of axial plasma guns [2].

Figure 20 shows traces for a pressure of 2 mTorr and 10 mTorr, respectively. It is seen that at 10 mTorr more ripples appear in the region of maximum attenuation at time delay of 120 microseconds as compared to 2 mTorr. Such oscillation have been observed for residual gas pressure of 5 mTorr to 200 mTorr. These could be attributed to oscillations set up by the fast moving plume when it encounters residual gas above a certain pressure. At 200 mTorr there are more than one sequence of oscillations as seen in Fig. 21a. For comparison, Fig. 21b shows the trace for a floating probe pick up located at 20 cm from the flash plate, with background pressure = 200 mTorr. It is seen that the probe pick up signal also shows a sequence of oscillations in the time period of 0 to 200 microseconds. (It is to be noted that the time scales for the two traces are different, namely 100 μs/div and 50 μs/div, respectively). Furthermore, the microwave absorption is influenced by the entire plasma column, whereas the probe pick-up tracks the time sequence at one location only. However, similarity in the two traces indicates that time fluctuations in the plasma have a major role in giving fluctuations in the backscattered signal. This is as distinct from fluctuations that could be caused by a frequency shifted backscattered signal beating with a fraction of the incident signal if both were to reach the detector. Such a frequency shift can arise from time variation in the plasma density, or from doppler shift due to reflection from a moving front in the plasma, such as the layer at critical density. In other words, the evidence from the probe pick-up oscillations tilts the likely cause in the favor of local oscillations of plasma density itself.

6 Discussion of Results

Experiments with floating as well as biased Langmuir probes have been carried out and their results were compared with data on backscatter of microwaves from a pulsed plasma column generated by plasma guns that are oriented axially or radially at one end of the plasma tube.

Langmuir probe data confirm that plasma which is generated has two components. One of these appears early and proceeds rapidly along the tube, compared to the second one. The first one has a higher temperature and dies off more quickly than the second one. An increase of pressure of the background gas slows down the velocities with which the peaks of pick-up signal propagate down the tube.

As a result of the fact that the plasma guns are located off-axis, the plasma density on the axis is not the maximum in any given axial location. This lack of uniformity in the lateral direction is more pronounced near the flash plate and in the earlier phases of time after plasma trigger.

The axial profiles of pick-signal have been evaluated at various time intervals. For axially oriented guns the profile remains high in the flash plate region as time progresses. However, for radial guns it comes down with time such that the peak occurs further down the axial dimension. These profiles are more complex than an Epstein profile moving axially in time. This would have a direct bearing on modelling of the plasma interaction with microwaves.

A simple model based on a cold collisional plasma and Epstein profile gives an increased attenuation of incident signal due to increased collision frequency as pressure of background gas increases. This was the motivation for studying the phenomena at varying pressure of the background gas. However, the increase of pressure introduces additional phenomena which are disadvantageous, such as ripple in the magnitude of attenuation with time.

Compared to axially oriented plasma guns, radially oriented guns tend to give a plasma that moves more slowly, and has less rapid fluctuations. Accordingly, the attenuation in backscatter is comparatively uniform in time especially when the pressure is low.

In further studies it would be worthwhile to measure more precisely the attenuation attainable with radial plasma guns using a power gating technique to increase the dynamic

range of the measurement. Langmuir probes located off-axis at the radius at which the plasma guns are located can give further confirmation of the extent of lateral non-uniformity of plasma density. The probe may be located at azimuthal angles directly in front of the guns as well as in between them. Framing camera studies can provide overall pictures of the plasma distribution at specific times. These would show the lateral as well as axial profiles of emitted light and their evolution in time.

Acknowledgements

We thank J. Pyle for technical assistance. This work was supported by AFOSR.

References

1. W.W. Destler, J.E. Degrange, H.H. Fleischmann, J. Rodgers, and Z. Segalov, J. Appl. Phys. **69**, 6313 (1991).

2. A. Singh, W.W. Destler, P. Catravas, and J. Rodgers, J. Appl. Phys. **72**, 1707 (1992).

3. R.J. Vidmar, IEEE Trans. Plasma Sci. **PS-18**, 733 (1990).

4. J.E. Scharer, O.C. Eldridge, S.F.R. Chang, Y.S. Zhang, M. H. Bettenhousen, and N.T. Lam, IEEE Trans. Plasma Sci. **PS-21**, 271 (1993).

5. M. Laroussi and J.R. Roth, IEEE Trans. Plasma Sci. **PS-18**, 366 (1993).

6. O. Auciello and D.L. Flamm, Eds., *Plasma Diagnostics*, Vol. I, Chap. 3, N. Hershkowitz, "How Langmuir Probes Work," pp. 114-181, Academic Press.

FIGURE CAPTIONS

Fig. 1. Schematic diagram of experimental set-up for measuring interaction of microwaves with plasma column.

Fig. 2. Schematic diagram of set-up for 'floating' Langmuir probe measurements.

Fig. 3. Detection circuit for floating probe.

Fig. 4. Detection circuit for biased probe.

Fig. 5. General case of a probe characteristic.

Fig. 6. Floating probe pick up signal as a function of time, for background pressure = 1 mTorr, V_{charge} = 8 kV; (a) z = 30 cm from axial guns, (b) z = 115 cm from axial guns, (c) z = 30 cm from radial guns.

Fig. 7. Average velocity of propagation of peaks in the fast and slow components of plasma for axial and radial guns, as functions of the range of distance covered.

Fig. 8. Average velocity of propagation of peaks of fast and slow components of plasma from $z = 0$ to z= 45 cm as functions of pressure of background gas for axial plasma guns.

Fig. 9. Profiles of probe pick-up voltage for the case of axial plasma guns for pressure $\approx$ 1 mTorr for time delay parameters (a) from 50 μs to 400 μs, and (b) from 400 μs to 800 μs.

Fig. 10. Profiles of probe pick up voltage for radial plasma guns for pressure $\approx$ 1 mTorr for time delay parameters (a) from 50 μs to 400 μs, and (b) from 400 μs to 700 μs.

Fig. 11. Maximum in the envelope of slower component of plasma as a function of axial distance of probe , with background pressure as parameter.

Fig. 12. Contours of constant value of pick-up signal as a function of axial distance of probe from flash plate, and the time delay; a) pressure of background gas $\approx$ 1 mTorr, b) pressure of background gas = 20 mTorr.

Fig. 13. Boundary of the critical density layer as a function of axial distance from flash plate and the time delay; pressure $\approx$ 15 mTorr.

Fig. 14. Langmuir probe characteristic synthesized from shots with different bias potentials on the probe, for $z = 75$ cm, time delay = 200 μs, and pressure $\approx$ 1 mTorr.

Fig. 15. Synthesized Langmuir probe characteristic while tracking the two main peaks on the trace, for $z = 50$ cm, pressure $\approx$ 1 mTorr, (a) for first peak corresponding to the fast component of the plasma, (b) for second peak corresponding to the slower component of the plasma.

Fig. 16. Time evolution of plasma density as obtained from bias probe measurements, for $z =$ 75 cm, $p \approx$ 1 mTorr.

Fig. 17. Trace of pick up signal versus time for applied bias of -10 V, $z = 75$ cm, $p \approx 1$ mTorr, showing two peaks.

Fig. 18. Schematic diagram of modified microwave circuit for measurement of backscatter of microwaves.

Fig. 19. Time variation of backscattered signal, with traces at two levels of oscilloscope sensitivity, for pressure $\approx$ 2 mTorr, frequency = 13.77 GHz, $V_{charge} = 8$ kV.

Fig. 20. Time variations of backscattered signal for same parameters as Fig. 19 but with pressure = 10 mTorr; (a) time base 200 μs/div, (b) time base 10 μs/div.

Fig. 21. Time variations of a) backscattered signal, and b) pick up from floating probe for pressure = 200 mTorr.

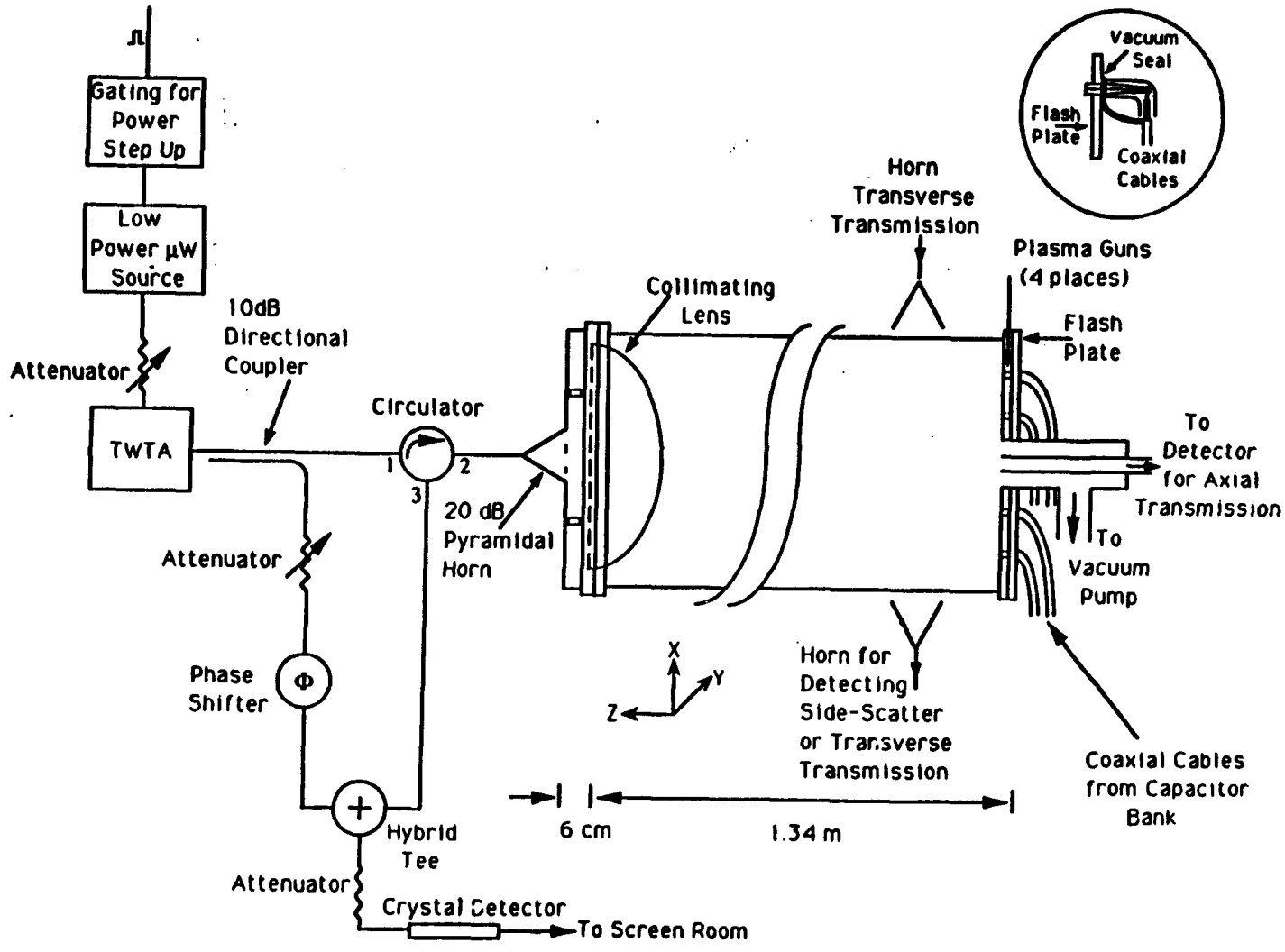

Fig. 1. Schematic diagram of the experimental set up.

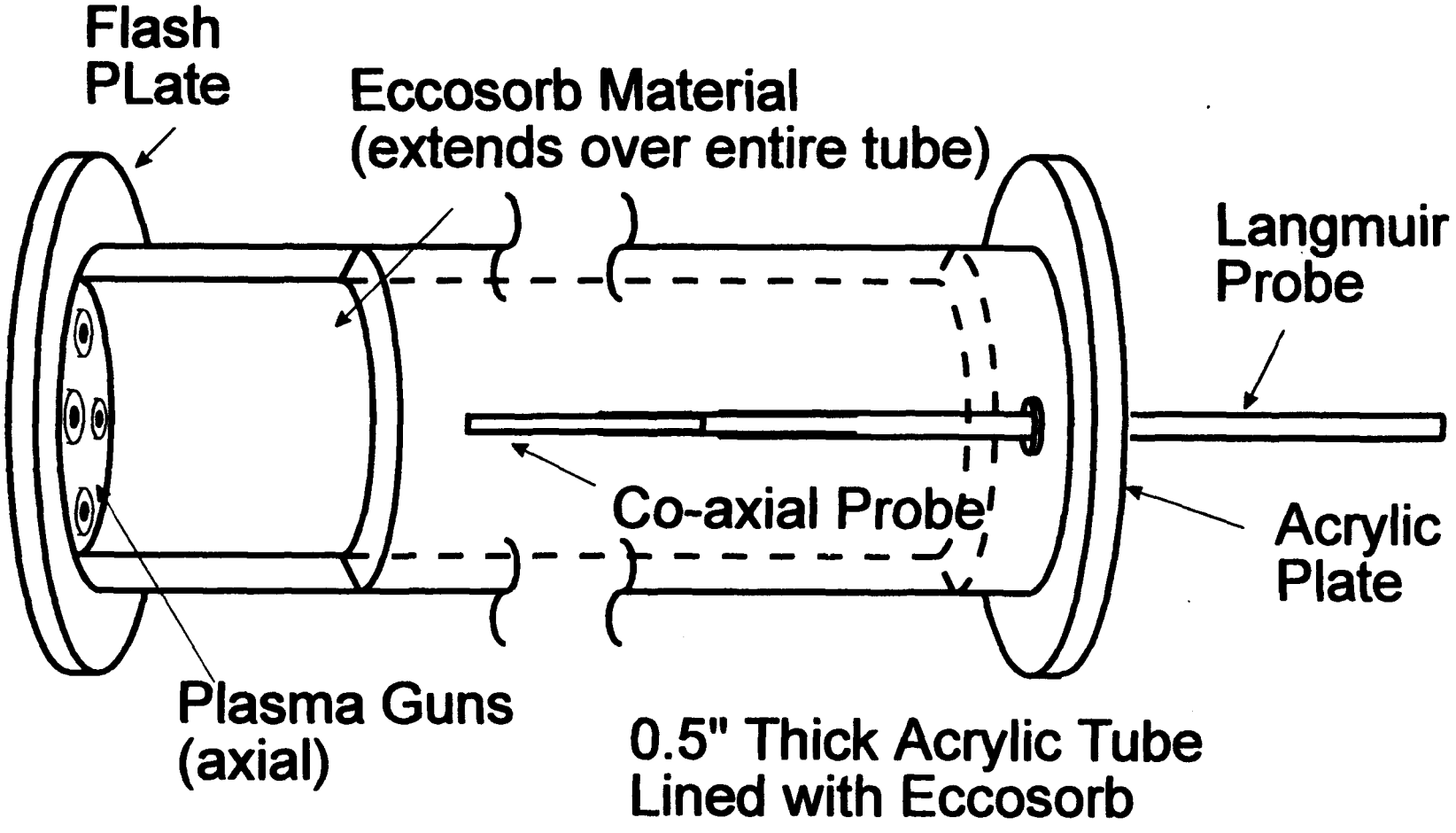
Flash
PLate
Eccosorb Material
(extends over entire tube)
Langmuir
Probe
Co-axial Probe
Acrylic
Plate
Plasma Guns
(axial)
0.5" Thick Acrylic Tube
Lined with Eccosorb

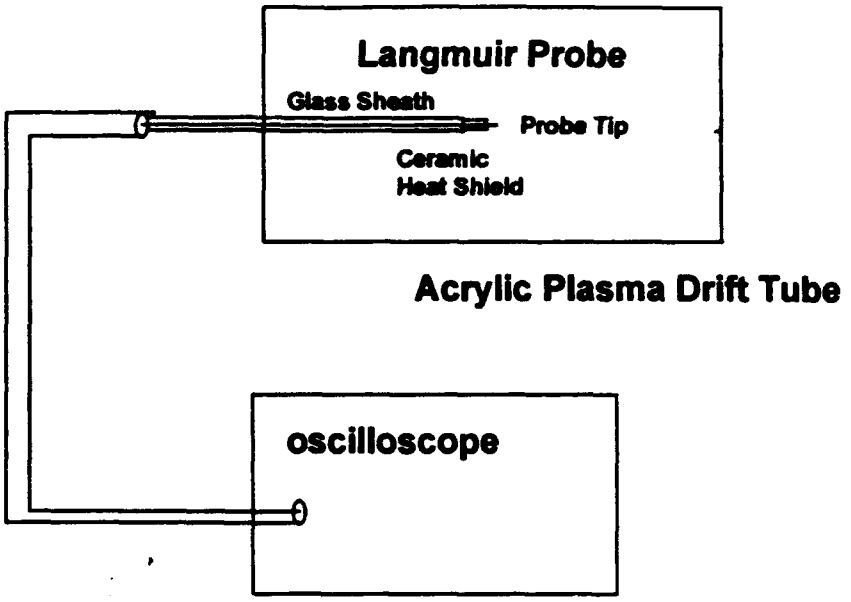
Langmuir Probe
Glass Sheath
Probe Tip
Ceramic
Heat Shield
Acrylic Plasma Drift Tube
oscilloscope

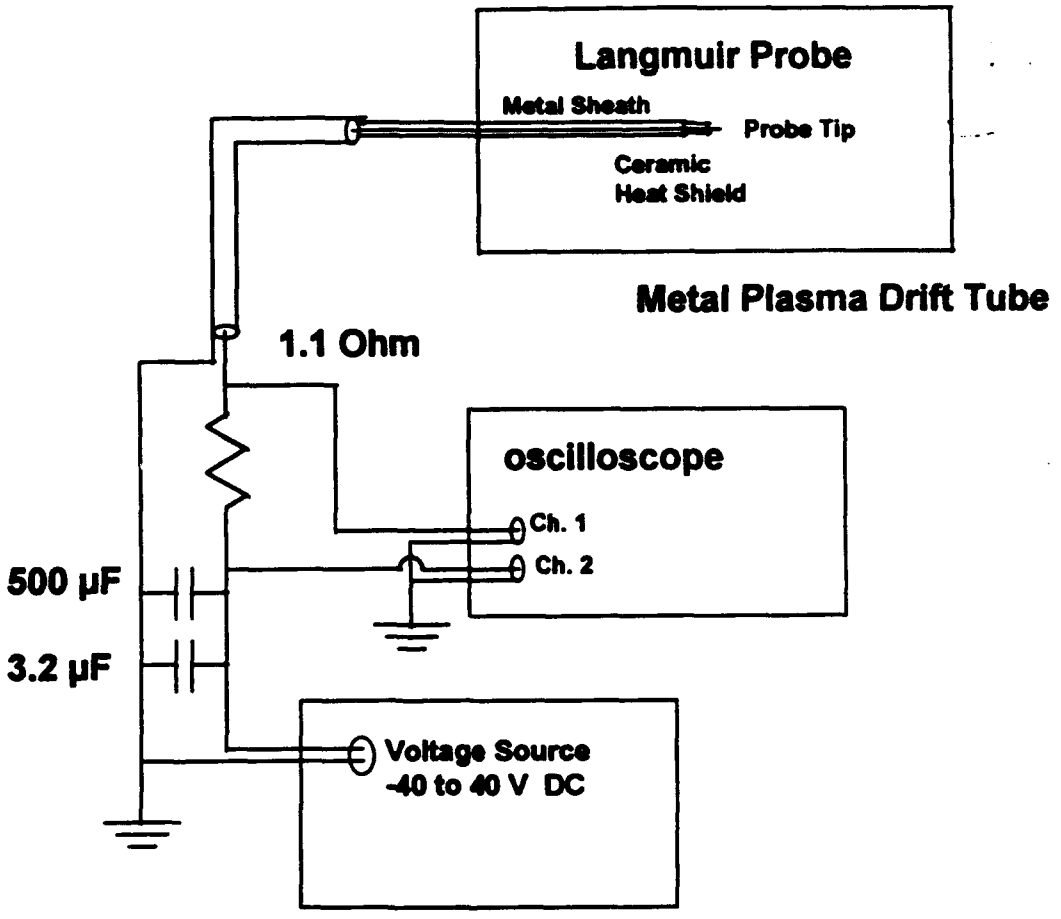
Langmuir Probe
Metal Sheath
Probe Tip
Ceramic
Heat Shield
Metal Plasma Drift Tube
1.1 Ohm
oscilloscope
Ch. 1
Ch. 2
500 µF
3.2 µF
Voltage Source
-40 to 40 V DC

Fig 4

Fig 5

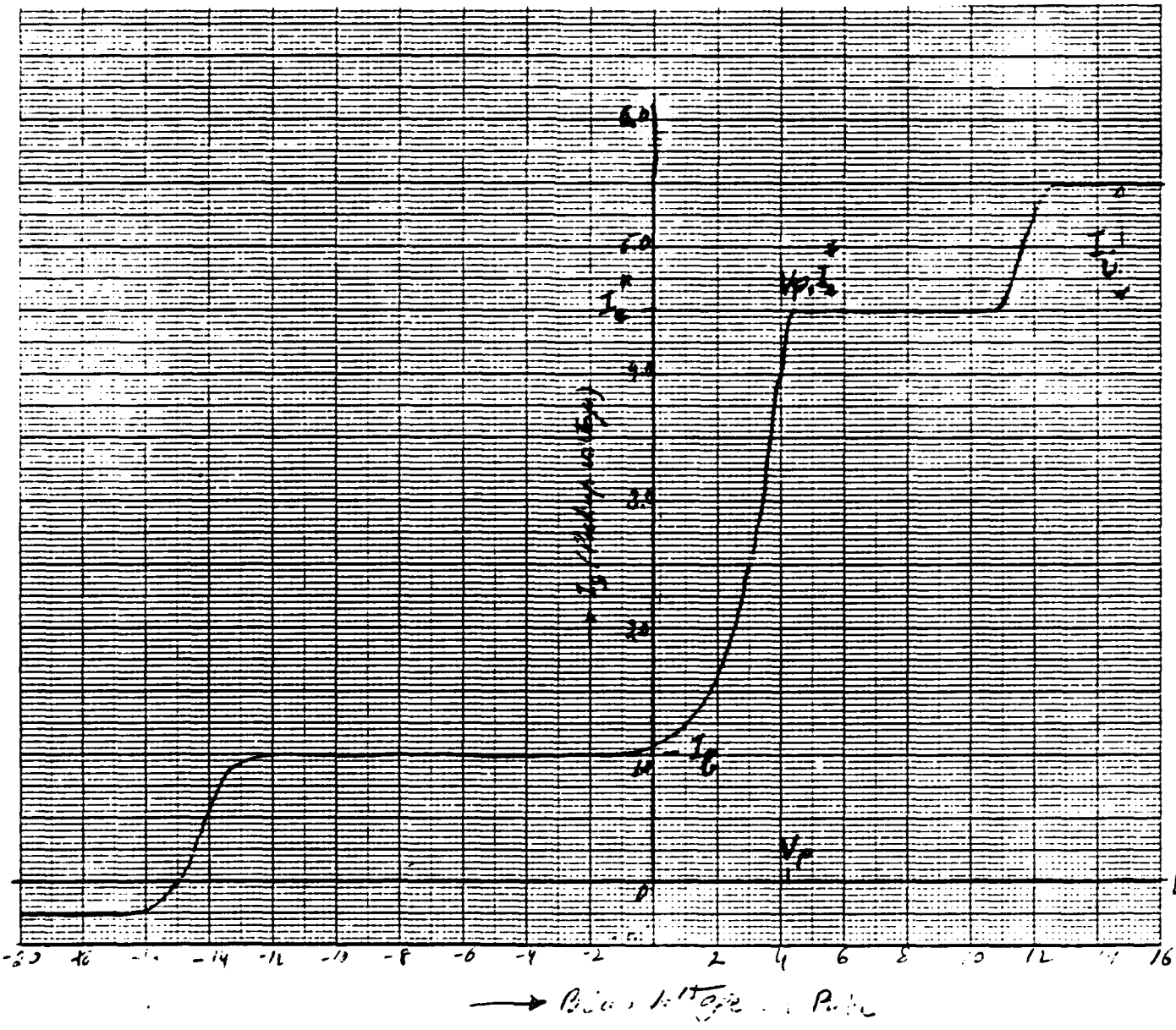

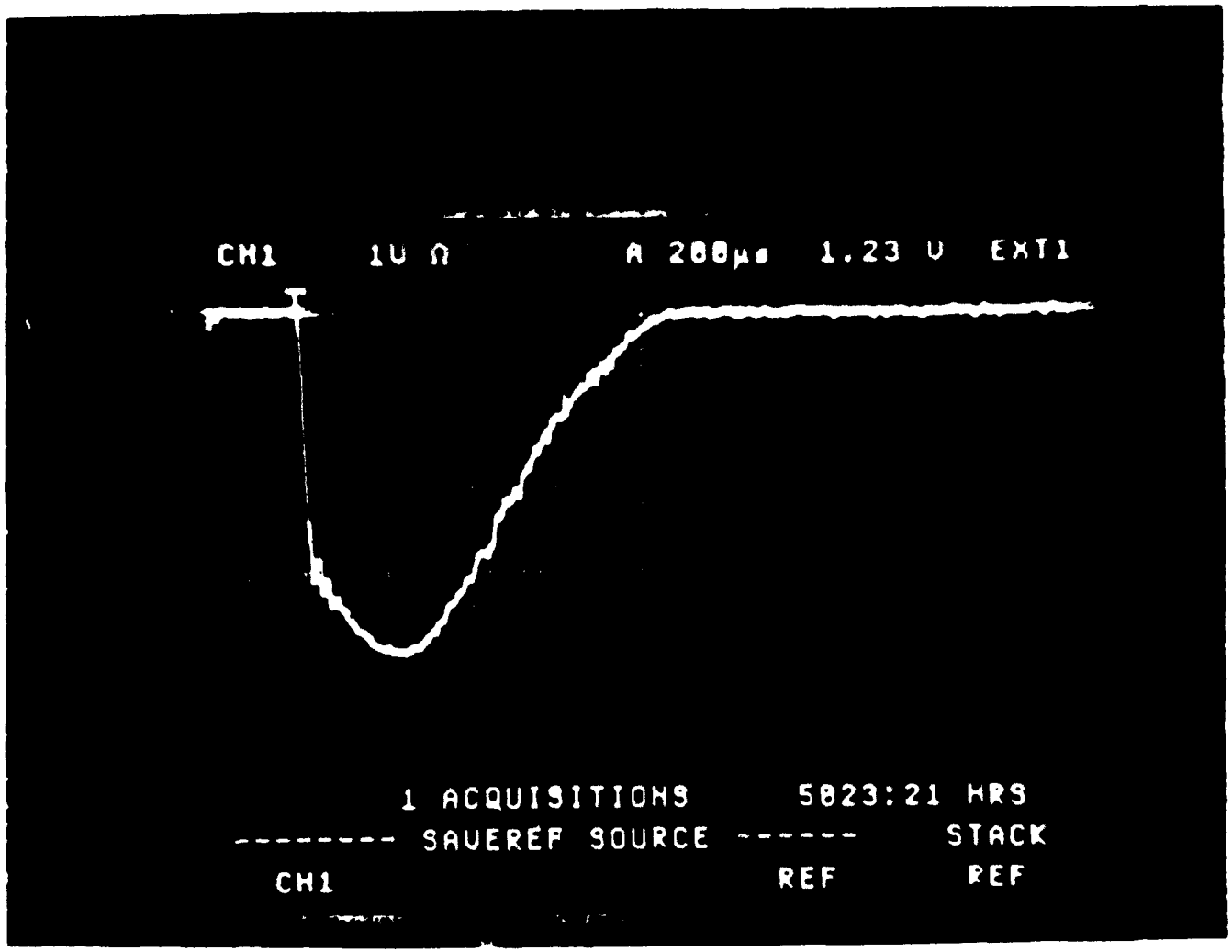
CH1 1U Ω A 200µs 1.23 V EXT1
1 ACQUISITIONS 5823:21 HRS
SAVEREF SOURCE
CH1 REF STACK REF

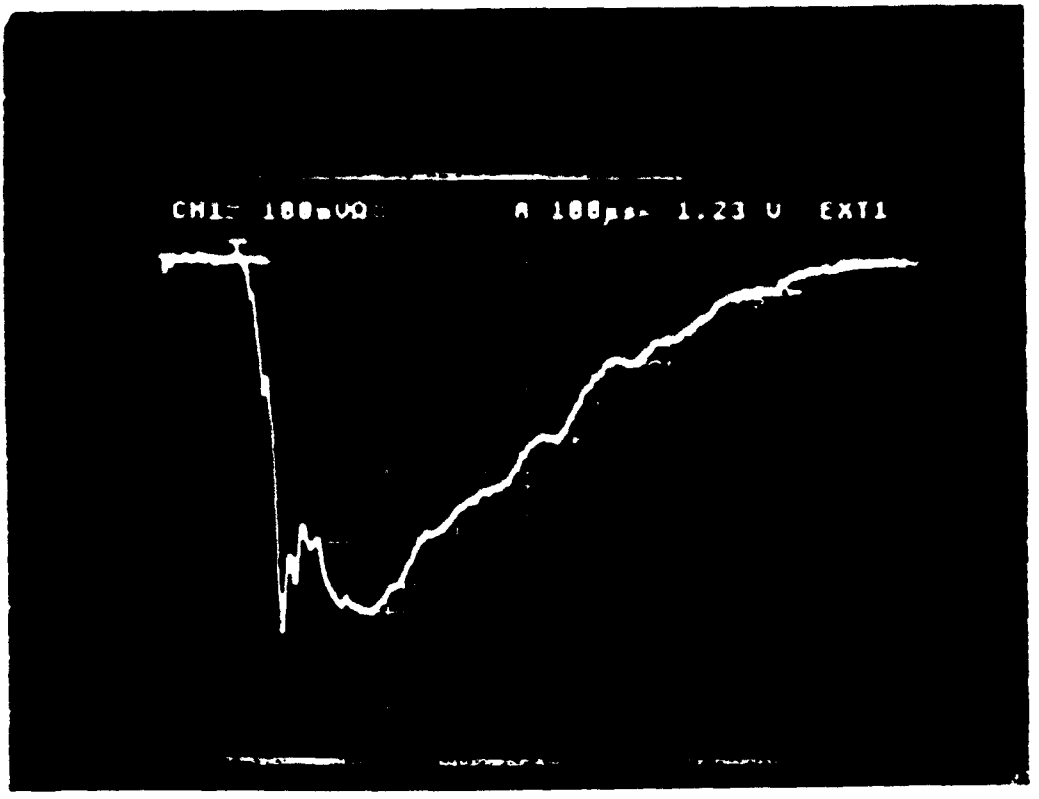

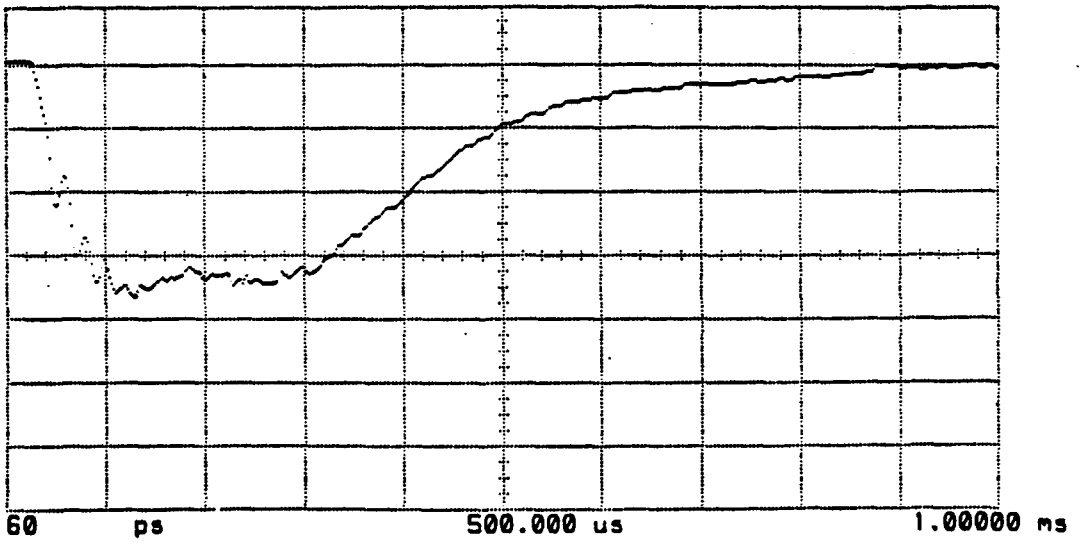

Ch. 1 = 1.000 Volts/div
Timebase = 100 us/div
Offset = -3.000 Volts
Delay = 500.000 us

Fig 6 a and 6e

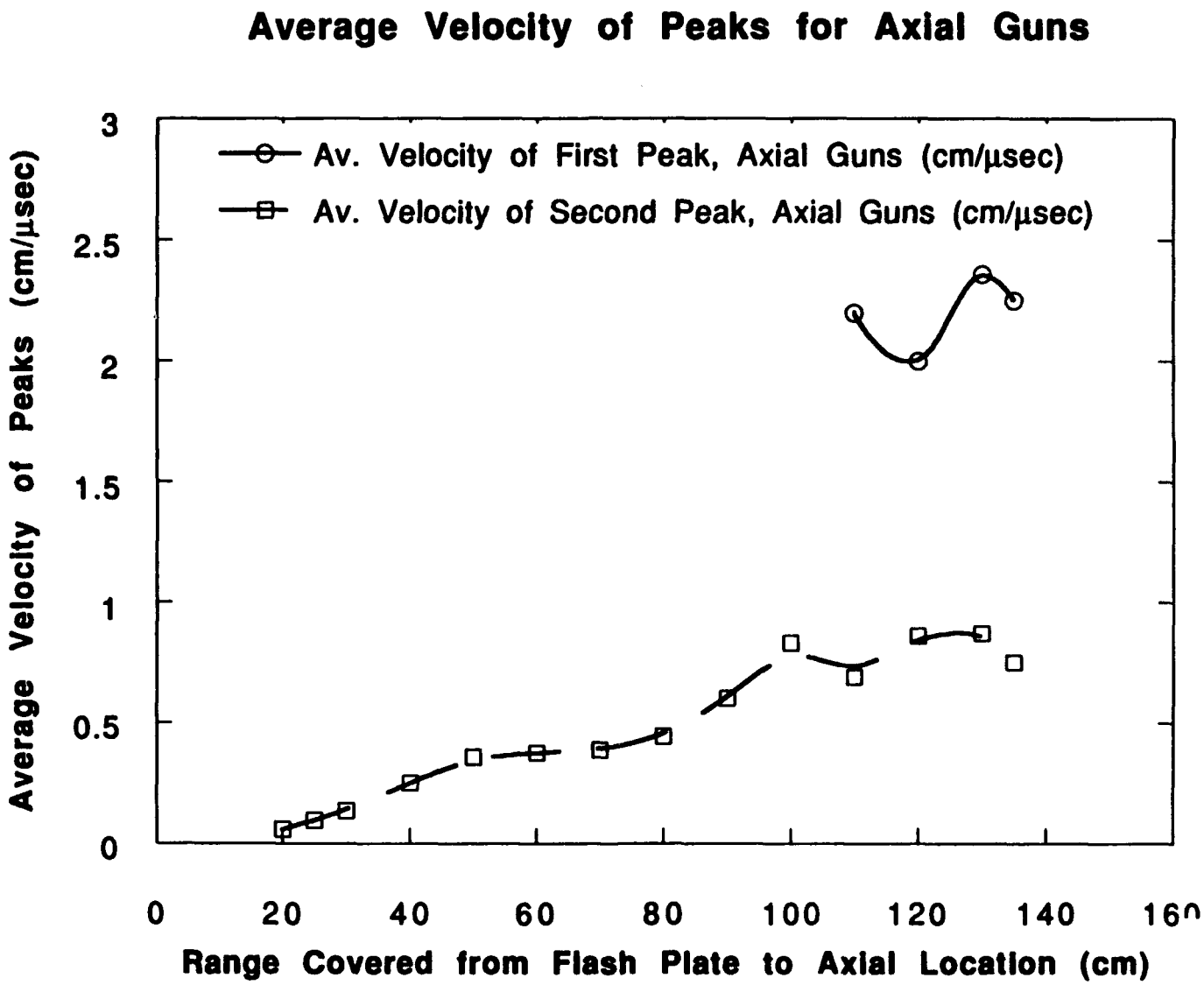
Average Velocity of Peaks for Axial Guns
Av. Velocity of First Peak, Axial Guns (cm/µsec)
Av. Velocity of Second Peak, Axial Guns (cm/µsec)
Average Velocity of Peaks (cm/µsec)
3
2.5
2
1.5
1
0.5
0
0
20
40
60
80
100
120
140
160
Range Covered from Flash Plate to Axial Location (cm)

Fig 7a

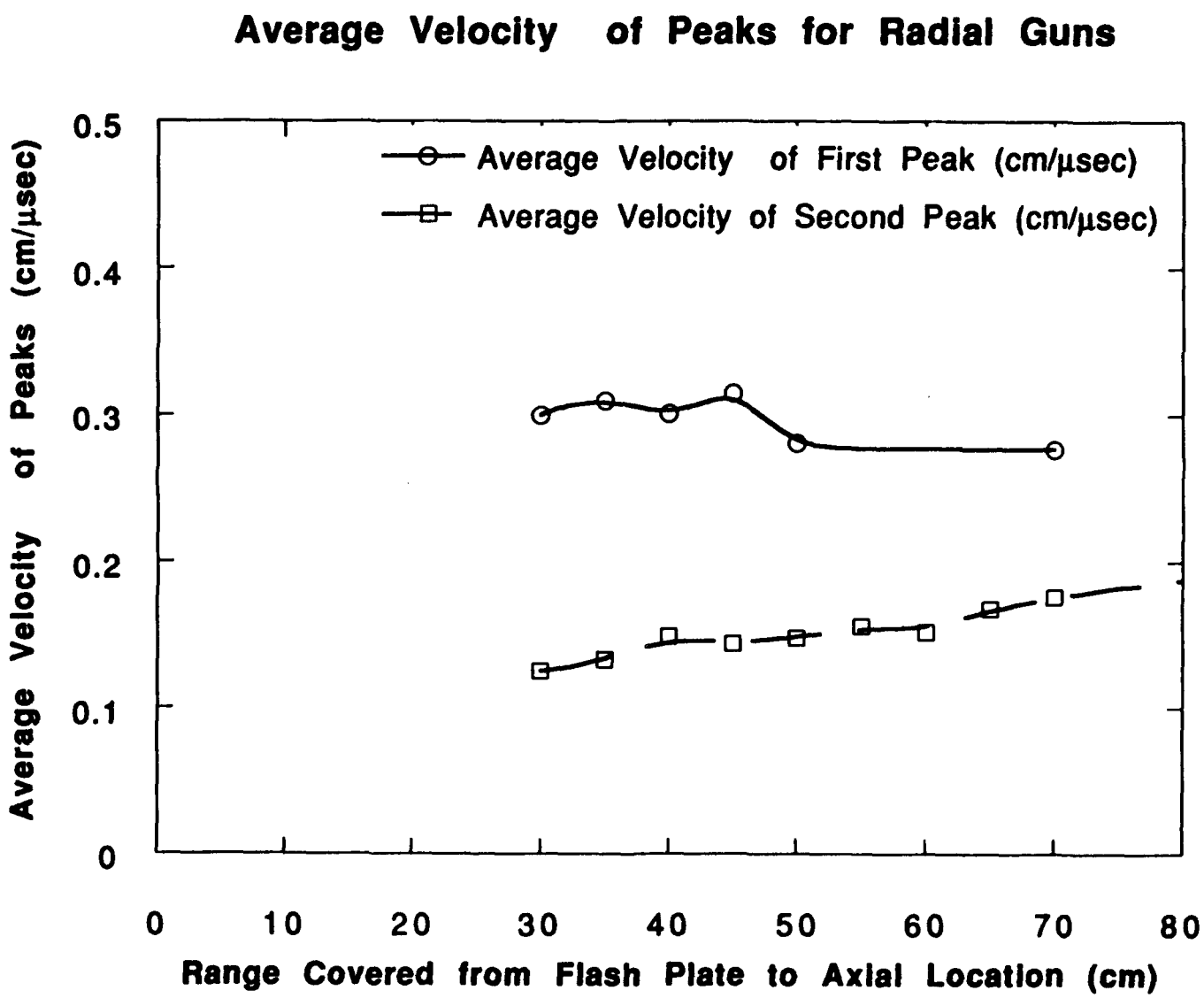
Average Velocity of Peaks for Radial Guns
Average Velocity of First Peak (cm/µsec)
Average Velocity of Second Peak (cm/µsec)
Average Velocity of Peaks (cm/µsec)
0.5
0.4
0.3
0.2
0.1
0
0
10
20
30
40
50
60
70
80
Range Covered from Flash Plate to Axial Location (cm)

Fig 76

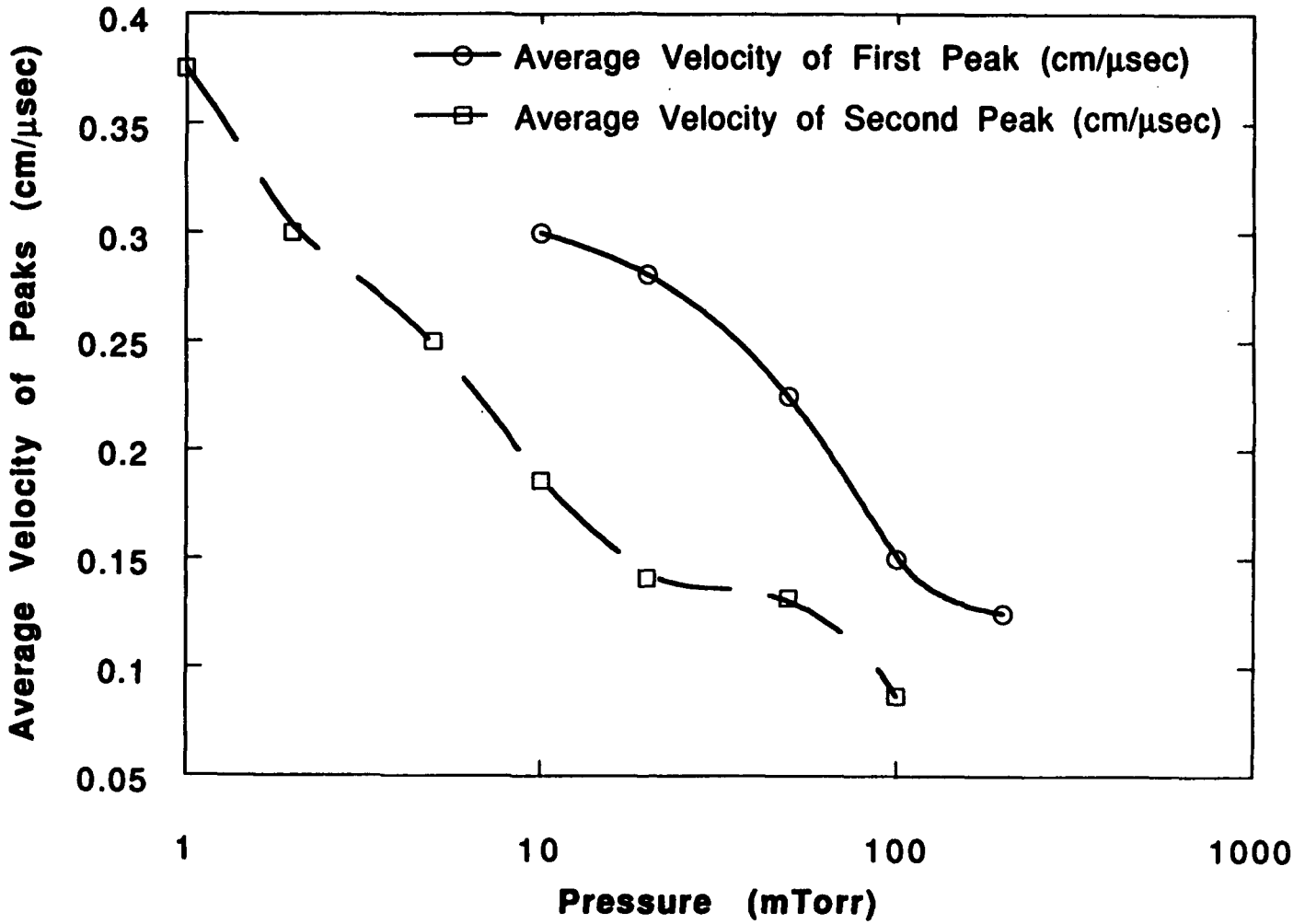
Average Velocity of First Peak (cm/µsec)
Average Velocity of Second Peak (cm/µsec)
Average Velocity of Peaks (cm/µsec)
0.4
0.35
0.3
0.25
0.2
0.15
0.1
0.05
1
10
100
1000
Pressure (mTorr)

Fig 8

Hard Vac - Coaxial Probe
< 1 mTorr

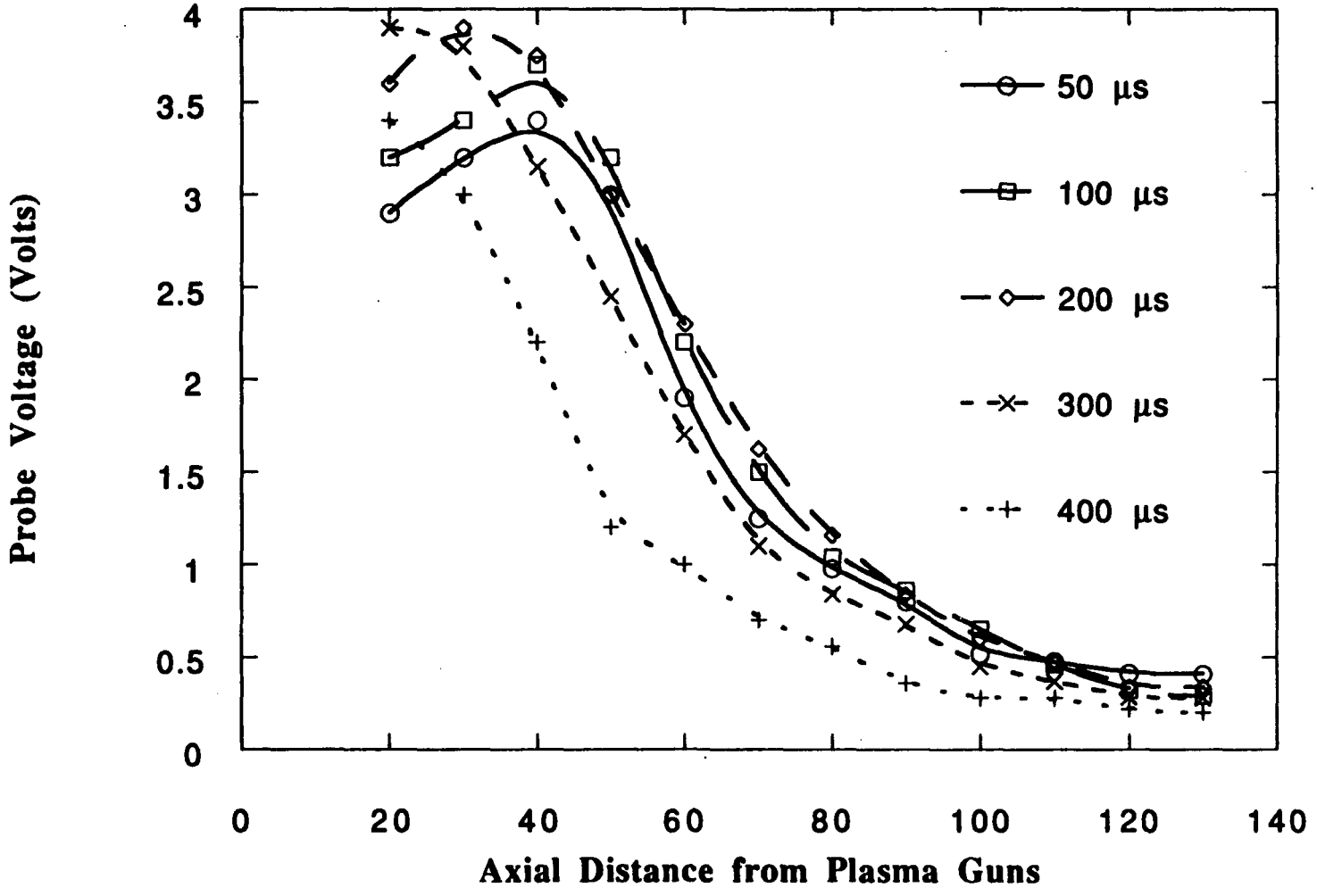

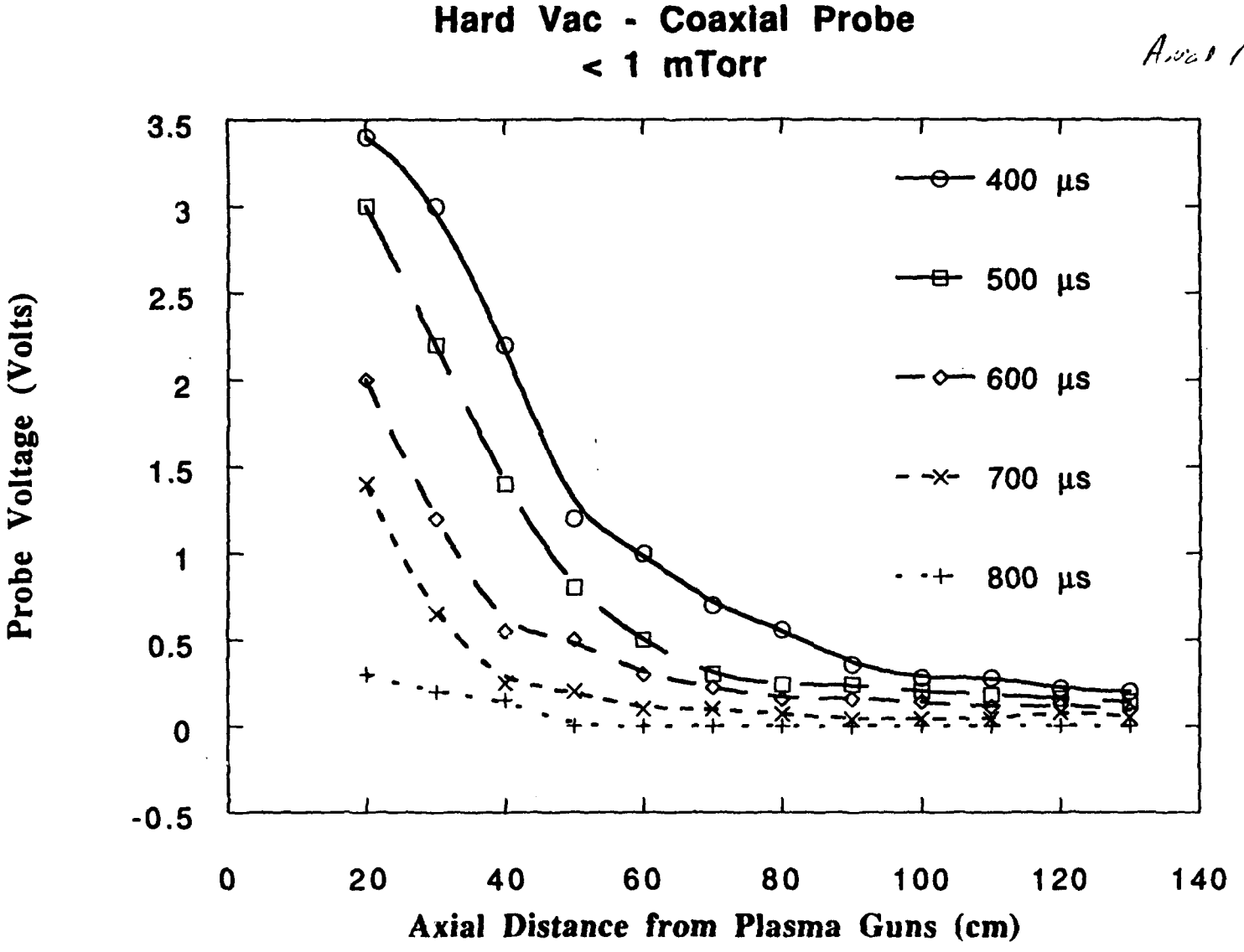
Hard Vac - Coaxial Probe
< 1 mTorr
Axial Plasma Guns
Probe Voltage (Volts)
3.5
3
2.5
2
1.5
1
0.5
0
-0.5
400 µs
500 µs
600 µs
700 µs
800 µs
0
20
40
60
80
100
120
140
Axial Distance from Plasma Guns (cm)

Fig. 1

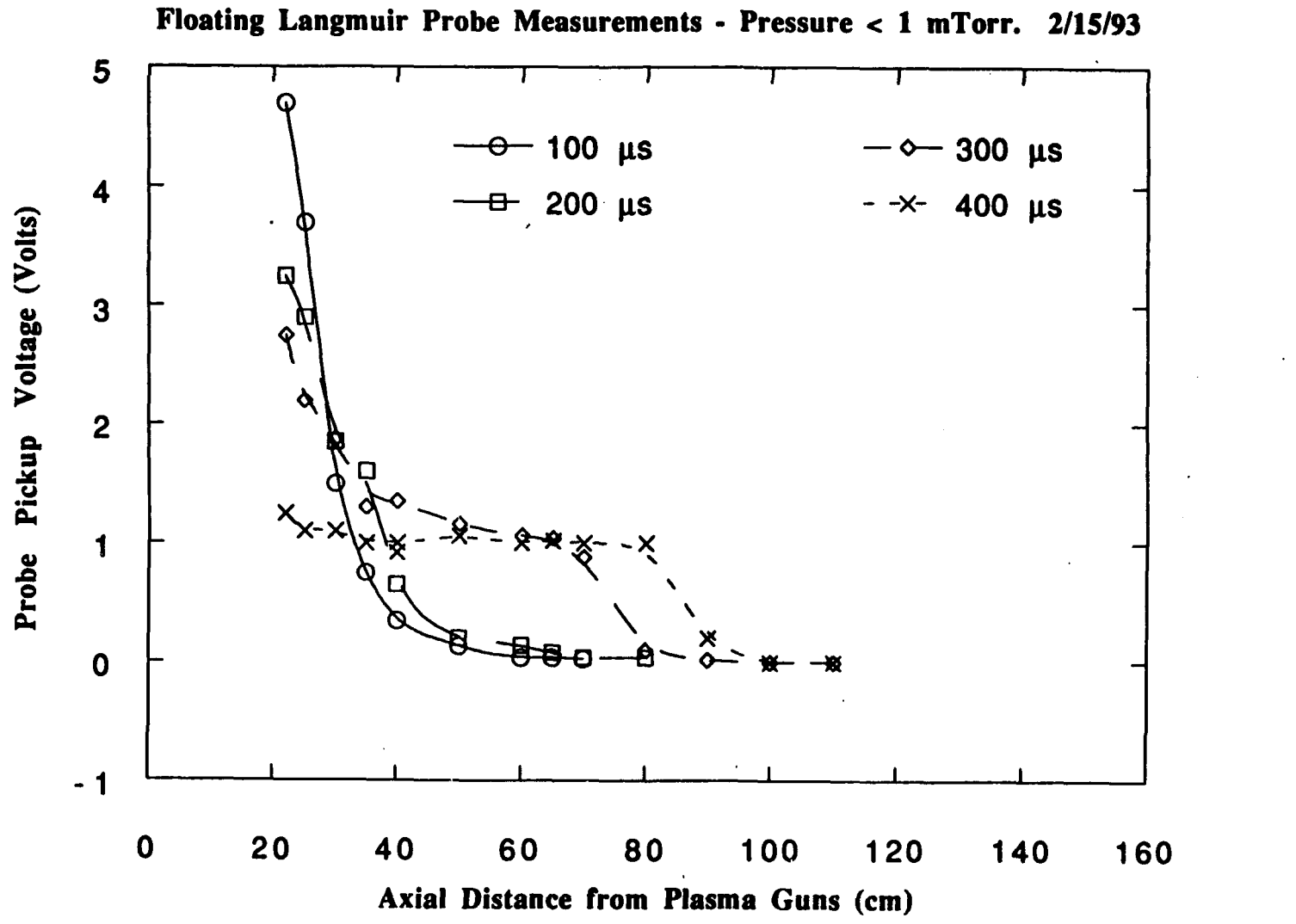
Floating Langmuir Probe Measurements - Pressure < 1 mTorr. 2/15/93
Probe Pickup Voltage (Volts)
5
4
3
2
1
0
-1
100 µs
200 µs
300 µs
400 µs
0
20
40
60
80
100
120
140
160
Axial Distance from Plasma Guns (cm)
plot hard vac 1234

Fig 10a

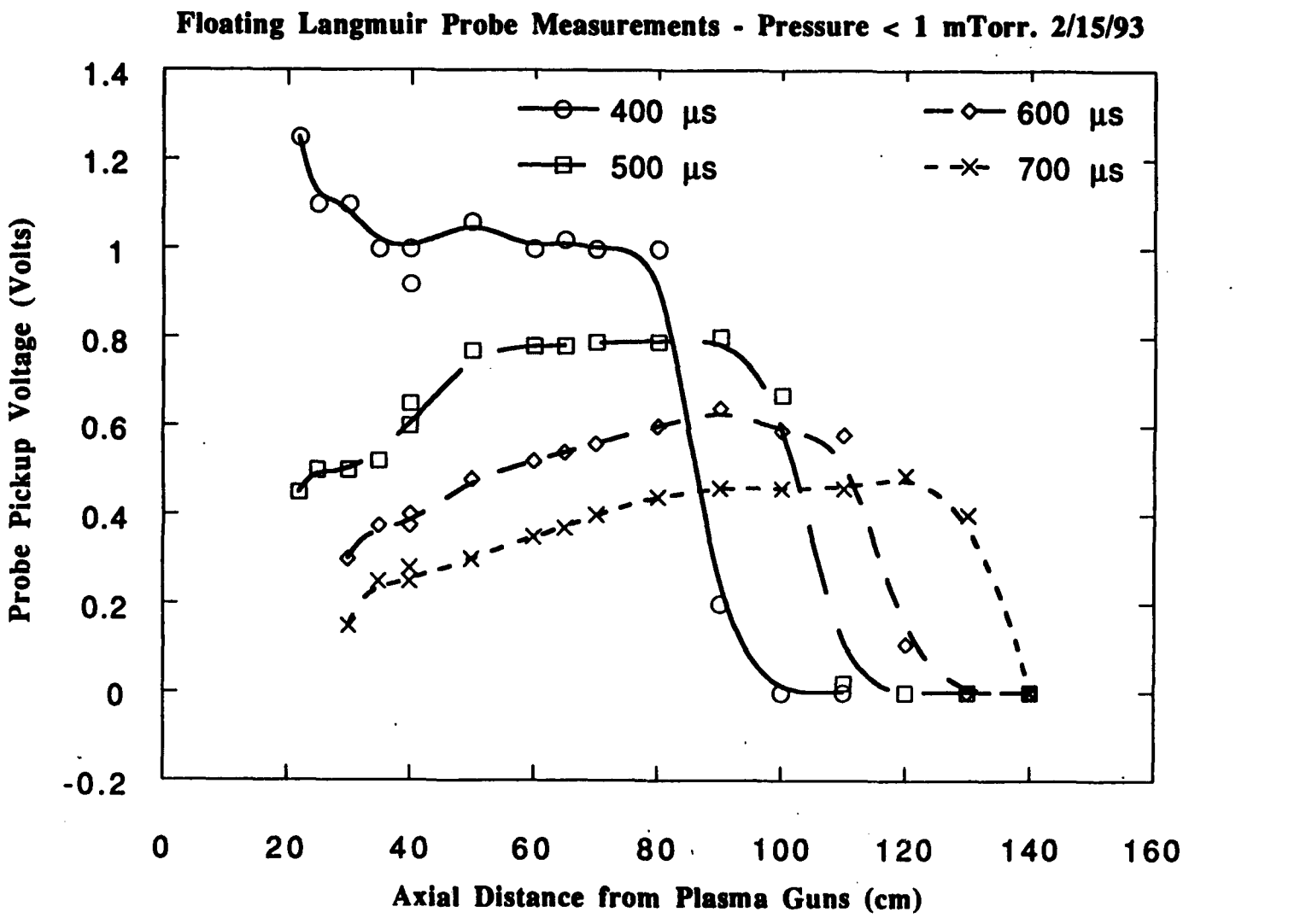
Floating Langmuir Probe Measurements - Pressure < 1 mTorr. 2/15/93
400 µs
500 µs
600 µs
700 µs
Probe Pickup Voltage (Volts)
1.4
1.2
1
0.8
0.6
0.4
0.2
0
-0.2
0
20
40
60
80
100
120
140
160
Axial Distance from Plasma Guns (cm)
plot high vac 4567

Fig 10 b

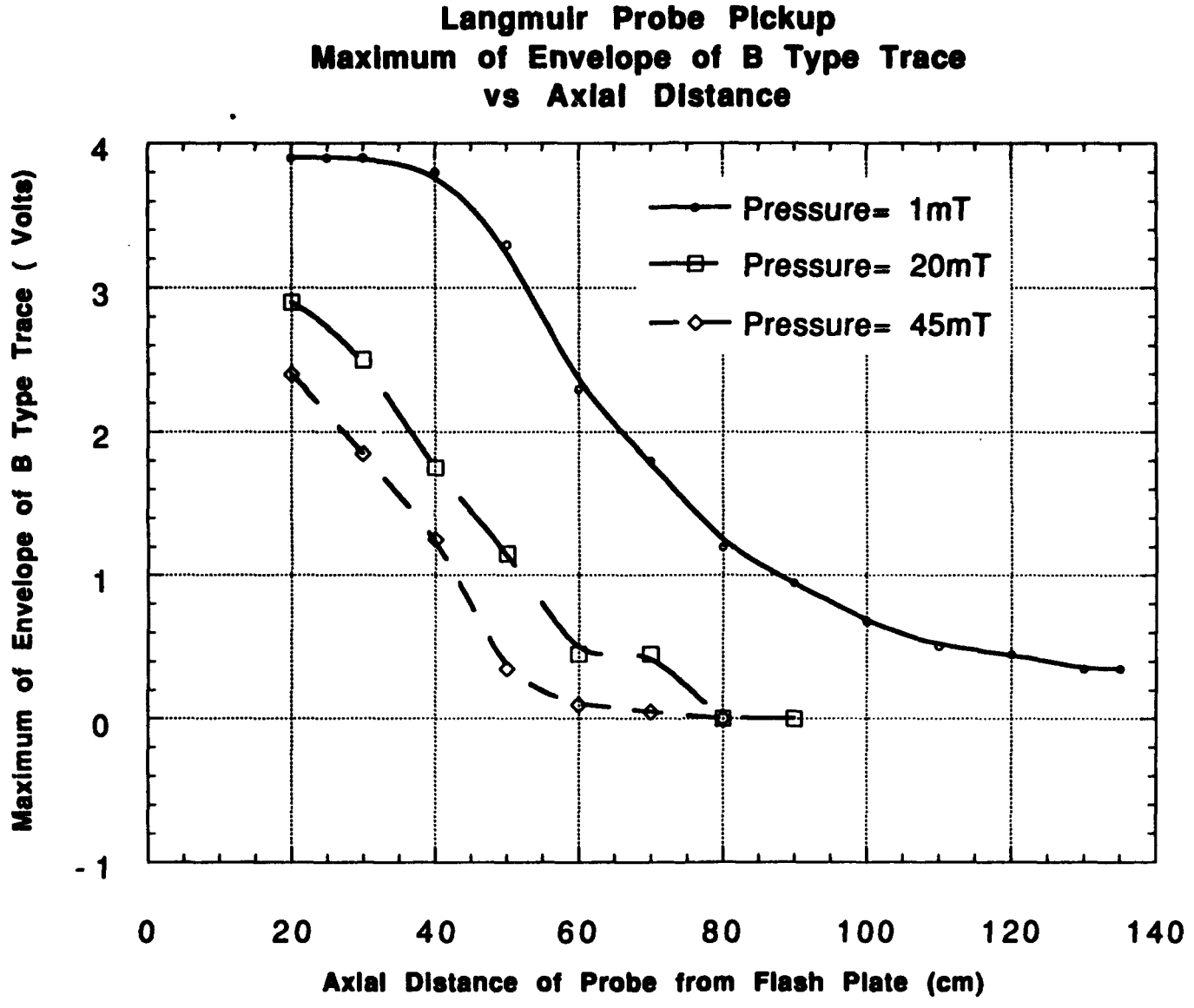
Langmuir Probe Pickup
Maximum of Envelope of B Type Trace
vs Axial Distance
Maximum of Envelope of B Type Trace (Volts)
4
3
2
1
0
-1
0
20
40
60
80
100
120
140
Axial Distance of Probe from Flash Plate (cm)
Pressure= 1mT
Pressure= 20mT
Pressure= 45mT

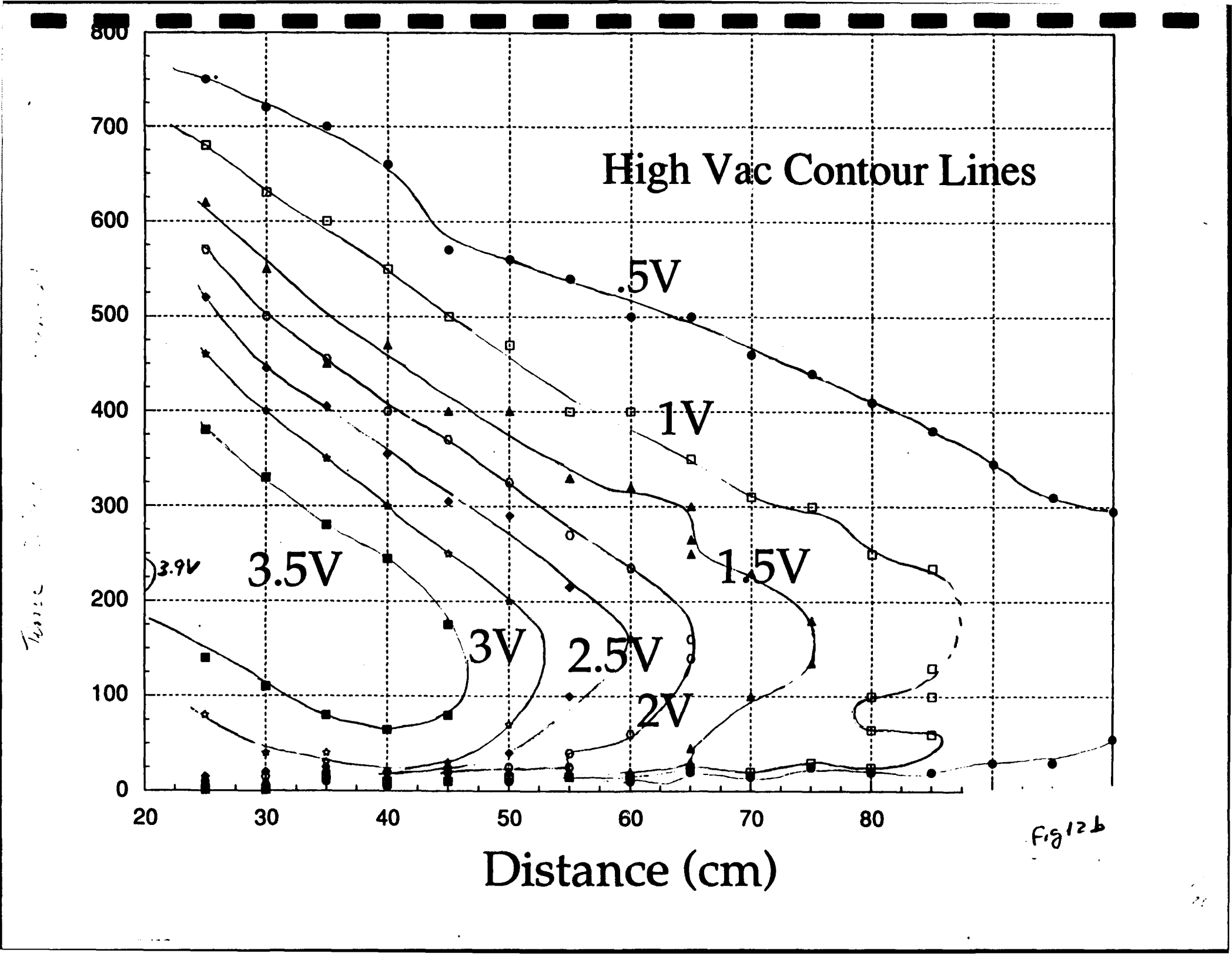
High Vac Contour Lines
.5V
1V
1.5V
2V
2.5V
3V
3.5V
3.9V
800
700
600
500
400
300
200
100
0
20
30
40
50
60
70
80
Distance (cm)

Fig 12b

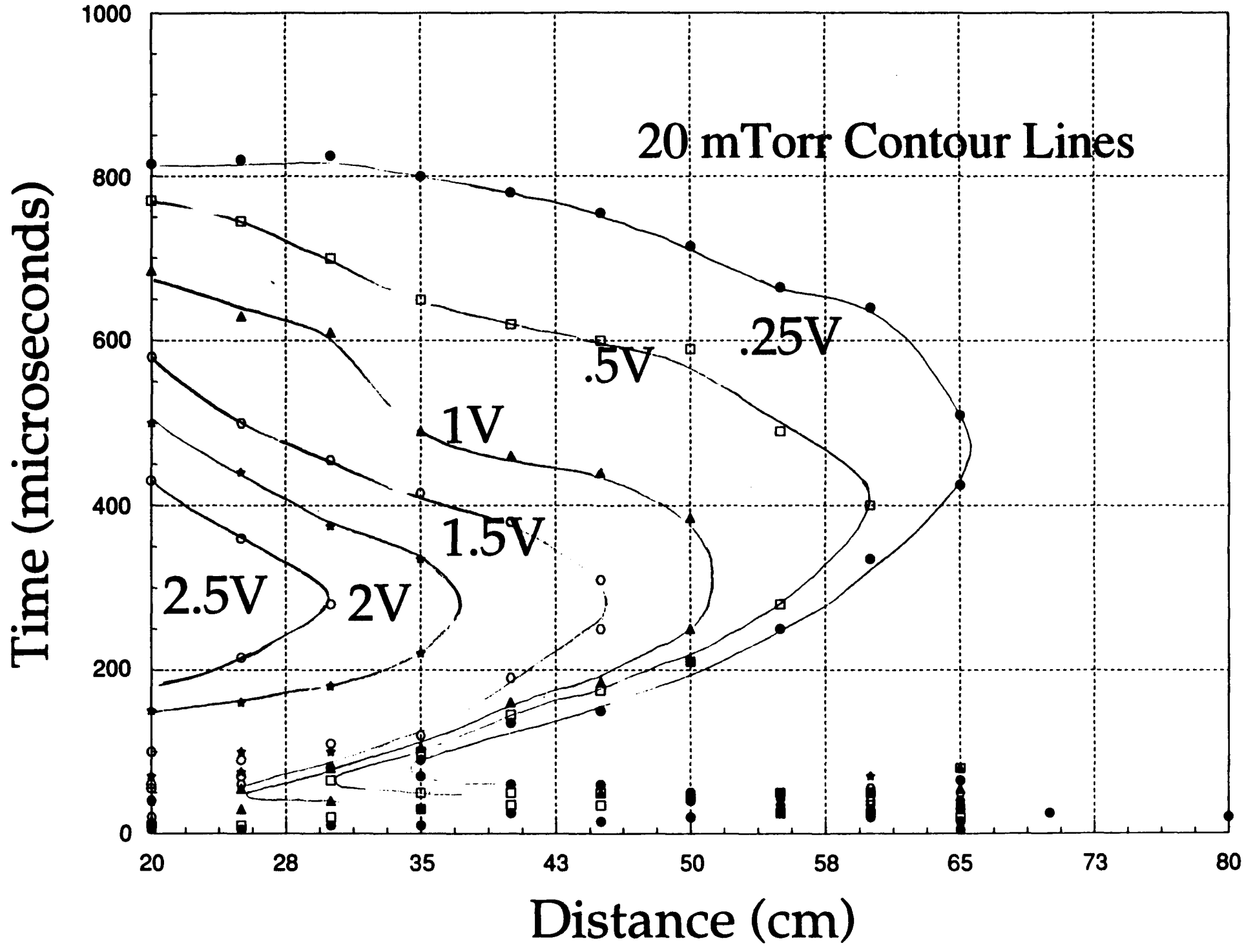
20 mTorr Contour Lines
.25V
.5V
1V
1.5V
2V
2.5V
Time (microseconds)
Distance (cm)
1000
800
600
400
200
0
20
28
35
43
50
58
65
73
80

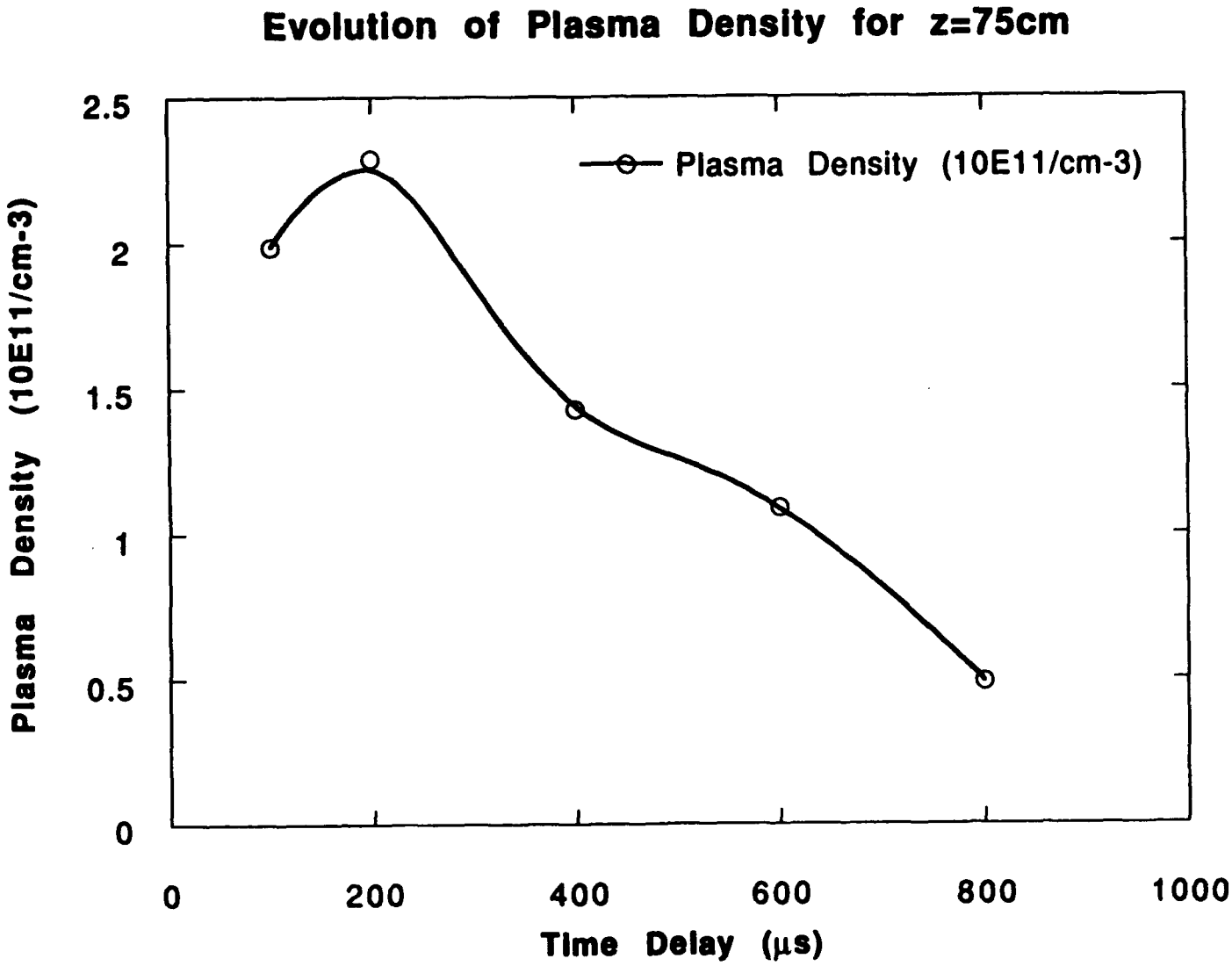
Evolution of Plasma Density for z=75cm
Plasma Density (10E11/cm-3)
Plasma Density (10E11/cm-3)
2.5
2
1.5
1
0.5
0
0
200
400
600
800
1000
Time Delay (μs)

Fig 16

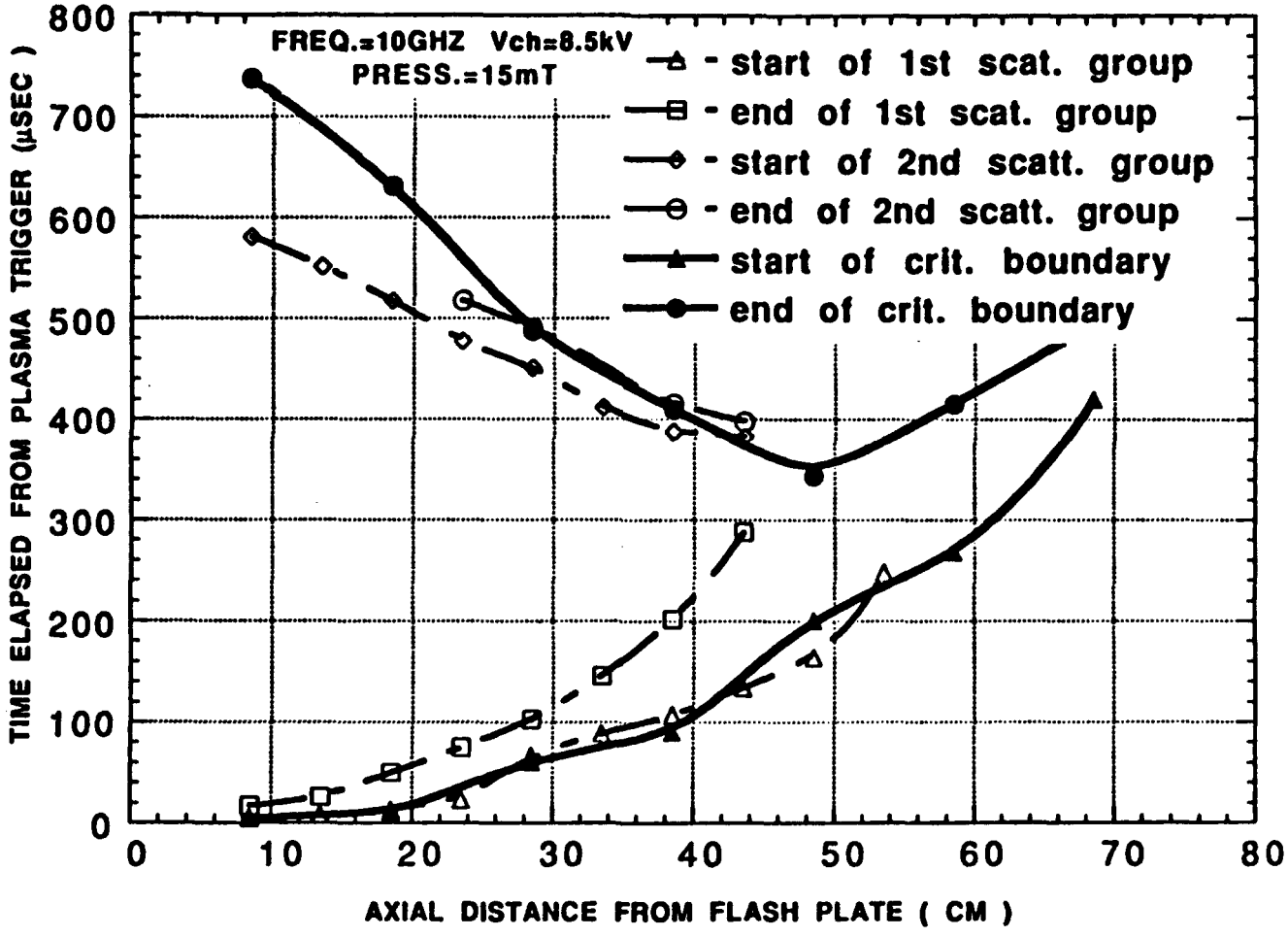

~~Fig. 19a~~. Correlation of sidescattered signal with critical density boundary. Frequency = 10 GHz, pressure = 15 mTorr, incident microwave power level = 19 W, charging potential = 8.5 kV.

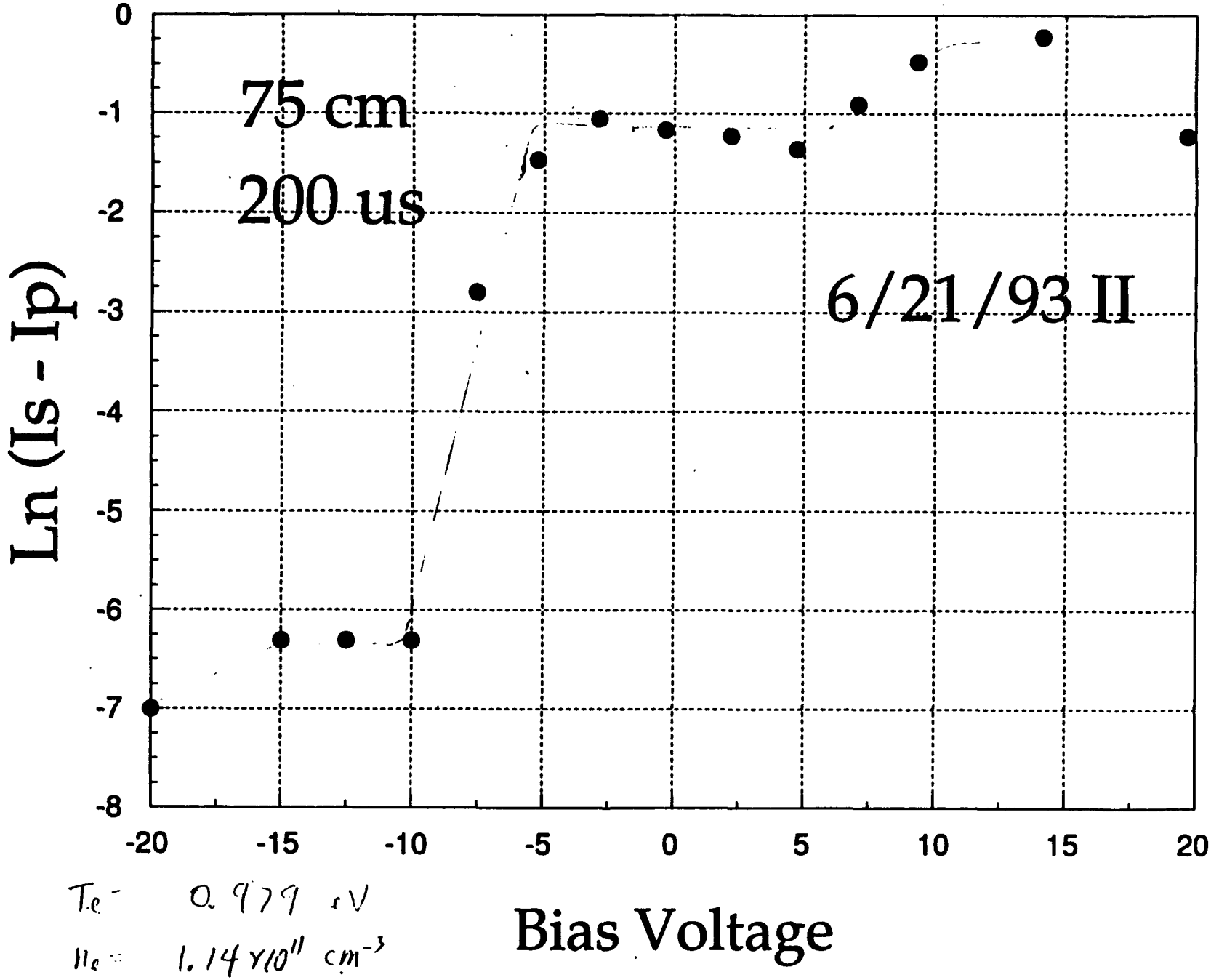

T_e = 0.979 eV

n_e = 1.14×10^{11} cm^{-3}

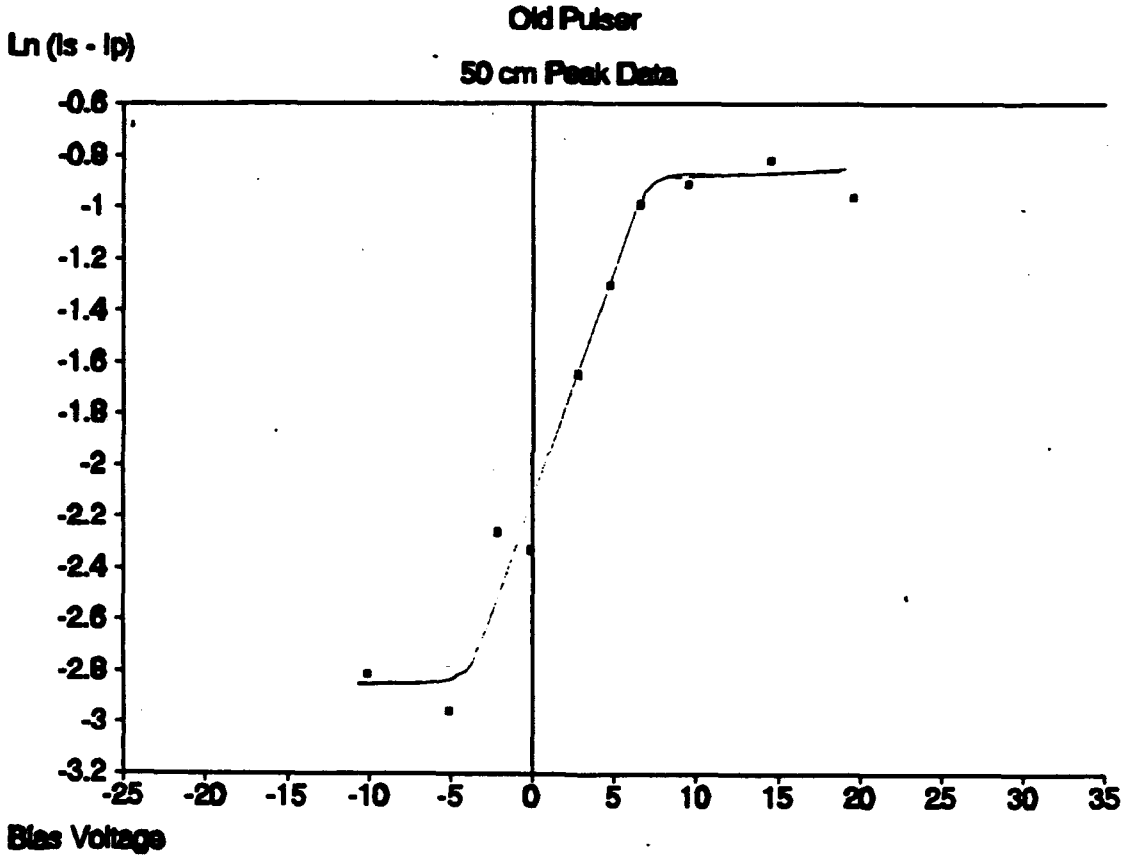
Old Pulser
50 cm Peak Data
Ln (Is - Ip)
-0.6
-0.8
-1
-1.2
-1.4
-1.6
-1.8
-2
-2.2
-2.4
-2.6
-2.8
-3
-3.2
-25
-20
-15
-10
-5
0
5
10
15
20
25
30
35
Bias Voltage

Fig 15a

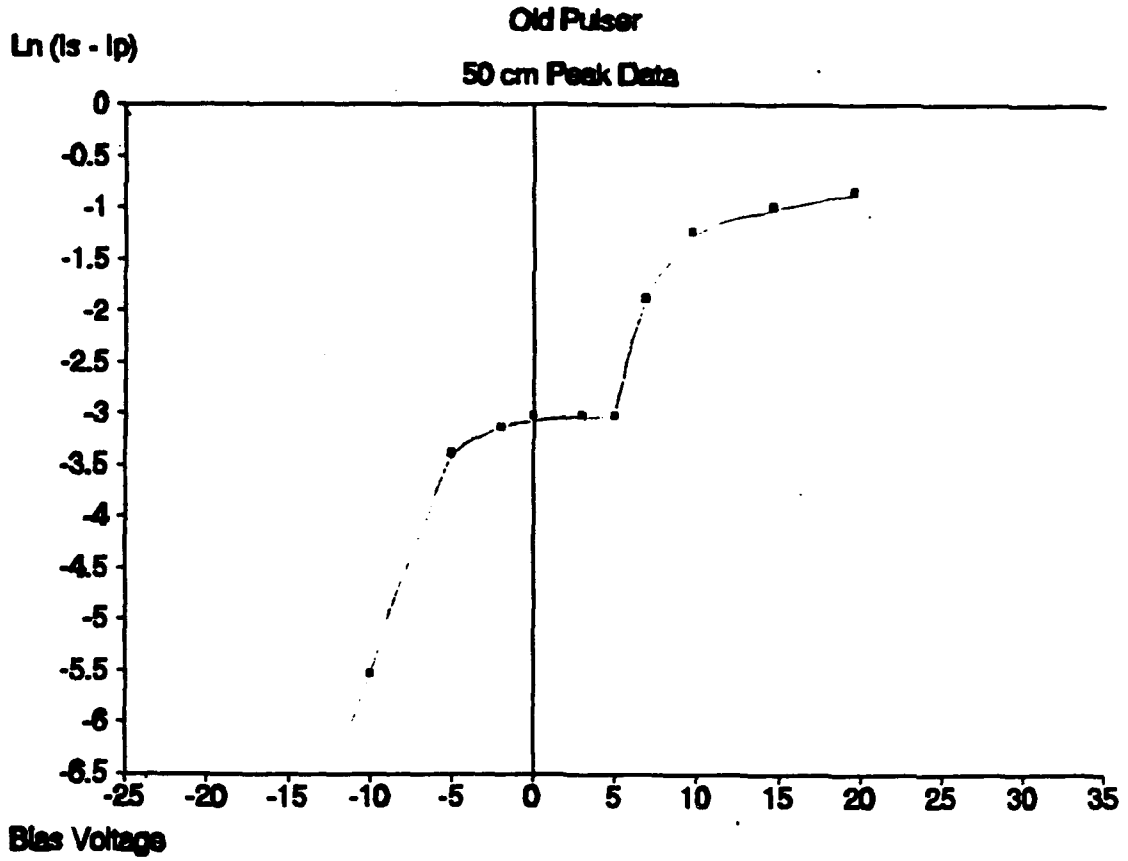

2.32 eV

2.32 eV

Fig 15

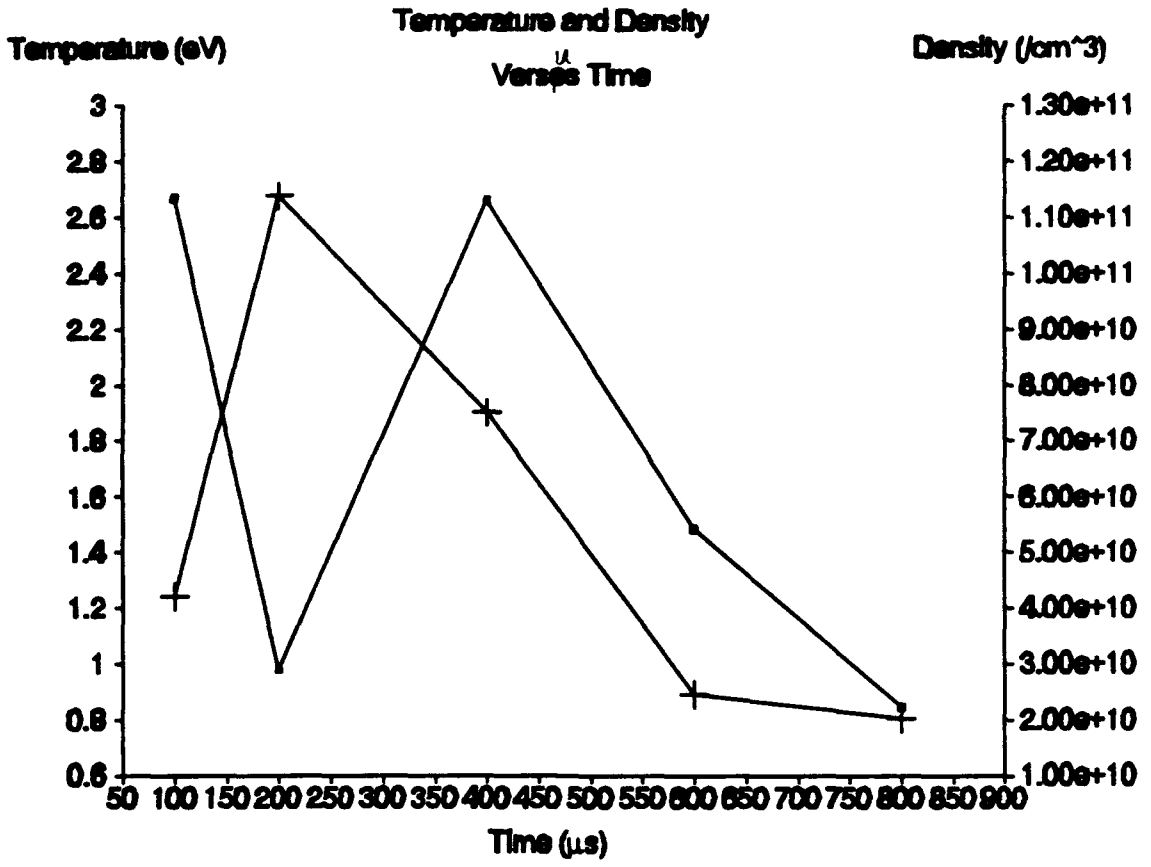
Temperature and Density
Versus Time
Temperature (eV)
Density (/cm^3)
3
2.8
2.6
2.4
2.2
2
1.8
1.6
1.4
1.2
1
0.8
0.6
1.30e+11
1.20e+11
1.10e+11
1.00e+11
9.00e+10
8.00e+10
7.00e+10
6.00e+10
5.00e+10
4.00e+10
3.00e+10
2.00e+10
1.00e+10
50 100 150 200 250 300 350 400 450 500 550 600 650 700 750 800 850 900
Time (μs)

Fig 16

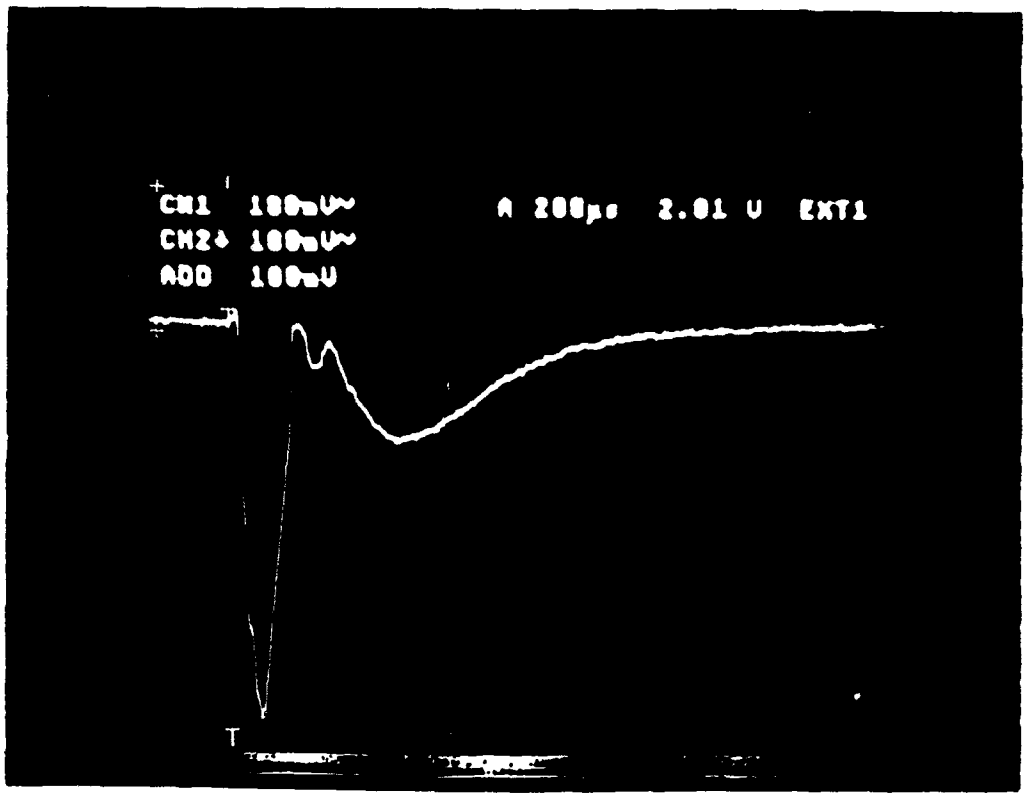

Fig 17

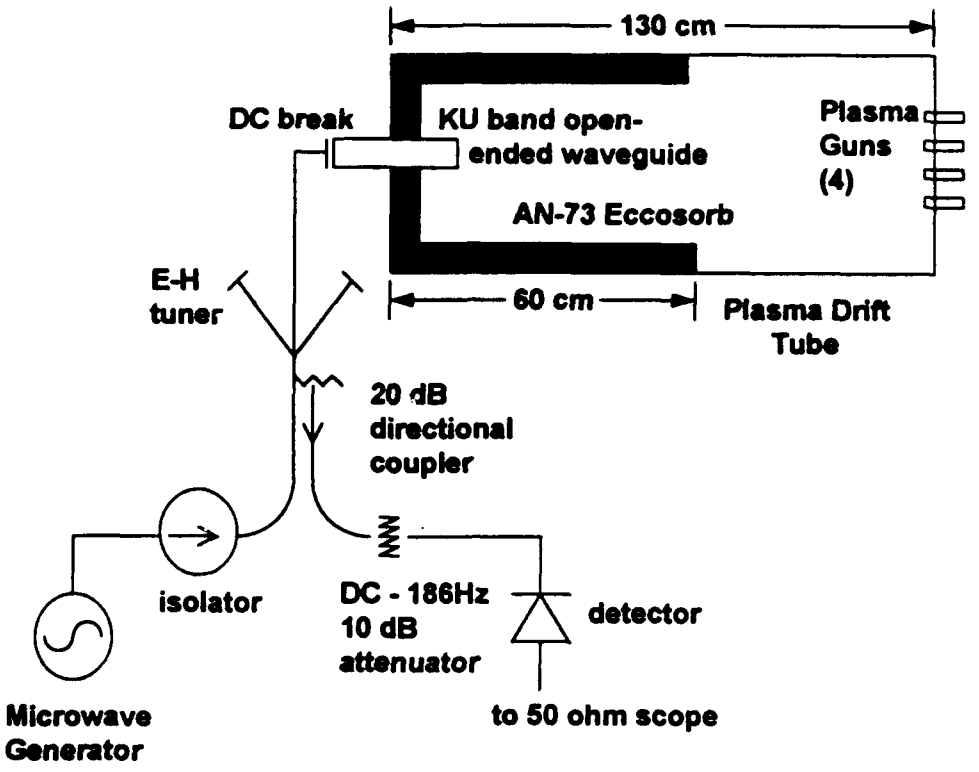
130 cm
DC break
KU band open-
ended waveguide
Plasma
Guns
(4)
AN-73 Eccosorb
E-H
tuner
60 cm
Plasma Drift
Tube
20 dB
directional
coupler
isolator
DC - 186Hz
10 dB
attenuator
detector
Microwave
Generator
to 50 ohm scope

Fig 12

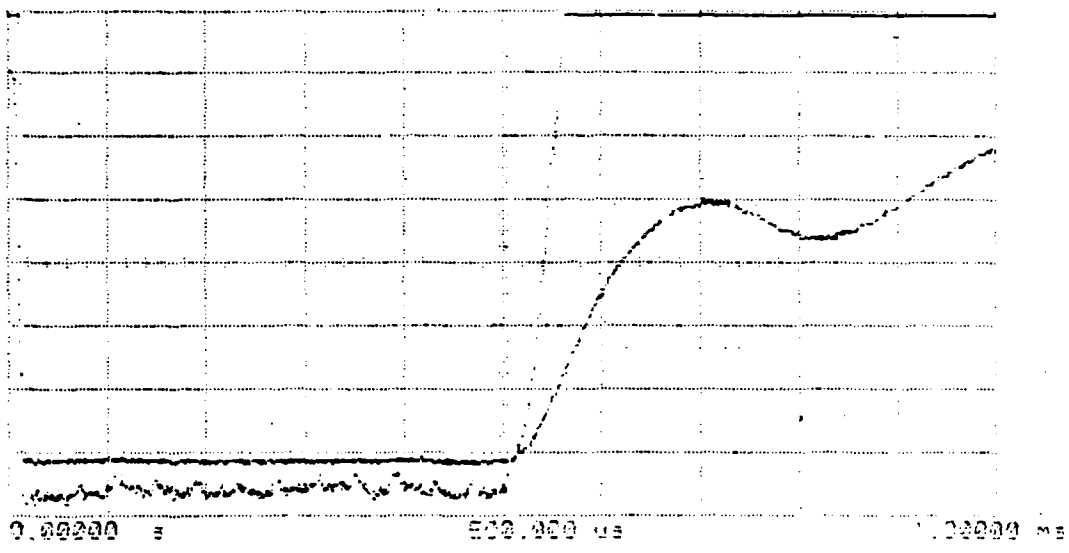

Ch. 1	=	1.000 mVolts/div	Offset	=	3.000 mVolts
Ch. 2	=	5.000 mVolts/div	Offset	=	15.00 mVolts
Timebase	=	100 us/div	Delay	=	0.00000 s

Fig 19

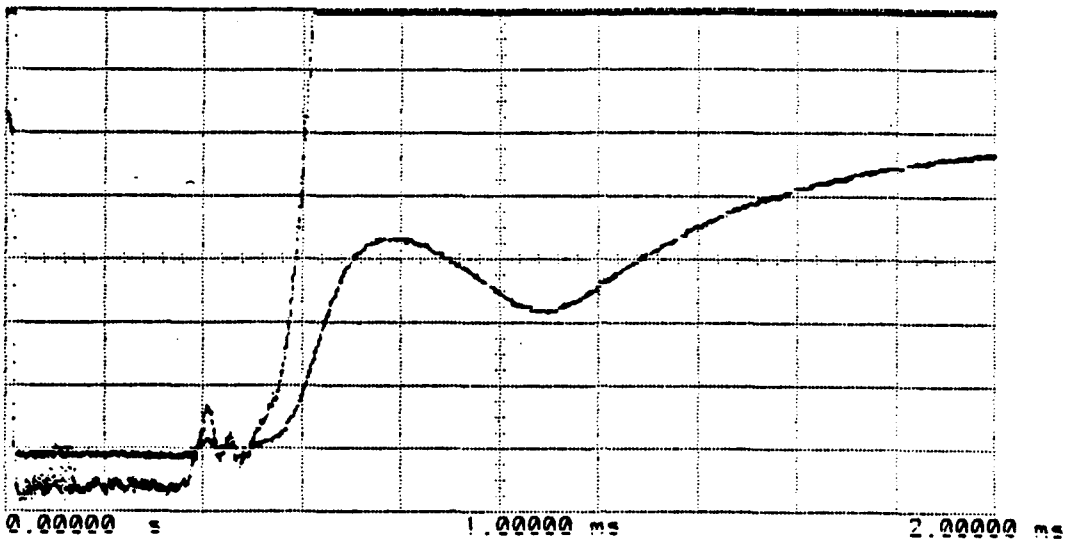

Ch. 1	=	1.000 mVolts/div	Offset	=	3.000 mVolts
Ch. 2	=	5.000 mVolts/div	Offset	=	15.00 mVolts
Timebase	=	200 us/div	Delay	=	0.00000 s

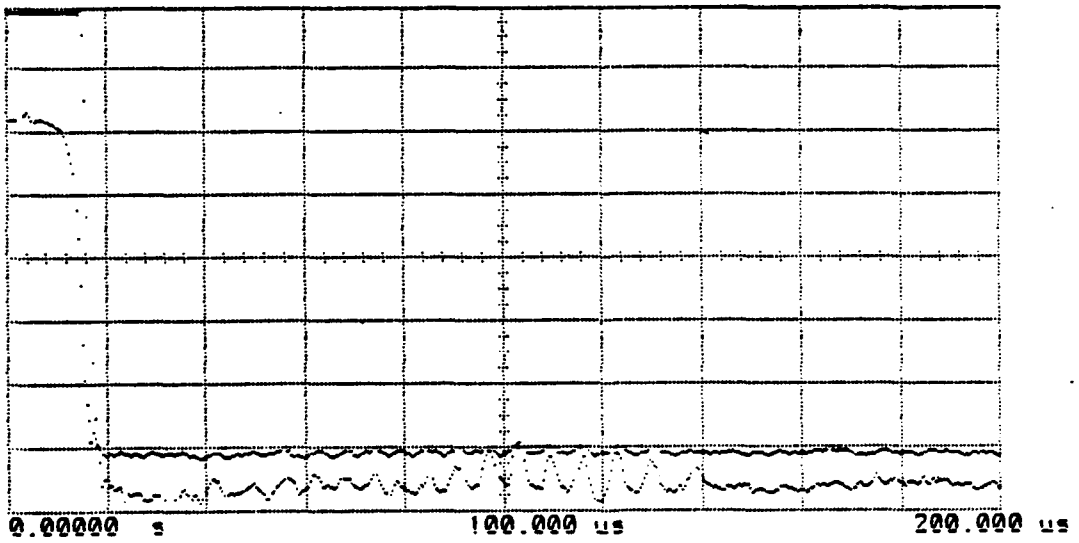

Ch. 1	=	1.000 mVolts/div	Offset	=	3.000 mVolts
Ch. 2	=	5.000 mVolts/div	Offset	=	15.00 mVolts
Timebase	=	20.0 us/div	Delay	=	0.00000 s

Fig 20,9, 20b

a)

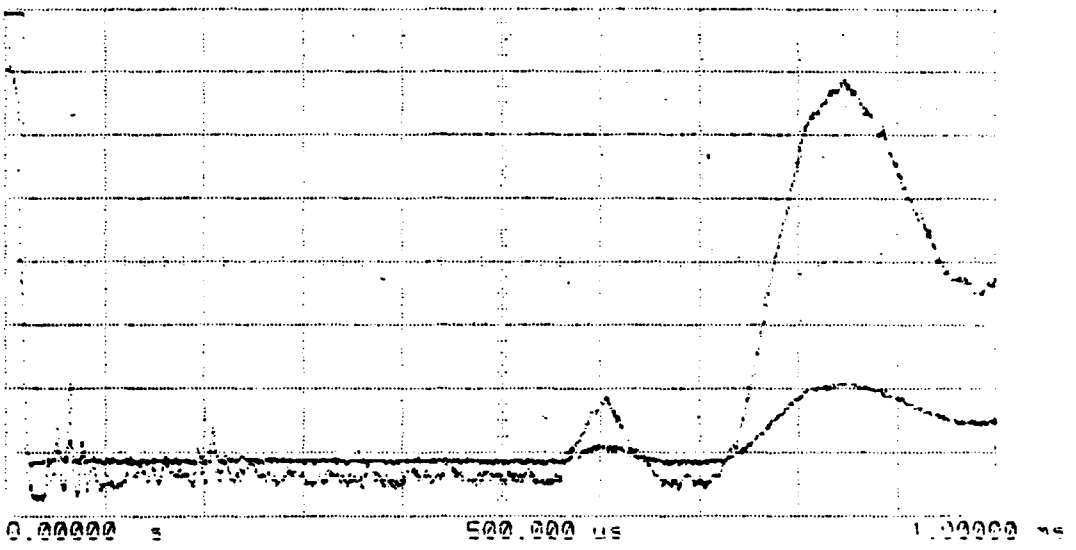

Ch. 1	=	1.000 mVolts/div	Offset	=	3.000 mVolts
Ch. 2	=	5.000 mVolts/div	Offset	=	15.00 mVolts
Timebase	=	100 us/div	Delay	=	0.00000 s

b)

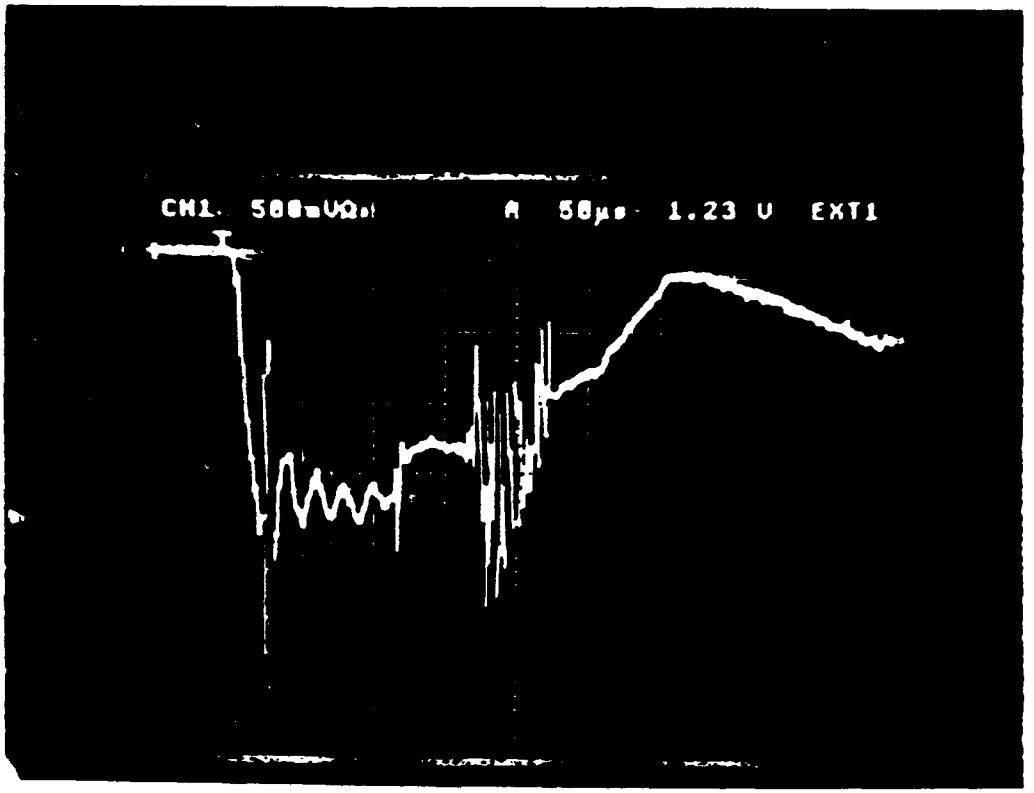

Fig 21 a, 21b